

# Gold Nanoparticles Based Novel Solid Catalysts

## Synthesis, Characterization and Application

Dissertation

zur

Erlangung des akademischen Grades

doctor rerum naturalium (Dr. rer. nat.)

der Mathematisch-Naturwissenschaftlichen Fakultät

der Universität Rostock



vorgelegt von

(M.Sc.) Ahmad Alshammari

geboren am 16.05.1980

in Hail, Saudi Arabia

Rostock 25.10.2010

---

**Dekan:** Prof. Dr. Christoph Schick

**1. Gutachter:** Prof. Dr. Axel Schulz

**2. Gutachter:** Prof. Dr. Angelika Brückner

**3. Gutachter:** Prof. Dr. Ralf Ludwig

**4. Gutachter:** Prof. Dr. Martin Köckerling

**5. Gutachter:** Dr. habil. Andreas Martin

**6. Gutachter:** Dr. habil. Wolfgang Baumann

**7. Gutachter:** Dr. habil. Hendrik Kosslick

**8. Gutachter:** PD Dr. Evgenii Kondratenko

---

**Tag der Promotion:** 14.12.2010

---

## Abstract

Catalysis using gold nanoparticles (AuNPs) is a topic of great interest due to their various beneficial properties towards different catalytic reactions of both academic and industrial importance. The catalytic activity of AuNPs is directly related to their size, shape and distribution particularly in the nanometer range. In this thesis, the preparation, characterization and application of a variety of AuNPs were studied. In particular, sol-method route has been employed for the synthesis of colloidal AuNPs and impregnation technique for supported and promoted AuNPs. The catalyst supports used are MgO, CaO, Al<sub>2</sub>O<sub>3</sub>, TiO<sub>2</sub> and ZrO<sub>2</sub> and their corresponding metal oxy-fluorides. Depending upon the suitability of the technique, the bulk and surface properties of these unsupported (colloidal), supported and promoted AuNPs were investigated by different characterization methods such as UV-Vis, DLS, ICP-OES, XRF, TGA, BET, XRD, XPS, solid-state NMR, SEM, TEM, etc. The content of Au is confirmed by ICP, which is in line with the nominal values. UV-Vis, DLS, SEM and TEM gave complementary evidence on the tendency of changes in the size and distribution of AuNPs. No reflections correspond to gold could be seen from the XRD patterns particularly in the fresh samples. However, XPS showed the presence of Au in the near-surface-region. The catalytic properties of the samples were examined for three different reactions in both liquid and gas phase conditions. For instance, unsupported catalysts (colloidal) were tested in homocoupling of phenylboronic acid to biphenyl as a model reaction. Supported AuNPs were checked as catalysts for the oxidation of benzyl alcohol to benzaldehyde and also for the oxidation of cyclohexane to adipic acid in glass reactor and autoclave. In addition, the promoted AuNPs were exclusively used for gas phase ammoxidation of 2-methylpyrazine to 2-cyanopyrazine in a fixed bed reactor. The particle size of colloidal AuNPs is found to vary in the range from 2 to 20 nm. The smallest particles gave the best performance in the coupling of phenylboronic acid. Among all supported and promoted AuNPs, TiO<sub>2</sub> supported one displayed superior performance in the above-mentioned reactions. The superior performance of this catalyst is undeniably attributed to the smaller size of AuNPs. Besides, good correlation between activity and Au particle size could be achieved. Overall, it can be stated that the particle size of gold has shown a strong influence on the catalytic performance of the samples.

### Keywords:

Gold catalysts, Colloidal AuNPs, Supported and promoted AuNPs, Liquid and gas phase oxidations, Metal oxide and oxy-fluoride catalyst carriers.

## Zusammenfassung

Die Katalyse unter Verwendung von Goldnanopartikeln (AuNPs) ist von großem akademischem und industriellem Interesse. Die katalytische Aktivität von AuNPs hängt in hohem Maße von deren Partikelgröße im Nanometerbereich, Morphologie und Dispersität ab. In der vorgelegten Arbeit wird die Synthese, Charakterisierung und Anwendung einer Reihe von nanopartikulären Goldkatalysatoren untersucht. Für die Synthese kolloidaler Goldpartikel dienten Sol-Methoden, während Imprägnierungstechniken für die Präparation geträgerter und promotierter AuNPs eingesetzt wurden. Verwendete Katalysatorträger waren MgO, CaO, Al<sub>2</sub>O<sub>3</sub>, TiO<sub>2</sub> und ZrO<sub>2</sub> sowie ihre korrespondierenden Metalloxyfluoride. Die Eigenschaften dieser kolloidalen, geträgerten und promotierten AuNPs wurden, je nach Möglichkeit, mittels verschiedener Analysemethoden untersucht, wie UV-Vis, DLS, ICP-OES, XRF, TGA, BET, XRD, FTIR, Raman, XPS, Festkörper-NMR, SEM, TEM, etc. Der Goldgehalt wurde mittels ICP-OES bestimmt und war in Übereinstimmung mit den theoretischen Werten. Über UV-Vis, DLS, SEM und TEM wurden sich gegenseitig ergänzende Informationen zu Veränderungen in den Partikelgrößen und -verteilungen erhalten. In den Pulverdiffraktogrammen von Gold-Trägerkatalysatoren konnten keine Gold zuzuordnenden Beugungsreflexe gefunden werden, auch nicht in den frischen Proben. Hingegen wurden Goldspezies an der Oberfläche geträgerter Katalysatoren mittels XPS-Messungen nachgewiesen. Die katalytischen Eigenschaften der neu hergestellten Materialien wurden sowohl in Flüssigphasen- als auch Gasphasenreaktionen getestet. So wurden kolloidale Goldkatalysatoren in der Homokupplung von Phenylboronsäure zu Biphenyl ; geträgerte AuNPs in der Oxidation von Benzylalkohol zu Benzaldehyd und auch von Cyclohexan zu Adipinsäure im Glasreaktor und im Autoklaven eingesetzt. Promotierte Au-Trägerkatalysatoren wurden hingegen in einem Festbettreaktor in der Gasphasenammoxidation von 2-Methylpyrazin zu 2-Cyanopyrazin getestet. Die Partikelgröße kolloidaler AuNPs variierte im Bereich von 2 bis 20 nm, wobei die kleinsten Partikel die höchste Aktivität in der Homokupplung von Phenylboronsäure zeigten. TiO<sub>2</sub> war von allen verwendeten Trägern das am besten geeignete Material, damit geträgerte Goldpartikel waren in den genannten Reaktionen am aktivsten, was aber ebenso an der sehr geringen Partikelgröße der Goldspezies auf Titania liegt.

### Stichwort:

Au-Katalysatoren, Kolloidales AuNPs, Geträgerte und promotierte Au-Trägerkatalysatoren AuNPs flüssigkeit und gasphasenoxidationen, Metalloxide und oxy-fluoride as Katalysatorträ



## Acknowledgements

All the admirations are for almighty God, who helped me in difficulties and gave me enough strength and ability to accomplish this research work. It is also a pleasure to thank many people who made this thesis possible. First and foremost, I would like to thank my advisor, **Dr. habil. Andreas Martin**, Head of the Department, Heterogeneous Catalytic Processes, Leibniz Institute for Catalysis (LIKAT) for his excellent guidance, encouragement, inspiring discussions, valuable suggestions and support throughout my entire doctoral work. I also greatly appreciate the freedom that he gave me to pursue my ideas. I would deeply like to thank my co-advisor Dr. Angela Köckritz (Group leader, LIKAT) for her patient help and support throughout my investigations.

Special thanks go to Prof. Axel Schulz, Head of Department for Material Design, for accepting my registration at Rostock University under his supervision. I equally thank Dr. habil. H. Kosslick for his willing help and useful discussions.

I also take this opportunity to profusely thank Dr. V. Narayana Kalevaru (Group leader, LIKAT), for his valuable suggestions and follow up action, which gave me the opportunity to learn more during the course of my Ph.D. studies. His guidance is indeed an important part of my learning.

I also extend my thanks to Dr. M. Kant, Dr. U. Armbruster, Dr. (Mrs.) C. Fisher, Dr. M. Schneider, Dr. M-M. Pohl, Dr. J Radnik, Dr. N. Dhachapally, Dr. H. Atia, Dr. P. Patil, Mr. R. Eckelt, Mrs. J. Kubias and Mrs. R. Bienert and also other analytical staff of LIKAT for their help in testing and characterizing my catalysts.

I would also like to thank Prof. Matthias Beller (Director of LIKAT) for allowing me to work in a reputed institute like LIKAT.

Special thanks go to the colleagues from KACST particularly **Prince Dr. Turki Al-Saud**. It is my pleasant duty to thank him for all kind of support and for having trust in me. I am also delighted to thank Prof. Dr. Soliman Alkowtir and Dr. Hamid Al-Migrin, for their unforgettable help and encouragement to study abroad.

Last, but not the least, I also extend my thanks to my parents, my wife **Monirah Aladeem** and my children (Turki and Nirasan) for always being on my side, cherishing and supporting me.

**A. Alshammari**

## Plan of the thesis

The contents of the present thesis have been divided into six chapters on the basis of the introduction / reviewed literature, experimental / characterization techniques applied, and finally on the catalytic application of prepared catalysts.

**Chapter 1** deals with the general introduction about gold catalysis and thorough literature survey concerning its importance, some basic concept and the catalytic applications. Objectives of the thesis are also given.

**Chapter 2** describes the preparation of un/supported gold catalyst, the experimental procedures for the physico-chemical, surface, bulk, particle size characterizations and evaluation of the catalysts for liquid and gas phase reactions are described.

**Chapter 3** begins with the optimization of the gold particles size by varying the reaction parameters (T, pH, etc.). The influence of the reactions conditions, nature of reductants, and combination of reductants on the size, morphology, formation mechanism and stability of colloidal AuNPs is also discussed.

**Chapter 4** presents a comprehensive study of the physico-chemical properties of supported and promoted gold catalysts over different kind of supports including metal oxides and their corresponding fluorides. Bimetallic and used catalysts have been also studied. These catalysts are characterized by BET surface area, ICP, XRF, EDX, NMR, XRD, TGA, DTA, IR, XPS, TEM and SEM.

**Chapter 5** includes three different sections. Section 5.1 shows an example of the application of unsupported gold catalysts (colloidal). The evaluation of supported gold catalysts for oxidation of benzyl alcohol and cyclohexane are described in section 5.2. The application of promoted gold catalysts for ammoxidation of 2-methylpyrazine (2-MP) are also given in section 5.3. The optimization of process parameters for the oxidation of cyclohexane and ammoxidation of 2-MP is also presented.

**Chapter 6** summarizes and concludes the results of the investigations; possible outlook of future researches using gold catalysts are also shown.

\* \* \*

# Contents

<b>Abstract</b> .....	<b>iii</b>
<b>Acknowledgements</b> .....	<b>v</b>
<b>Plan of the thesis</b> .....	<b>vi</b>
<b>Contents</b> .....	<b>vii</b>
<b>1. General Introduction and Literature Survey</b> .....	<b>1</b>
1.1. Metal nanoparticles for catalysis.....	2
1.2. Background on the use of gold in catalysis .....	3
1.2.1. Importance of gold nanoparticles in catalysis.....	4
1.2.2. Theoretical background.....	4
1.2.3. Literature survey on gold catalysts .....	12
1.3. Objectives of the thesis .....	16
<b>2. Equipment and Experimental Methods</b> .....	<b>18</b>
2.1. Sample preparation .....	19
2.1.1. Preparation of colloidal AuNPs.....	19
2.1.2. Preparation of supported AuNPs.....	20
2.1.3. Preparation of promoted gold catalysts .....	21
2.2. Characterization methods.....	22
2.2.1. Bulk techniques .....	22
2.2.2. Surface area measurements .....	23
2.2.3. Surface techniques.....	23
2.2.4. Particle size and shape determination.....	24
2.2.5. Other techniques and software .....	24
2.3. Catalytic activity measurements .....	25
2.3.1. Experimental set-up .....	26
2.3.2. Catalyst testing and products analysis .....	26
<b>3. Formation, Structural Characterization and Stability of Colloidal AuNPs</b> .....	<b>28</b>
3.1. Influence of the reaction parameters on formation, size & shape of AuNPs.....	29
3.1.1. Influence of temperature .....	29
3.1.2. Influence of initial gold concentration .....	30
3.1.3. Influence of the reductants concentration.....	31
3.1.4. Influence of initial pH-value of HAuCl <sub>4</sub> solution .....	32
3.1.5. Influence of gold precursor.....	33

3.2. Effect of nature of reductant on the size and shape of AuNPs .....	33
3.2.1. Optical observation.....	33
3.2.2. Zeta potential measurements.....	34
3.2.3. UV-Vis spectroscopy.....	34
3.2.4. Dynamic light scattering (DLS) investigations .....	35
3.2.5. Transmission electron microscopy (TEM) study.....	35
3.2.6. X-ray diffraction (XRD) and Energy dispersive x-ray (EDX) analysis .....	36
3.3. Long-term stability of the colloidal AuNPs .....	37
3.3.1. Optical observations.....	38
3.3.2. Zeta potential measurements.....	38
3.3.3. UV-Vis spectroscopy.....	39
3.3.4. DLS investigations .....	40
3.3.5. TEM study .....	40
3.4. Effect of the reductants combination on the size and stability of AuNPs .....	41
3.4.1. Zeta potential measurements.....	41
3.4.2. UV-Vis spectroscopy.....	42
3.4.3. DLS investigations .....	42
3.4.4. TEM study .....	42
3.5. Formation growth mechanism of colloidal AuNPs .....	43
3.5.1. Formation of colloidal AuNPs with sodium citrate .....	43
3.5.2. Formation of colloidal AuNPs with tannic acid.....	47
3.5.3. Formation of colloidal AuNPs by combination of SC and TA.....	48
<b>4. Characterization of Supported, Promoted, Bimetallic and Spent Au Catalysts....</b>	<b>52</b>
4.1. Supported gold catalysts .....	53
4.1.1. XRF and ICP results.....	53
4.1.2. EDX analysis.....	54
4.1.3. Thermal analysis .....	54
4.1.4. Solid state NMR investigations.....	57
4.1.5. BET surface area .....	58
4.1.6. XRD analysis.....	59
4.1.7. X-ray photoelectron (XPS) study.....	60
4.1.8. TEM study .....	61
4.1.9. SEM study.....	65
4.2. Characterization studies of promoted gold catalysts .....	65
4.2.1. XRF and ICP results.....	65
4.2.2. XRD analysis.....	66

4.2.3. BET surface area .....	66
4.2.4. TEM and EDX study.....	67
4.3. Characterization studies of bi-metallic catalysts .....	68
4.3.1. BET surface area and ICP results of bi-metallics .....	68
4.3.2. XRD analysis.....	68
4.3.3. TEM and EDX studies .....	69
4.4. Characterization of spent mono-metallic Au solids.....	70
4.4.1. Optical observations.....	70
4.4.2. BET surface area .....	70
4.4.3. XRD analysis.....	71
4.4.4. TEM study .....	71
<b>5. Catalytic Activity of Colloidal AuNPs, Supported and Promoted Au Catalysts ....</b>	<b>73</b>
5.1. Application of colloidal AuNPs in liquid-phase reactions .....	74
5.1.1. Colloidal gold nanoparticles as catalyst.....	74
5.1.2. Homocoupling of phenylboronic acid to biphenyl .....	74
5.2. Application of supported AuNPs in liquid-phase reactions .....	74
5.2.1. Supports used and their roles in general.....	74
5.2.2. Oxidation of benzyl alcohol to benzaldehyde using supported Au catalysts.....	75
5.2.3. Oxidation of cyclohexane using supported Au catalysts.....	78
5.2.4. Optimization of the reaction conditions.....	81
5.2.5. Oxidation of cyclohexane using bi-metallic catalysts.....	87
5.2.6. Correlation between activity and particle size on the performance of catalyst ...	89
5.3. Application of promoted Au catalysts in gas-phase reaction ammoxidation .....	90
5.3.1. The role of Au as a promoter on ammoxidation activity of 2-methylpyrazine .....	91
5.3.2. Performance of Au promoted V <sub>2</sub> O <sub>5</sub> catalysts on oxide carriers .....	92
5.3.3. Performance of Au promoted V <sub>2</sub> O <sub>5</sub> catalysts on metal oxy-fluorides.....	92
5.3.4. Influence of temperature on the catalytic activity of V <sub>2</sub> O <sub>5</sub> -Au/TiO <sub>2</sub> solid .....	93
<b>6. Conclusions .....</b>	<b>95</b>
6.1. Summary and conclusions .....	96
6.2. Outlook .....	99
<b>References .....</b>	<b>101</b>
<b>Appendix .....</b>	<b>105</b>

---

## 1. General Introduction and Literature Survey

---

*This chapter describes the aim of the research presented in the thesis. Some theoretical background information regarding catalysis concepts at the nanoscale level is outlined. In addition, catalysis by gold is reviewed in more detail including its potentiality for a variety of reactions.*

---

## 1.1. Metal nanoparticles for catalysis

Nanoscale materials (e.g. nanoparticles) can be defined as those having characteristic length scale lying within the nanometric range, i.e. in the range between one and several hundreds of nanometers [1]. Within this length scale, the properties of matter are sufficiently different from individual atoms or molecules and from bulk materials [2,3]. Therefore, their study has been recently recognized as a new area of science, which is generally termed as *Nanoscience*. In fact, this field began about forty years ago but in recent times, such materials continue to play a growing and tremendous interest due to their promising applications from both academic and industrial points of view. In general, the potential application of nanoparticles in various fields is illustrate in Fig. 1.

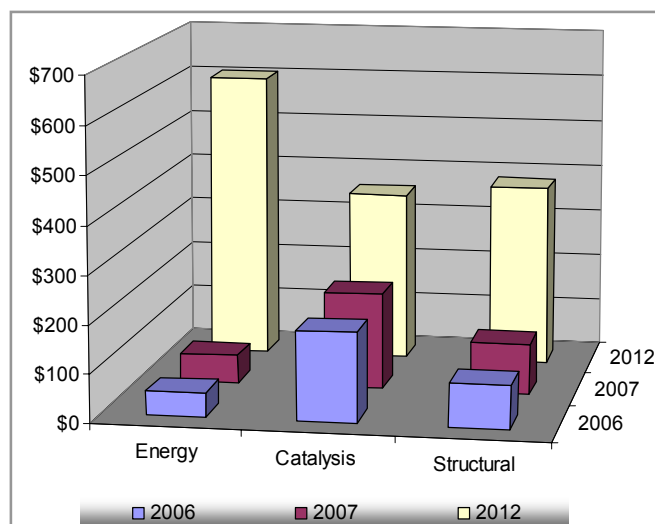


**Fig. 1.** Global market for nanoparticles in energy, catalytic and structural applications, 2006-2012 (Source: BBC research).

Coming to the applications of nanoparticles, the global market of the catalysts at nanoscale level was worth close to \$200.6 million in 2007 as shown in Fig. 1. The market of this field is projected to grow and reach above \$350 million/year in 2012. Fig. 1 also represents the global market for nanoparticles in energy and structural applications comparing with catalysis. Energy and structural application are estimated to reach \$604 and \$357 million in 2012, respectively, while \$420 for catalysis.

Metal nanoparticles (MNPs) have also been attracted in scientific research and industrial applications, due to their unique large surface-to-volume ratios and quantum-size effects [4,5,6]. Since heterogeneous metal catalysts usually work on the surface of metals, the MNPs, which possess much larger surface area per unit volume or weight of metal than the bulk metal, have been considered as promising materials particularly for catalysis. Industrial noble metal catalysts are usually composed of inorganic supports

having large surface areas and highly dispersed metals on the supports, which are prepared by different techniques. The metal particles are mostly composed of one or more metal particles (ensembles) with various sizes and shapes. MNPs often strongly interact with the inorganic supports, thus resulting in the different shapes of polyhedral particles. Transition metals have often been used in the form of metal particles dispersed onto inorganic supports such as silica gel, alumina, activated charcoal and so on. Dispersed particles on an inorganic support have advantages over metal powders in several ways such as i) high dispersion / effective utilization of MNPs, ii) good thermal stability, iii) provide high surface area, iv) reduce the cost of expensive metals etc. Among various metals investigated, gold nanoparticles in particular have been the subject of extensive research in recent times.

## 1.2. Background on the use of gold in catalysis

Historically, gold has always been regarded as being catalytically inactive. The intrinsic catalytic capabilities of group VIII metals (Cu, Ag and Au) can be ascribed to the optimum degree of d-band vacancy [7,8]. The elements of Cu, Ag and Au have fully occupied d-bands. Because of their relatively low ionization potentials, Cu and Ag readily lose electrons to yield d-band vacancies and hence they are potentially able to be catalytically active. As a matter of fact, in the chemical industry, Cu is used for methanol synthesis and Ag is used for ethylene oxide synthesis. In contrast, Au has a high ionization potential and accordingly has a poor affinity towards molecules. It was demonstrated by early surface science studies and density functional calculations that no dissociative adsorption of H<sub>2</sub> and O<sub>2</sub> occurs below 473 K on Au and therefore Au should not be catalytically active for hydrogenation and oxidation reactions [9,10]. For these reasons, gold received very little attention by the catalysis community in the past. However, in the late 1970s, Bond and co-workers [11] reported that the hydrogenation of alkenes and alkynes using the Au/SiO<sub>2</sub> catalyst gave interesting results, but afterwards some further investigations were however extended to oxidation reactions again using supported gold catalysts. This work was then regarded as the first hint that Au might not always necessarily be poorly active when dispersed as small particles (< 5 nm). In 1980s, there were two important observations made by Hutchings et al. [12] and Haruta et al. [13], which completely changed the general perception of gold and highlighted the special attributes of gold as an effective heterogeneous catalyst. Hutchings successfully predicted that gold would be the best catalyst for acetylene hydrochlorination [12], whereas Haruta discovered that gold nanoparticles are very active for low temperature CO oxidation reaction [13].



### 1.2.1. Importance of gold nanoparticles in catalysis

Catalysis using supported gold nanoparticles (AuNPs) has attracted a dramatic growth of interest due to its greater potentiality, which is directly related to its particle size. Therefore, when gold is prepared as very small particles with diameter of less than 10 nm, it turns to be a highly active catalyst. However, such phenomenon is completely disappeared as the particle size grows into the micrometer range. The importance on the usage of gold catalysts is clearly evidence from an explosion in the number of academic publications dealing with AuNPs recent times (Fig. 1.2). In other words, the number of publications appeared in 1980s is just <100, which is remarkably increased to over 1600 publications until 2009. In the year 2010 alone (October), there have been over 1550 publications, which undeniably indicate extreme importance of gold in catalysis. In addition, some books and several comprehensive reviews have also been published on this topic. Besides, patents activity was not much before 1990s but has increased noticeably since then and is now fairly steady at about 25 patents per annum.

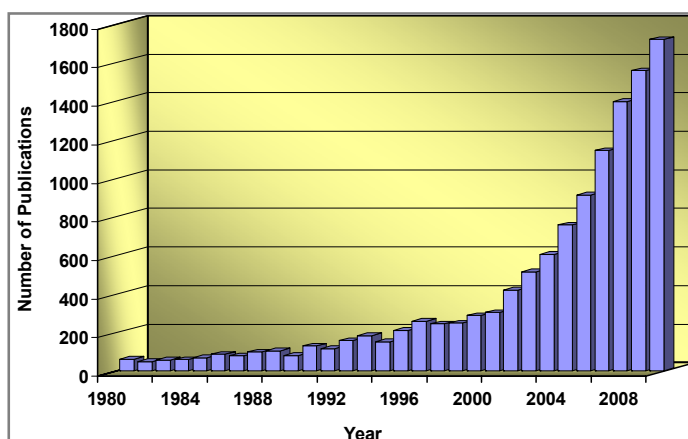


Fig. 1.2. Publications on gold catalysis in the academic literature (source: SciFinder Scholar).

### 1.2.2. Theoretical background

- Why gold nanoparticles active?

It was historically believed that the gold is the least reactive metal and was even called “the noblest of all the metals” [14]. The low chemical activity of gold is due to the filled 5d shell and relatively high value of first ionization potential, as a result, the Au catalysts have shown poor chemisorption properties [15]. Despite such belief, the interest in the use of Au in heterogeneous catalysis has been dramatically increased in recent times. Such increased interest is however based on the experimental evidence; for instance, its surprisingly high activity in the low temperature oxidation of CO [16]. Nevertheless, the reason for such catalytic activity and the reaction mechanism are still controversial.

Therefore, several studies have been devoted to understand gold's activity particularly for CO oxidation. Goodman and his group [17] focused on the Au cluster size in model catalysts and discussed quantum size effects to explain that the beginning of the catalytic activity obtains together with the appearance of a band gap in the clusters (Fig. 1.5(a)). Later on, it was suggested that the bi-layered morphology of Au cluster that is electron-rich in nature facilitates the dissociation of O<sub>2</sub> and such phenomenon is assumed to be responsible for high activity [18]. Moreover, changes of the electronic structure due to Au-Au bond contraction in small particles was also discussed as a reason for the activity by Bokhoven [19]. Other studies linked the active site to low-coordinated Au atoms (Fig. 1.2(b)) [20], especially at the corner sites [21]. Haruta [8] and Bond [22] have also used Au catalysts for different reactions. They suggested that the active site is located at the Au/support edge interface and includes cationic Au (Fig. 1.2(c)). Based on spectroscopic data (e.g. IR) for the presence of cationic Au along with zerovalent Au<sup>0</sup> during CO oxidation, it was proposed that the active site is composed of Au<sup>0</sup> and Au<sup>+</sup> species at the perimeter interface (Fig.1.2 (e)). On the other hand, it has also been reported that Au particles anchor at defects sites such as O<sub>2</sub> vacancies (F centers), which transfer electron density to the Au particles or atoms (Fig. 1.2(d)). This negative charge improves the catalytic activity for the low-temperature CO oxidation by facilitating O<sub>2</sub> dissociation and CO adsorption.

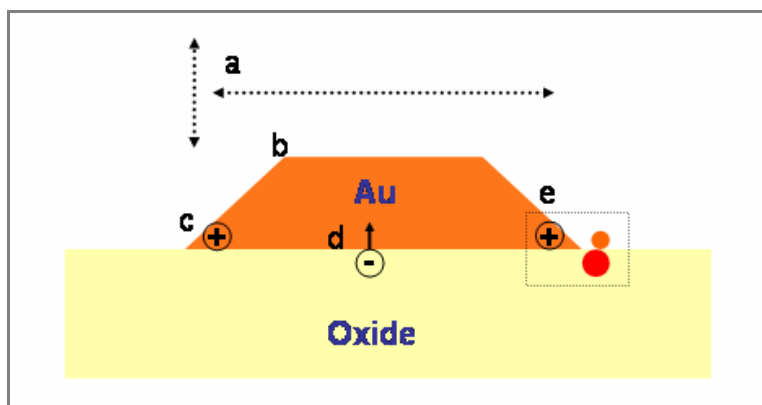


**Fig. 1.2.** Models proposed for explaining the catalytic activity of Au/oxide catalysts: (a) Cluster size effects, (b) low-coordinated Au atoms, (c) cationic gold, (d) electron transfer from F centers of the support to the Au particle, (e) ensembles of Au<sup>0</sup>, Au<sup>+</sup>, and support-bound OH groups.

- Properties of gold nanoparticles

### *Physical properties*

As mentioned above, gold is unique among various metallic elements because of its resistance to oxidation and corrosion, which makes it very effective for its usage in jewelry. Gold is a late transition metal belonging to group VIII of the periodic table along

with Cu and Ag. It has an atomic mass of 196.97 amu; M.P. 1064 °C, density = 19.6 g/cm<sup>3</sup>. The electron affinity of Au is greater than that of O<sub>2</sub> and the redox potential of Au<sup>+</sup>/Au<sup>0</sup> couple is +1.5 V. The yellow color of Au is caused by optical absorption in the visible region, which is due to the relatively low band gap between the 5d band and the Fermi level [23].

### *Chemical properties*

Gold exhibits a wide range of oxidation states. The +1 and +3 states are common, but this property is somewhat different from other metals of the same group, the +5 state of Au is also known in [AuF<sub>6</sub>]<sup>-</sup>. Three monohalides exist, but not the fluoride, because this ion is too electronegative to form a stable bond. In addition, the high electronegativity of Au gives rise to another unique feature of its chemistry. For instance, auride anion (Au<sup>-</sup>) is well documented, the compound CsAu being salt-like [24]. For such reason, Au will not react directly with other electronegative elements (e.g. sulfur or O<sub>2</sub>) and will be only dissolved in aquaregia (HCl : HNO<sub>3</sub> = 1 : 3 v/v).

### *Extraordinary surface area and chemical reactivity*

At the nanoscale, there is a huge increase in the surface-to-volume ratio of any material, in general. Surprisingly, it was demonstrated elsewhere [25] that the surface area (SA) increases significantly when the diameter of spherical particles of gold is reduced (Fig. 1.3).

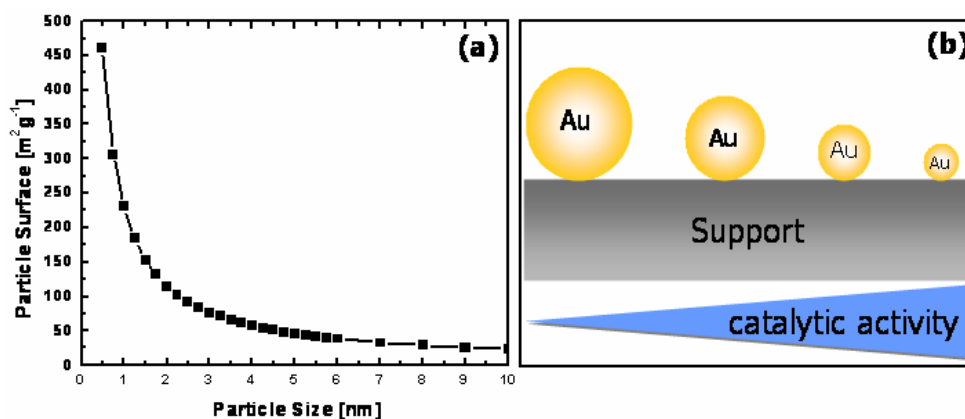


Fig. 1.3. Relation between the size of AuNPs with their surface area (a) and catalytic activity (b).

### *Optical properties*

The optical properties of AuNPs are strongly depended on the particle size and shape [26]. A striking property of colloidal AuNPs is its intense color. For example, bulk Au has a yellowish color in reflected light, caused by a reduction in reflectivity for light at the blue end of the spectrum, whereas the thin Au films have blue color in transmission.

This characteristic blue color changes to orange passing different color as the particles size reduced to smaller size due to the changes in the so-called surface plasmon resonance. Such effects of optical properties of small AuNPs are dominated by the collective oscillation of conduction electrons as a result of the interaction with electromagnetic radiation (known as “surface plasmon resonance”, SPR or “localized surface plasmon resonance” [27,28]).

- Catalytic application of gold nanoparticles

AuNPs are widely used in various fields starting from pollution control, chemical processing, fuel cells to electronics. The summary on the commercial application of AuNPs in different areas is presented in Table 1.1.

**Table 1.1.** Commercial applications of gold catalysts

Field of applications	Examples
Pollution and emission control	<ul style="list-style-type: none"> <li>• Low temperature air purification</li> <li>• Catalytic wet air oxidation</li> <li>• Automotive emission control</li> </ul>
Chemical processing	<ul style="list-style-type: none"> <li>• Production of vinyl chloride</li> <li>• Direct production of hydrogen peroxide</li> <li>• Production of nylon precursors</li> </ul>
Hydrogen economy Fuel cell application	<ul style="list-style-type: none"> <li>• Water-gas shift in H<sub>2</sub> production</li> <li>• Oxidation removal of CO from H<sub>2</sub> (PROX)</li> <li>• Gold as an electrocatalyst</li> </ul>
Sensor to detect poisonous or flammable gases in solution, or air	<ul style="list-style-type: none"> <li>• Detecting of carbon monoxide</li> <li>• Detecting of nitrogen oxides</li> </ul>

- Preparation of gold nanoparticles

In general, preparation of AuNPs can be classified into two main categories: i) unsupported particles and ii) supported particles, as shown in Table 1.2. In this thesis, our materials were prepared according to the methods, which are marked in blue color (Table 1.2). These three selected methods are discussed below in more detail.

**Table 1.2.** Preparation techniques for unsupported & supported gold nanoparticles

Unsupported AuNPs		Supported and promoted
Monometallic system	Bimetallic system	
Chemical reduction	Co-reduction of mixed ions	Adsorption technique
Photochemical irradiation	Successive reduction of metal ions	Grafting AuNPs onto support
Sonochemical irradiation	Reduction of double complexes	Deposition-precipitation
Electrochemical reduction	Electrochemical reduction	Impregnation
Metal vapor condensation	-	Co-precipitation

### *Chemical reduction*

The formation of AuNPs by chemical methods can be carried out by reduction of metal ions with chemical reductants or decomposition of metal precursors with external energy. For the first time, Turkevich demonstrated a method for preparing gold metal suspension by one-step chemical reduction of  $[\text{AuCl}_4^-]$  using sodium citrate as reducing agent [29,30]. In special cases, combination of two or more reductants can also be used. The chemical reductants include molecular hydrogen, ascorbic acid, alcohols, tannic acid, hydrazine, citrate, etc. Energy provided from the outside involves photo-energy (ultra-violet and visible light), electricity, thermal energy (heat), sonochemical energy, etc. In order to produce metal nanoparticles with a narrow size distribution, stabilizers are important particularly in case of gold nanoparticles. On the other hand, it is difficult to obtain stable colloidal dispersions of metal nanoparticles without stabilizers. Some of the advantages of chemical reduction method are briefly summarized below:

- the procedure is very simple
- it yields relatively stable metal colloids that are easy to isolate as dry powders
- the particle size distribution is narrow
- it is suitable for multi-gram synthesis and easy to scale up with reproducibility

### *Co-reduction of mixed ions*

Co-reduction of mixed ions is similar to chemical reduction in many ways. However, this method is mainly used for preparing bi-metallic nanoparticles. The preparation of the colloidal dispersions of bimetallic nanoparticles containing gold can be prepared using chemical methods [5,31]. Co-reduction is the simplest preparative method of bimetallic nanoparticles. In this method metals ions of two or more metals are usually reduced by a suitable reductants (e.g. citrate) [29]. The average diameter of bimetallic nanoparticles depends on the metal composition.

### *Adsorption of AuNPs onto support by impregnation*

The most widely used method to obtain supported AuNPs onto different supports by impregnation is known as adsorption of colloids [32]. In a simplistic way, this method involves the preparation of colloidal Au mixture first, which is followed by addition of support under stirring. The slurry thus obtained is evaporated, oven dried and calcined to obtain the catalyst. Different kinds of supports can be used (e.g.  $\text{TiO}_2$ ,  $\text{Al}_2\text{O}_3$ ,  $\text{SiO}_2$ ,  $\text{ZrO}_2$  etc.).

- Characterization of gold nanoparticles

The complete characterization of MNPs is somewhat complex. Difficulties arise not only from their smallness but also from the different shape of polyhedra, size, distribution etc.

It is known that no single technique can give complete information on the properties of materials under investigations. Therefore, it is essential to characterize the samples using various techniques for gaining deeper insights on the structure, size and catalytic properties. In view of this, the present samples are analyzed by various sophisticated methods and the information that can be obtained from those methods is listed below in Table 1.3.

**Table 1.3.** Techniques for the study of small particles of gold [33]

Method	Information obtained
Light scattering	Size and size distribution in solution
UV-Vis spectrum	Formation of colloidal nano-gold (plasmon band)
NMR	Molecular physics, crystals and non-crystalline materials
X-ray diffraction	Crystal structure and size, chemical composition
XPS	Surface composition of the catalyst
TEM, SEM	Size and Morphology
EPMA, EDX	Element and distribution
STM, AFM	Size and structure

- Stability of gold nanoparticles

The interest in the stability of AuNPs is propelled in the last two decades, i.e. after realizing the fact that the catalytic activity of AuNPs is considerably depended on its size. Unfortunately, the naked colloidal nanoparticles are thermodynamically unstable and exhibit poor long-term stability mainly due to agglomeration. Such agglomeration is much easier particularly with the gold particles owing to stronger attraction between them. Therefore, the stabilization of such particles is essential to prevent agglomeration. The possibilities for preventing agglomeration for long-term periods can be achieved by coordination to ligands/anionic species or by supporting them on a solid surface. More details of these two methods are described below.

i) Ligand route

There are two fundamental modes to maintain the stability of colloidal AuNPs system using ligands/anionic species route. These two modes for stabilization are steric and electrostatic [34]. Steric stabilization method involves that organic species added to the system adsorbing onto the particle surface, preventing a close contact of the single gold particles. These materials are generally polymers (e.g. polyvinyl alcohol, PVA) [35]. On the other hand, electrostatic or charge stabilization method involves the interaction of anionic species such as halides or polyoxoanions with the co-ordinatively unsaturated surface metal atoms, which results in the formation of a diffuse electrical double layer

and consequently a coulombic repulsion between the particles. Each mode has its own advantages and disadvantages. Steric stabilization mode is simple, which needs only the addition of suitable stabilizers (e.g. polymers). However, in some cases the use of stabilizer is undesirable e.g. the choice of polymer will affect the size and shape of colloidal MNPs formed. The stabilizer used can sometimes passivate the nanoparticles surface as a result a drastic loss of the catalytic activity might be occurred. In contrast, electrostatic stabilization mode has other benefits of stabilizing a system by simply changing the concentration of ions in the system. This is a reversible process and is also potentially inexpensive. The difference in the interaction using these two methods is shown below in Fig. 1.4.

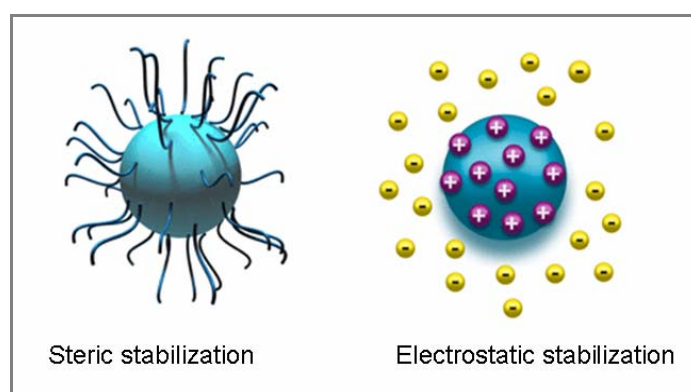


**Fig. 1.4.** Schematic representation of colloidal AuNPs system stabilization modes.

## ii) Solid route

Besides the use of ligands/anionic species to prevent the agglomeration of colloidal AuNPs, supporting of the metal particles onto a solid is an alternative route to stabilize small particles. Several kinds of solid support can be used for this purpose (e.g.  $\text{TiO}_2$ ,  $\text{Al}_2\text{O}_3$ ,  $\text{SiO}_2$ , etc.).

- Factors affecting catalytic activity of gold catalyst

The catalytic activities of gold catalysts in different reactions are notably affected by several factors, such as effect of preparation method, particle size, nature of support and so on.

### *Effect of particle size*

It was already mentioned earlier that the catalytic activity of Au depends on its particle size [36,37,38]. Therefore, the size of the metal particles is one of the most important factors that need to be tuned in a suitable way to obtain improved performance. The total surface area per unit amount of metal particles increases in proportion to the square of the diameter ( $d^2$ ) of the particles. Thus, the surface-to-volume ratio increases

with decreasing particle size, if the fcc (face-centered-cubic) structure is assumed. The other effects that can be observed when the size of gold particles decreased are:

- the fraction of the surface atoms increases
- more defect sites. In many cases, catalysis only occurs at specific sites on the catalyst surface, such as the so-called "steps".
- a large fraction of the atoms encounters the surface of support, and the length of the edge per unit mass of metals gets higher.

Moreover, When a Au particle decreases in size, a greater proportion of atoms are found at the surface. Since reactions occur at surfaces, this leads to much more reactivity for a given mass in nanoparticulate form. Furthermore, it is obvious that for millimeter and micrometer-sized particles the surface atoms can be neglected with respect to their contribution to the average coordination number.

#### *Effect of preparation method*

It is known from the literature [e.g. 39] that the method of preparation has a significant effect on the properties of supported gold catalysts, which in turn affect the catalytic activity. Numerous methods [13,40,41] for preparing gold catalyst have been reviewed earlier. One of the most widely used methods to prepare active gold catalysts is impregnation [42]. In this method,  $\text{HAuCl}_4$  is first reduced to AuNPs and then impregnated further onto the support. By using this method, it is possible to achieve an average Au particle size of 1-2 nm. However, the drawback of this method is that the presence of chloride ions originating from the gold precursor (e.g.  $\text{HAuCl}_4$ ). In order to avoid contamination of chloride ions, gas phase grafting method using monodispersed colloidal AuNPs stabilized by a suitable polymer is also tried [43,44]. However, the size of resulting AuNPs is somewhat large (ca. 10 nm). Additionally, other methods such as deposition-precipitation or co-precipitation method are used for preparing highly active gold catalysts. The selection of suitable pH value during precipitation is very important in each of these methods. Au size in the range of 1-2 nm could also be obtained using these methods. Irrespective of method of preparation applied, thermal treatment shows an important influence on the catalytic activity of gold catalysts [45]. Literature reports indicate that the catalysts are generally calcined at mild temperatures between 100 and 200 °C, (e.g. Au/TiO<sub>2</sub> [46], Au/Fe<sub>2</sub>O<sub>3</sub> [47], and Au/MnO<sub>x</sub> [48]) to avoid sintering so that the solids can show better performance than those calcined at higher temperatures.

#### *Effect of support*

It has been shown earlier that the primary role of the support is to prevent the agglomeration of nano-metal particles [49]. In addition, the support provides good



thermal stability, high surface area (i.e. high dispersion of active component), which are essential ingredients for obtaining highly active and selective catalysts. It is also reported that the interaction between the support and AuNPs has an important influence on the catalytic activity [50]. For instance, in the CO oxidation using either pure gold particles or pure titania showed no catalytic activity at 227 °C. However, nano-gold particles deposited on titania support displayed a reasonable good catalytic performance even at 25 °C, which clearly indicates the significant role of support [51]. Moreover, the choice of the support is an essential issue to perform the reaction catalyzed by nano-gold. For example, CO oxidation can also be carried out by AuNPs supported on different supports (e.g. TiO<sub>2</sub>, CaO, etc.) except acidic ones (e.g. Al<sub>2</sub>O<sub>3</sub>) and activated carbon. It was reported for example that Mg(OH)<sub>2</sub> is the best support for Au in CO oxidation at sub-ambient temperatures [52], but that deactivation occurs after 3 months. The effect of the support was explained on the basis of the structure of the as-prepared catalyst.

### 1.2.3. Literature survey on gold catalysts

A significant contribution in the field of Au catalysis was made by Hutchings and Haruta groups. Hutchings and his co-workers realized in the late 1980s that the very high standard electrode potential of Au (+1.5 V) makes AuCl<sub>3</sub> a very effective catalyst for the acetylene hydrochlorination [53]. However, the most important breakthrough came in 1987s by Haruta et al. [13], who showed that Au-based catalysts prepared in a suitable manner are very active in oxidation of CO even at sub-ambient temperature. Since then, a lot of research has been carried out by various scientists through out the globe, mostly in the field of CO oxidation [54,55]. Comprehensive review may be found [56,57] on such investigations. Later on, Au-based catalysts were tested for other reactions as well, i.e. NO<sub>x</sub> reduction [58,59], hydrogenation of unsaturated hydrocarbons [60], WGS reaction [61], NH<sub>3</sub> oxidation [62], total oxidation of volatile organic compounds (VOCs) [63], and preferential oxidation of CO in the presence of H<sub>2</sub> (PROX) [64]. Additionally, gold catalyst has been used in industrial application. The first known catalyst for this purpose is Au-Pd bimetallic catalyst formulation, which includes potassium acetate for the production of vinyl acetate monomer from ethylene, acetic acid, and oxygen [65]. Many other types of chemical reactions have been catalyzed using heterogeneous supported nano-gold catalysts [66,67]. However, due to the enormous volume of literature, we will show briefly only some selected examples, which have been investigated in this thesis. For instance, the related reactions of the present thesis are oxidation of benzyl alcohol, oxidation of cyclohexane, and ammoxidation of 2-methylpyrazine. Thus, a brief introduction to these three topics is given below.

- Oxidation of benzyl alcohol to benzaldehyde

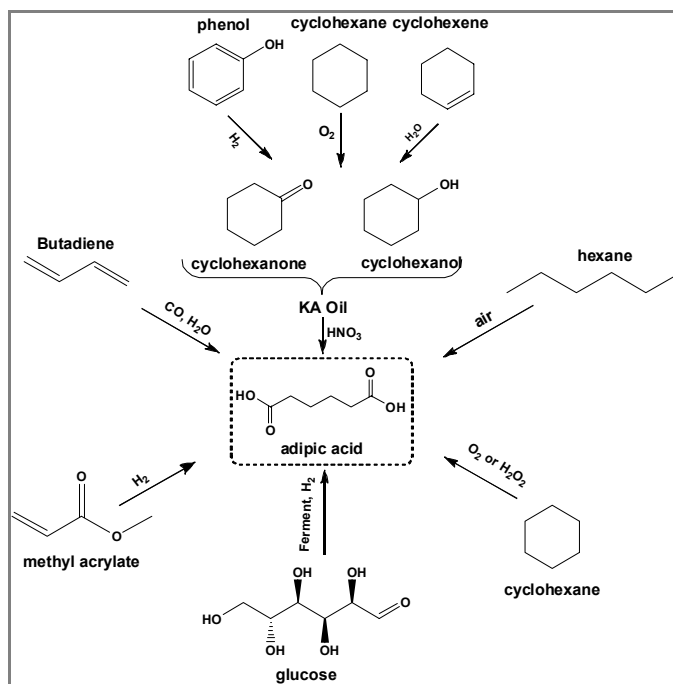
The oxidation of alcohols to useful chemical intermediates and fine chemicals with high selectivity represents an essential and demanding target in green chemistry [68]. Prati and her group demonstrated that Au/C catalysts can be used for selective oxidation of alcohols and polyols [69,70]. Rossi and co-workers showed that supported Au catalysts are effective for gas-phase oxidation of volatile alcohols to the corresponding aldehydes and ketones [71]. Moreover, Hutchings et al. used Au/graphite catalysts for the oxidation of glycerol to glyceric acid and claimed 100% selectivity of target product [72,73]. Recently, Corma and co-workers have shown that Au/CeO<sub>2</sub> catalyst is highly active and selective in the oxidation of alcohols [74]. Synthesis of benzaldehyde from the oxidation of benzyl alcohol is also one such good example for alcohol oxidation. Benzaldehyde is widely used in the production of perfumery, pharmaceutical and agrochemicals. Hutchings and co-workers have also proved that Au supported on TiO<sub>2</sub> is used on the oxidation of benzyl alcohol to benzaldehyde with O<sub>2</sub> [75]. Recently, this group studied the effect of the method preparation of Au–Pd alloy particles supported on TiO<sub>2</sub> and investigated the activity of such catalysts for the selective oxidation of benzyl alcohol [76]. Against this background, our initial study is focused on the oxidation of benzyl alcohol (BA) because this reaction is often employed as a model reaction for alcohol oxidations. In addition, this molecule has been selected due to its relatively high reactivity and the main product is a non-enolizable aldehyde thus reducing the number of possible side products. In this study, AuNPs supported by different metal oxides and their corresponding oxy-fluorides have been tested towards benzyl alcohol oxidation.

- Oxidation of cyclohexane to adipic acid

The selective oxidation of cycloaliphatic hydrocarbons to dicarboxylic acids, in particular, cyclohexane (CH) to adipic acid (AA) is indeed an industrially important reaction. The target product, adipic acid, is an extremely important commodity chemical for the manufacture of polyamides (e.g. nylon 6,6), polyurethanes, polyesters, carpets, plasticizers (e.g. PVC), and for the production of intermediates for pharmaceuticals, insecticides etc. [77,78]. Furthermore, it is also used in medicine and food products for different applications. In 2008, the global consumption of AA was around 2.5 million metric tons. Of which, the highest consumption rate is recorded in Western Europe (ca. 800,000 tonnes) followed by USA (ca. 700,000 tonnes), while the lowest in Eastern Europe (ca. 20,000 tonnes). The overall (worldwide) growth rate for AA is about 3 % per year, which is expected to reach 5-7 % by 2012. The highest growth rate of 12% is expected in Asia-Pacific region. These statistics clearly show that there is a great demand for this commodity chemical (AA) in the global market and hence research in

this direction to develop new and economically attractive routes is certainly of high commercial significance.

The current production process of AA on a commercial scale involves two-steps. The first step deals with the oxidation of CH to produce mainly a mixture of cyclohexanone (-One) and cyclohexanol (-Ol), the so-called KA-oil process (KA = Ketone and Alcohol) at around 150 °C and at 10-20 bar of air using a cobalt or a manganese catalyst. In the second step, the resulting mixture of KA is subsequently converted into AA using nitric acid as an oxidant [79]. The majority of AA available in the market is made through KA-oil process according to the steps mentioned above. The main drawback of this method is to maintain very low conversion levels of CH ( $X = \leq 5\%$ ) to obtain high selectivity of KA products (70-85%) particularly in the first step, which involves large recycling (> 90 %) of un-reacted CH and hence incurs some additional costs. Another disadvantage of this method is concerning environmental issues. For instance, the usage of nitric acid as an oxidant in the second step of this process undeniably generates certain amounts of  $\text{NO}_x$  in the product stream, which in turn can cause acid rain, promote formation of smog, destroys ozone layer and so on. Therefore, there is a need to look for other alternatives or develop new and attractive routes that can avoid usage of environmental unfriendly reagents. Various possible routes that can be used for producing are illustrated in Scheme 1. Although different opportunities exist, the direct oxidation of CH to AA in one step using  $\text{O}_2$  as an oxidant is indeed an effective and economic approach, which is also the main task of the present invention.



**Scheme 1.1.** Summary of the different alternative pathways for AA production.

Even though some of the above processes (see Scheme 1.1) are being practiced commercially, most of them suffer from high costs due to multi-step operations and handling large waste disposal. On the other hand, some process options for AA production in absence of HNO<sub>3</sub> usage were also proposed by various research groups in different patents (e.g. GB 1304 855 (1973) [80] and US 3390174 (1968) [81]). Nevertheless, these approaches gave only poor selectivities (S = 30-50%) of desired products. An additional problem of most of these processes is usage of soluble homogeneous catalysts, which leach out during the course of the reaction and pose difficulty of separation after the reaction. Moreover, the usage of solid catalyst in the direct oxidation of CH to AA is also known from the prior art. For example, F.T. Starzyk et al. [82] have applied "iron phthalocyanine encapsulated in Y-zeolite" as a catalyst for the direct oxidation of CH to AA. However, this process strongly suffers from much longer induction periods, i.e. the catalyst requires about 300 h to reach CH conversion of ca. 35 % and needs 600 h to get higher amounts of adipic acid in the product stream, which makes the process commercially unattractive.

Furthermore, efforts were also made by various researchers to use gold-based catalysts for the direct oxidation of CH to AA, but to the best of our knowledge all such attempts went unsuccessful until now. For instance, various gold catalysts such as Au/graphite [83], Au/MCM-41 [84], Au/SBA-15 [85], Au on CeO<sub>2</sub> [86], SiO<sub>2</sub> [87] and Al<sub>2</sub>O<sub>3</sub> [88] supports were applied for the said reaction, which gave only cyclohexanol and cyclohexanone as major products without any adipic acid in the product stream. Using such catalyst systems, the conversion of CH was varied in the range from 6 to 20 % but again almost no adipic acid formation was reported. However, the selectivity of both cyclohexanol and cyclohexanone products together were found to be in the range of 17 to 90 % depending upon the catalyst system used and reaction conditions applied.

On the whole, it can be stated that the catalyst systems used in the prior art are completely different from ours. The goal of the present invention is therefore to provide a direct method for producing AA in a single step with acceptable selectivity from the oxidation of CH using effective and potential catalyst compositions. The work also aims to supply an easy method for preparing the catalyst and its use in the said oxidation reaction.

- Ammoxidation of 2-methylpyrazine to 2-cyanopyrazine

Ammoxidation is a liquid or gas phase partial oxidation with selective insertion of nitrogen in to an alkyl group (also -OH & -CHO groups) attached to olefinic, aromatic or hetero aromatic hydrocarbons to produce nitriles in a continuous process. Thus, ammoxidation combines both oxidation and ammonolysis in a single step with the

involvement of suitable catalyst. Ammoxidation of alkyl aromatics and heteroaromatics has been the subject matter of great interest in recent times because the nitriles are useful organic intermediates for preparing various useful chemicals of high commercial significance. Ammoxidation technique has become popular since 1960s and has many advantages compared to classical methods of nitrile synthesis. Ammoxidation of 2-methylpyrazine (MP) in particular is an industrial important reaction, because the target product, 2-cyanopyrazine (CP), is an essential intermediate in the production of pyrazinamide, an effective anti-tubercular drug. It is often used in combination with other anti-tuberculosis medications. For instance, pyrazinamide is used in combination with isoniazid and rifampicin in the treatment of tuberculosis. However, it is never used on its own. Interestingly, pyrazinamide is used to reduce the whole treatment period considerably (e.g. in combination with rifampicin only 2 months). Many studies have revealed that vanadia based solids [89] and vanadium phosphorus oxides (VPOs) [90] and Mo-based are normally reported to be effective catalysts for different ammoxidation reactions [91,92]. However, to the best of our knowledge, Au-containing catalysts have never been applied for ammoxidation reactions. Recently, much attention is paid to the synthesis of the nanocatalytic materials (e.g. Au-based) with desired properties with high surface areas. Particularly, during the last couple of decades the interest in the gold containing catalysts is very rapidly increased due to their unique properties including high activity at low temperatures in many important reactions [8]. Keeping these aspects in mind, we have now tried to add small amounts of gold to the vanadia-based ammoxidation catalysts in the direction of improving their performance. In this thesis, quite recently and for the first time, a new class of supported vanadia-gold catalysts are synthesized and tested towards ammoxidation of MP. A strong synergistic effect between Au and  $V_2O_5$  is noticed during the ammoxidation of MP. These  $V_2O_5$ -Au catalysts are prepared using different oxide carriers such as  $TiO_2$ ,  $Al_2O_3$ ,  $ZrO_2$ , MgO and CaO. In addition, the corresponding oxy-fluorides of the above-mentioned supports are also used as novel supports for the first time and tested their catalytic performance in the ammoxidation of MP to CP.

### 1.3. Objectives of the thesis

The objectives of the thesis are focused mainly on three main aspects concerning synthesis, characterization and testing of both colloidal and solid gold catalysts:

- i) To improve tailor-made preparation of colloidal AuNPs the special emphasis was devoted to synthesize very small and stable Au particles considering various aspects and additionally supported and promoted solid catalysts. The details are listed here:

- the objective is to use colloidal-method for the synthesis of AuNPs in presence and absence of stabilizers
  - optimisation of synthesis conditions (e.g. influence of temperature, pH, metal precursor, stirring speed etc.) for obtaining small AuNPs
  - to check the influence of various reducing agents on the size, shape and distribution of AuNPs
  - to check the effect of reductants combination (i.e. simultaneous usage of two or more reductants during synthesis) on the size and stability of AuNPs
  - to establish the formation mechanism of AuNPs
  - synthesis of supported and promoted solid AuNPs by means of impregnation technique and using different catalyst carriers
- ii) Characterization of both colloidal and supported/promoted solid AuNPs:
- characterization of colloidal AuNPs mainly by DLS, UV-Vis, and also some selected samples by TEM, SEM, and XRD to know their basic properties like particle size, shape, distribution, stability etc.
  - characterization of supported / promoted solid AuNPs by BET-SA, pore size distribution, ICP, XRF, TGA & DTA, XRD, HRTEM, SEM, EDX, XPS, solid state NMR etc. for better understanding of catalytic properties of the catalysts.
- iii) Catalytic testing of unsupported (colloidal) and supported / promoted solid gold catalysts for different reactions:
- to check the performance of Colloidal AuNPs in the homocoupling reaction in liquid phase, e.g. phenylboronic acid to biphenyl as a model reaction
  - to test the catalytic performance of supported mono metallic and bimetallic (e.g. Au-Pd, Au-Ag) gold catalysts for two different liquid phase reactions. For instance, oxidation of benzyl alcohol to benzaldehyde and oxidation of cyclohexane to adipic acid in liquid phase. Besides, optimization of reaction conditions (e.g. T, P, mole ratios etc.) for enhancing the yield of adipic acid is also part of objectives
  - to check performance of gold promoted catalysts (e.g.  $V_2O_5$ -Au) for gas phase ammoxidation of 2-methylpyrazine to 2-cyanopyrazine in a fixed bed catalytic reactor

---

## 2. Equipment and Experimental Methods

---

*In Chapter 2 methods to prepare unsupported (colloidal), supported and promoted gold catalysts are explored. In addition, bimetallic catalyst systems were also prepared. The experimental techniques employed for their physico-chemical, bulk, surface and particle size characterization are given. Furthermore, the experimental set-ups used for testing catalytic activity in for both liquid and gas phase conditions are described. The experimental procedure adopted for evaluation of the catalytic performance is also presented.*

---

## 2.1. Sample preparation

### 2.1.1. Preparation of colloidal AuNPs

- General procedure

Synthesis of gold nanoparticles (equation 2.1) was carried out in a highly simplified one-step chemical reduction of tetrachloroauric acid (HAuCl<sub>4</sub>, lab-prepared, see the Appendix), as shown in Fig. 2.1.

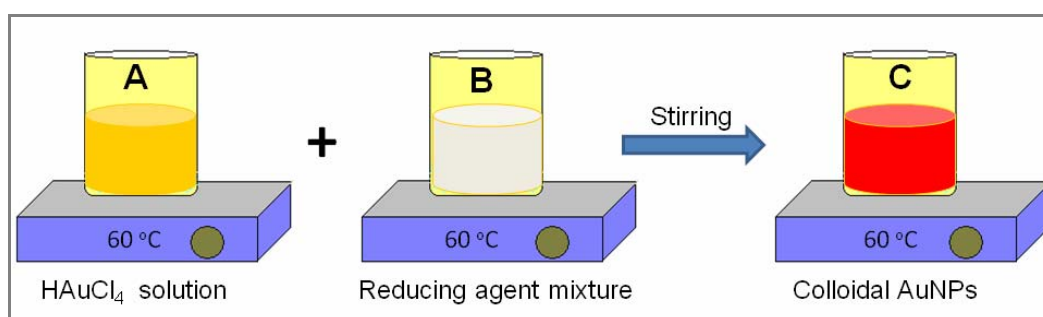
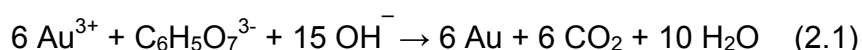


**Fig. 2.1.** Schematic procedure of colloidal gold nanoparticles synthesis.

**A:** 30 ml of a 1.0 mM HAuCl<sub>4</sub> solution was heated at 60 °C.

**B:** 8 ml of a 15 mM citric acid (CA) solution was heated to 60 °C.

**C:** mixture of A and B were mixed quickly under stirring (1000 rpm) until the formation of colloidal AuNPs was indicated by color and also further confirmed by DLS and UV-Vis techniques.

The same procedure was carried out using the various reductants such as sodium citrate (SC), iso-ascorbic acid (IA), sodium borohydride (SB), tannic acid (TA), sodium thiocyanate (ST). In a similar way, the preparation was also performed using the combination of two reductants simultaneously and the details are given below.

- Improvement of preparation method for getting small and stable AuNPs

With an intention to synthesize and stabilize small AuNPs using the procedure shown in Fig. 2.1, the following optimal experimental conditions were developed to obtain stable AuNPs ranging from 1 to 5 nm using TA/SC and ST/SC-Polyvinylpyrrolidone (PVP) combination, as reductant/stabilizers. In a typical experiment, the colloidal AuNPs are made up of two solutions: (A) 1 mL of 1% HAuCl<sub>4</sub> solution in 80 mL of water and 1 mL of 25 mM K<sub>2</sub>CO<sub>3</sub> solution were prepared, (B) the mixture contains 1 mL of 1% of TA in the presence of 1% SC (mainly as stabilizer) was prepared. Both solutions were heated separately to 60 °C. Then the solution of B was added quickly to solution A under



stirring (1000 rpm) until the formation of colloidal AuNPs, which is monitored by *in situ* UV-Vis. The same procedure was also used for other combinations (e.g. ST/SC-PVP).

- Formation mechanism of colloidal gold nanoparticles

With an intention to study the growth formation mechanism of colloidal AuNPs, the reduction of  $\text{HAuCl}_4$  using SC was chosen as a model reaction. From the colloidal mixture prepared according to Fig. 2.1, 2 ml aliquots of the reaction mixture were assayed for characterization at different reaction times (i.e. at different stages of reaction) ranging from 2 sec. to 60 min. The same procedure and similar reaction conditions / concentrations were applied for experiments with single SC or TA use (15.0 mM solution each) for comparison.

- Preparation of colloidal bimetallic AuNPs

A one-step chemical reduction of  $\text{HAuCl}_4$ -M colloids ( $M = \text{PdCl}_2, \text{AgNO}_3$ ) was carried out to prepare Au-Pd and Au-Ag bimetallic colloidal systems. For example, in the first step, tetrachloroauric acid ( $\text{HAuCl}_4 \cdot 3\text{H}_2\text{O}$ , Lab-prepared, 0.06 g) and potassium carbonate ( $\text{K}_2\text{CO}_3$ , Aldrich, 0.1 g) were dissolved in distilled water (600 mL). In the second step, an aqueous  $\text{PdCl}_2$  solution (M) was prepared by dissolving required amount of  $\text{PdCl}_2$  in 10 mL distilled water. This solution was heated to 50 °C for 10 minutes and a few drops of HCl was added to completely dissolve the  $\text{PdCl}_2$  precursor. The solution was then added to the gold chloride solution prepared in the first step followed by reduction of bimetallic solution using a mixture of 1% tannic acid (reducing agent) and 1% of sodium citrate (stabilizer) under stirring (1000 rpm) at 60 °C. In a similar way, Au-Ag bimetallic colloidal nanoparticles were also prepared.

### 2.1.2. Preparation of supported AuNPs

The preparation of supported AuNPs on different carriers including metal oxides and their corresponding oxy-fluorides was performed in three steps (Fig. 2.2).

Step 1: The first step involves the preparation of colloidal AuNPs by the reduction of  $\text{HAuCl}_4$  (0.06 g) in aqueous solution using 1% tannic acid, 1% sodium citrate and  $\text{K}_2\text{CO}_3$  (0.1 g), as shown in (section 2.1.1).

Step 2: In this step, the above-prepared colloidal AuNPs (step 1) were impregnated onto the support (e.g. CaO, 3 g).

Step 3: After impregnation (step 2), the slurry was vigorously stirred for 2 hours at room temperature and then the excess solvent was removed on rotary evaporator. The obtained solid was washed three times with water, and then oven dried 120 ° for 16 h. The dried sample was finally calcined at 350 °C for 5 h in air.

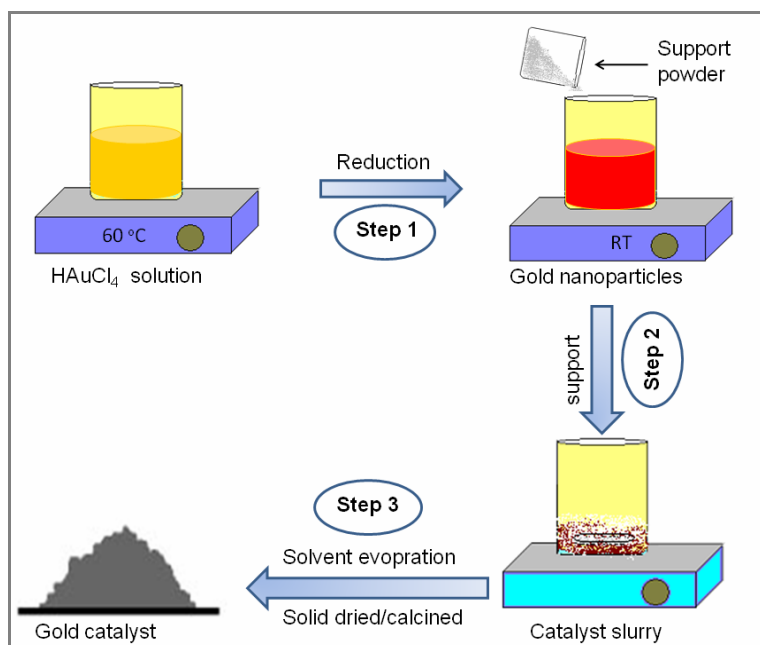


**Fig. 2.2.** Schematic procedure of supported gold nanoparticles preparation

All other supported catalysts were prepared using similar procedure but varying 10 different supports. Table 2.1 shows the type of supports used in this thesis. The content of Au is kept constant always at 1 wt%.

**Table 2.1.** Type of supports used in the preparation of gold catalysts

Series	Metal oxide support	Metal (oxy) fluoride support
1	MgO (lab-prepared)	$\text{MgF}_{2-x}(\text{OH})_x$ (lab-prepared)
2	CaO (lab-prepared)	$\text{CaF}_{2-x}(\text{OH})_x$ (lab-prepared)
3	$\text{ZrO}_2$ (lab-prepared)	$\text{ZrF}_{4-x}(\text{OH})_x$ (lab-prepared)
4	$\text{TiO}_2$ (commercial)	$\text{TiF}_{4-x}(\text{OH})_x$ (lab-prepared)
5	$\text{Al}_2\text{O}_3$ (commercial)	$\text{AlF}_{3-x}(\text{OH})_x$ (lab-prepared)

### 2.1.3. Preparation of gold promoted catalysts

A series of promoted catalysts with 10 wt% vanadia and 1 wt% gold were prepared according to the three-step procedure described below in Fig. 2.3.

**Step 1:** This step involves the preparation of 10 wt%  $\text{V}_2\text{O}_5$  solution in which ammonium metavanadate ( $\text{NH}_4\text{VO}_3$ , 0.39 g) was dissolved in distilled water (5 mL). An oxalic acid ( $\text{C}_2\text{O}_4\text{H}_2$ , 0.62 g) was added slowly under stirring into the  $\text{NH}_4\text{VO}_3$  solution till its complete dissolution.

**Step 2:** The Au/CaO catalyst obtained in (2.1.2) was impregnated with above-prepared  $\text{V}_2\text{O}_5$  solution (step 1).

Step 3: The slurry was stirred at 60 °C to remove the excess of solvent. The obtained solid was oven dried at 120 ° for 16 h. The dried sample was calcined at 450 °C for 5 h in air. The other vanadium- gold catalysts supported on different supports (Table 2.2) were also prepared and calcined in a similar manner.

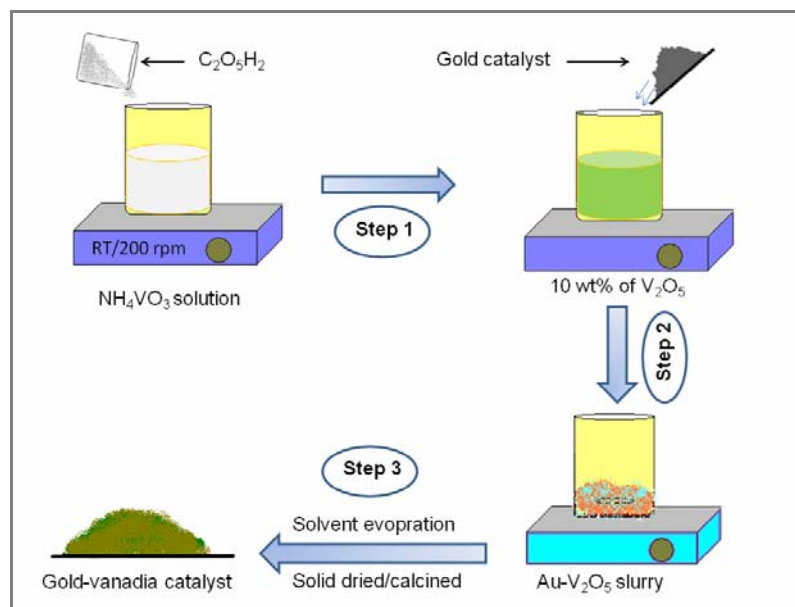


Fig. 2.3. Schematic procedure of promoted gold catalyst preparation.

## 2.2. Characterization methods

### 2.2.1. Bulk techniques

#### *Inductively Coupled Plasma*

Inductively coupled plasma (ICP) results of catalysts were obtained by instrument (model: optima 3000XL) PERKIN ELMER USA, using a microwave pressure digestion (MDS 200; CEM) with hydrofluoric and aquaregia.

#### *X-ray Fluorescence Spectrometry*

X-ray fluorescence (XRF) of the catalysts achieved using Philips PW 1480 X-ray spectrometer. Catalyst samples (50 mg) were pelleted using a dye and taken in the cell of XRF instrument for further determination.

#### *Energy Dispersive X-ray Analysis*

Energy dispersive X-ray spectroscopy (EDX) is an analytical technique used for the elemental analysis or chemical characterization of a sample, which is usually coupled with a SEM or TEM.

#### *Thermal Analysis*

Thermogravimetric and differential thermal analysis (TG-DTA) were performed with a TG apparatus (Shimadzu TGA-50). Catalysts of about 10 mg were heated from 20 to 900 °C at a rate of 5 °C/min and a flow rate of 25 mL/min in air atmosphere.

#### *Solid state Nuclear Magnetic Resonance Spectroscopy*

NMR studies ( $^{27}\text{Al}$  and  $^{19}\text{F}$ ) were performed on a Varian VNMRS 500 spectrometer using 4 mm MAS probes at room temperature and at the sample-spinning rate of 14.0 kHz.

#### *X-Ray Diffraction*

X-ray diffraction (XRD) results of the catalysts were recorded on a STADI P (STOE) setup with transmission geometry and equipped with a Ge primary monochromator with  $\text{CuK}\alpha$  radiation in the  $2\theta$  ranges from 5-60° and a position-sensitive detector. The diffraction peaks of the crystalline phase were compared with those standard compounds reported in the JCPDS Date file. The average crystallite size was calculated from the peak width using the Scherrer equation.

In addition, the particle size of Au may be estimated by using the Scherrer formula:

$$d = \frac{K \cdot \lambda}{\beta \cdot \cos \theta} \quad (2.2)$$

where  $d$  is the average crystal size (Å),  $K$  is the Scherrer constant (0.9) and  $\beta$  is the full width at the half-maximum (radians) of the peak [93]. This method, although widely used in characterization of powders, has some disadvantages. First, it estimates an average size of the metallic particles and gives no information about the size distribution of the metallic particles. Secondly, the sensitivity ranges between 3 nm and 50 nm. Thus, very small particles, below 5 nm are not detectable by X-ray diffraction technique.

#### **2.2.2. Surface area measurements**

BET surface areas (BET-SA) and pore size distribution of the catalysts were obtained on Micrometrics Gemini III-2375 (U.S.A) instrument by  $\text{N}_2$  physisorption at 77 K. Prior to the measurements, the known amount of the catalyst was evacuated for 2 h at 150 °C to remove physically adsorbed water.

#### **2.2.3. Surface techniques**

##### *X-ray Photoelectron Spectroscopy*

XPS analysis was carried out in an ESCALAB 220iXL spectrometer after exposure the sample to air at room temperature. Measurements were carried out at constant energy of 150 eV (survey), 25 eV (for quantification) and without charge compensation.

Monochromatic Al-K $\alpha$  radiation (1486.6 eV) was applied as the X-ray source. The binding energy scale was calibrated with pure and clean Cu, Ag, and Au samples.

#### 2.2.4. Particle size and shape determination

##### *Transmission Electron Microscopy*

TEM analysis was carried out using JEM-2100F high-resolution electron microscopy at a voltage of 200 kV. Sample preparation of unsupported gold particles (colloidal) for TEM is quite simple, involving the depositing of such materials on a carbon coated microgrid. However, supported AuNPs samples were dispersed in water/methanol and treated with ultrasound for 5 min, and then deposited on a carbon coated grid.

In addition, the results obtained from TEM have also been used to estimate the metallic surface area of gold. The calculations have been made by assuming that the gold particles are hemispherical in shape with the flat side on the support, according to the following formula:

$$S_{Au} = \frac{50000 \cdot W}{\rho \cdot d} \quad (2.3)$$

where  $W$  corresponds to the gold loading,  $\rho$  is the density of gold ( $19.3 \text{ cm}^3\text{g}^{-1}$ ) and  $d$  is the diameter of gold particles as determined by TEM (nm) or XRD (Å).

##### *Scanning Electron Microscopy*

SEM measurements were performed using a JSM-7401F instrument operating at 15 kV and coupled with facilities for quantitative analysis by means of energy dispersive spectroscopy (EDS). To prepare samples for SEM, samples were adsorbed on a silicon wafer and allowed to dry in air overnight.

#### 2.2.5. Other techniques and software

Colloidal AuNPs were characterized using the following techniques.

##### *Freeze-drying*

The colloidal AuNPs was dried using a Christ Alpha 2-4 freeze-dryer (LDC-1M control system). The gold colloids (100 ml) was placed in the freeze drier, frozen by liquid N $_2$ , and dried in the freeze drier chamber for 24 h. The chamber was then evacuated ( $4 \times 10^{-2}$  mbar) and freeze-drying process was started. At the end of the drying process, the temperature and the pressure were  $-25 \text{ }^\circ\text{C}$  and 0.1 mbar, respectively.

##### *Ultraviolet-Visible Spectroscopy (UV-Vis)*

The optical properties (absorbance) of colloidal solutions were acquired with a UV-Vis spectrometer (Avantes-2048, light source combined deuterium-halogen). The spectra

were collected over a range of 200-1100 nm (with an optical path length of 0.4 cm) as a function of reaction time by directly dipping the optical probe in the reaction vessel under constant stirring.

### *Dynamic Light Scattering*

Dynamic Light Scattering (DLS) measurements were determined out using a Zetasizer ZS ZEN 4003 (Malvern). A certain amount of the reaction solution was assayed and transferred to a cuvette for measurements at room temperature.

### *Zeta potential measurement*

The zeta potential data were obtained by a Zetasizer ZS ZEN 4003 (Malvern, U.K.). The measurements were carried out at 25 °C. Electrophoretic light scattering was used to detect the surface charge of the vesicles and the final obtained AuNPs.

### *Software used*

pH-value and temperature were monitored using a GMH 3530 device equipped with on-line software. The average particle diameter and size distribution were calculated using Java image tool software (ImageJ), based on the data of an average of 100-200 particles. The equation used for the estimation of these parameters based on HRTEM analysis is as follows:

$$\text{- the average diameter} \quad d_n = \frac{\sum n_i \cdot d_i}{\sum n_i} \quad (2.4)$$

$$\text{- the surface average diameter} \quad d_s = \frac{\sum n_i \cdot d_i^3}{\sum n_i d_i^2} \quad (2.5)$$

$$\text{- the dispersion} \quad d\% = \frac{100}{d_s} \quad (2.6)$$

where  $n_i$  is the number of particles of diameter  $d_i$ .

## **2.3. Catalytic activity measurements**

Herein, three types of catalysts, namely, unsupported AuNPs (colloidal), supported AuNPs and promoted AuNPs were used and their test has been done for three different experiments under liquid and gas phase conditions. This section shows in three parts on how the catalysts are evaluated and the products are analyzed.

### 2.3.1. Experimental set-up

- i) Synthesis of colloidal AuNPs were carried out in erlenmeyer flask under stirring on a hot plate equipped with temperature and pH sensor (Appendix figures - Fig. App. 1(a))
- ii) For liquid phase reactions under pressure, an autoclave with an associated control equipment has been used (Fig. App. 1(b))
- iii) Gas phase ammoxidation reaction was performed in a fixed bed tubular metal reactor (Fig. App. 1(c))

### 2.3.2. Catalyst testing and products analysis

- i) Homocoupling of phenylboronic acid to biphenyl

In this reaction, 0.11 g phenylboronic acid, 0.37 g potassium carbonate, and 10 mL water were placed in the reaction vessel. An aqueous solution of colloidal AuNPs (15 mL) was then added to the reaction vessel under vigorous stirring. Experiment was carried out at room temperature under aerobic conditions for 24 h. After that, the reaction was quenched with 0.5 M HCl solution and the products were extracted with AcOEt (10 mL, 4x). The combined organic layer was dried over Na<sub>2</sub>SO<sub>4</sub> and evaporated in vacuum. The products for this reaction were analyzed using high pressure liquid chromatography (Hitachi-4500 HPLC) equipped with a L4500A diode array detector.

- ii) Oxidation of benzyl alcohol to benzaldehyde

The oxidation of benzyl alcohol (BA) to benzaldehyde (BAI) was achieved in a stirred reactor (Parr autoclave, 100 mL). The reaction vessel was charged with 0.15 g of Au catalyst and BA (0.29 mol). The autoclave was flushed three times with O<sub>2</sub> before setting the initial reaction pressure of O<sub>2</sub> at 5 bar. Concerning the start-up procedure, this was performed with the O<sub>2</sub> line opened, and as the O<sub>2</sub> was consumed, it replaced from the cylinder, which maintains the overall pressure constant. The reaction mixture was stirred (1500 rpm) at 140 °C for 4 h unless otherwise stated. At the end of the reaction, the solid catalyst was separated by centrifugation. Besides, tests were also performed using a glass reactor consisting of 50 mL round-bottomed flask with a reflux-cooling condenser. 0.15 g of supported gold catalyst and 0.29 mol of BA were taken in a glass reactor under atmospheric pressure. Experiments were carried out using an oil bath at 140 °C for 20 h with continuous air bubbling unless otherwise stated. At the end of the reaction, the solid catalyst was separated by centrifugation. For the identification and analysis of the products, gas chromatograph (HP 6890 GC, equipped with an ultra-1 column (methyl siloxane) and a flame ionization detector (FID). Samples were taken at the end of reactions; 600 µL of product sample was added 400 µL of internal standard (ethylene glycol dibutyl ether) and 1 µL of this mixture was analyzed.

## iii) Oxidation of cyclohexane to adipic acid

Activity tests were carried out under pressure using a Parr autoclave (100 ml) according to the procedure described below. In a typical experiment, the reaction mixture consists of 0.3 - 0.4 g of supported gold catalyst, 5 mL of cyclohexane (CH), 25 mL of acetonitrile as solvent, and 0.1 g of tert-butyl hydroperoxide (TBHP), unless otherwise stated. These components were taken in an autoclave and flushed three times with O<sub>2</sub> before setting the initial reaction pressure of O<sub>2</sub> to 10 bar. Concerning the start-up procedure, it was performed with the O<sub>2</sub> line opened, and as the O<sub>2</sub> was consumed, it was replaced from the cylinder, which maintains the overall pressure constant. The stirring speed of reaction mixture was set to 1500 rpm in general and the reaction was performed at 150 °C for 4 h unless otherwise stated. At the end of the reaction, the solid catalyst was separated by centrifugation. In addition, this reaction was also performed using a glass reactor consisting of 50 ml round-bottomed flask with a reflux-cooling condenser. The reaction conditions used for glass reactor tests are similar to the ones performed in autoclave. Experiments were carried out using an oil bath at 150 °C for 5 h with continuous air bubbling. At the end of the reaction, the solid catalyst was separated by centrifugation. The identity of the reactions products for cyclohexane was confirmed by gas chromatograph (Agilent 6890 N) fitted with a HP-5 column and a flame ionization detector (FID). In order to obtain the acids in the ester form, 500 µl of product sample was esterified with 400 µl of trimethylsulfonium hydroxide in the presence of internal standard (3-pentanone, 100 µl). After such derivatization of acid to ester, 0.2 µl of this sample was injected off-line into GC and analyzed.

## iv) Ammoxidation of 2-methylpyrazine to 2-cyanopyrazine

The ammoxidation reaction of 2-methylpyrazine (MP) was carried out in a vertical fixed bed, continuous down flow micro-reactor under atmospheric pressure. In a typical experiment, about 1 g of the catalyst diluted with an equal amount of corundum grains was packed between two layers of quartz wool in the reactor. An aqueous mixture of MP (MP : water = 1 : 13 mole ratio) was fed into the reactor using HPLC pump. The molar ratio of the feed was kept at MP : H<sub>2</sub>O : NH<sub>3</sub> : air : N<sub>2</sub> = 1 : 13 : 7 : 26 : 22 and the GHSV (gas hourly space velocity) was 9506 h<sup>-1</sup> based on the total flow rate. The reaction temperature was monitored by a thermocouple with its tip located in the catalyst bed and connected by a PID-type temperature indicator cum controller. The reaction was carried out at various temperatures ranging from 360 - 420 °C. The liquid products collected from a ice cold trap were analyzed by gas chromatography (CP4FFAP-68) using an FID. The CO and CO<sub>2</sub> products were also analyzed by GC using GS Q column.



---

### 3. Formation, Structural Characterization and Stability of Colloidal AuNPs

---

*Chapter 3 is mainly dedicated to the results of colloidal AuNPs. For instance, the influence of reaction parameters on the formation, size & shape of AuNPs, dependence of AuNPs size and stability on the nature of reducing agents, optimization of synthesis conditions on the size and long-term stability of colloidal AuNPs are some of the important aspects that are presented in this chapter. Furthermore, the effects of the combination of reducing agents and formation mechanism using optimized conditions are also described.*

---

### 3.1. Influence of the reaction parameters on formation, size & shape of AuNPs

Several variables (e.g. temperature, initial concentration of gold, amount of reducing agent, pH-value of the starting material, etc.) are expected to have considerable influence on the formation, stability and size distribution of AuNPs during the course of the reduction of  $\text{Au}^{3+}$  in  $\text{AuCl}_4^-$  solution to atomic Au. The sodium citrate (SC) reduction method was selected as a model reaction to explore the effect of such parameter on the size, shape and stability of AuNPs; and the effect of each parameter is described individually in the following subsections.

#### 3.1.1. Influence of temperature

The reaction temperature is one of the most important parameters, which can affect the average size and distribution of the colloidal AuNPs. Therefore, the synthesis procedure was carried out particularly in the range of 40-80°C using  $\text{HAuCl}_4$  and SC at fixed proportions. Fig. 3.1(a) illustrates UV-vis spectra of AuNPs prepared at different temperatures. A slight broadening of the SP band was observed at 40 °C. The increase of the temperature from 40 to 60 °C was accompanied by shifting this band from 527.1 to 524.9 nm while further increasing of the temperature to 80°C caused a slight shift to 524.1 nm. Further confirmation of this study was carried out using DLS (Fig. 3.1(b)); the average size of AuNPs decreased from 26 to 13 nm measured immediately after synthesis when the reaction temperature was raised from 40 to 80 °C, respectively.

Additionally, SEM has been used to confirm the effect of reaction temperature of the resulting gold particles, as shown in Fig. 3.2. The resulting colloidal AuNPs at reaction temperature of 60 and 80 °C are found to have more or less comparable particle size (12-14 nm), as shown in Fig. 3.2(b) and (c), respectively. However, the reaction at 40 °C gave bigger particles with average size of 16 nm. Based on these observations, we concluded that an optimum temperature of 60 and 80 °C is suitable for the preparation of small AuNPs with reasonable stability. However, the particles prepared at high temperature seem to

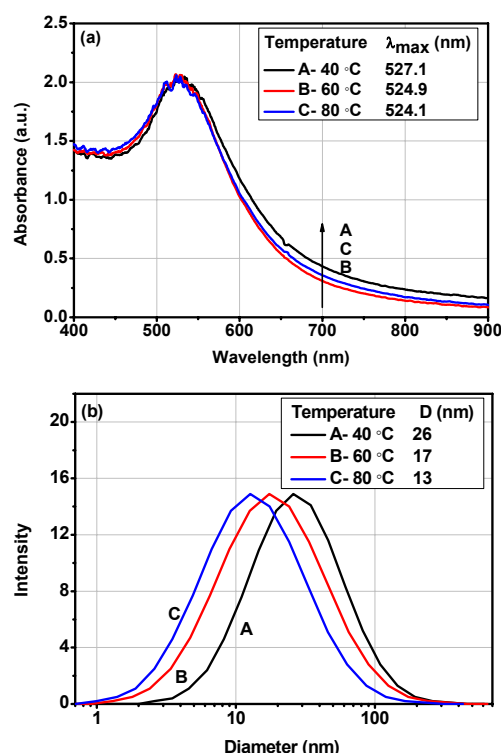


**Fig. 3.1.** UV-Vis spectra (a) and DLS distribution curves (b) of colloidal AuNPs prepared by reduction of 1.0 mM  $\text{HAuCl}_4$  with 15 mM SC at 40, 60 and 80 °C.

be less stable. Therefore, reaction temperature at 60 °C has selected for further reaction conditions.

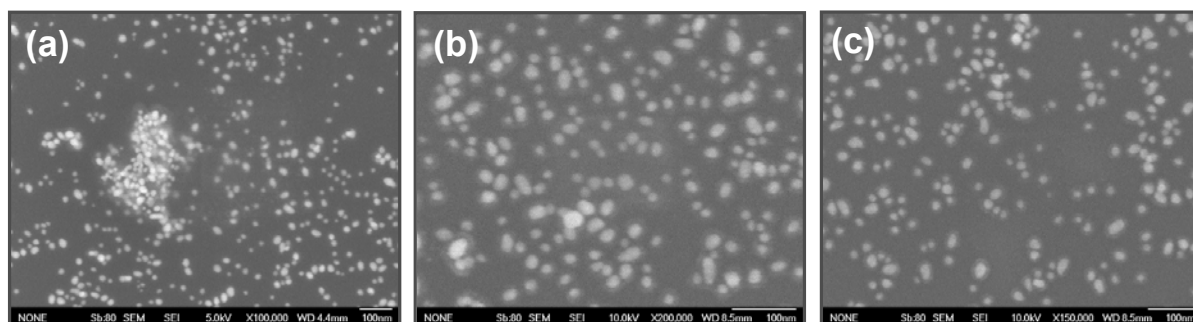


**Fig. 3.2.** SEM images of colloidal AuNPs prepared by reduction of 1.0 mM HAuCl<sub>4</sub> solution with 15 mM SC at (a)- 40, (b)- 60), and (c)- 80 °C.

### 3.1.2. Influence of initial gold concentration

Both average size and size distribution of nanoparticles can be altered by the concentration of the precursor [94]. To examine such phenomenon, different concentrations of HAuCl<sub>4</sub> solutions (0.05-2.0 mM) were applied and reduced by 15 mM SC and then the size of colloidal AuNPs was analytically monitored by various techniques such as UV-Vis and DLS. Figure 3.3(a) depicts UV-vis spectra of colloidal AuNPs prepared by using 0.05, 0.1, 0.5, 1.0 and 2.0 mM HAuCl<sub>4</sub> solutions and reduction with SC at 60 °C after completion of the reaction. The increase of HAuCl<sub>4</sub> concentrations induced an increase in the intensity of the SP bands and also a shift to lower wavelengths from 538 nm to 523 nm, indicating that the size and amount of AuNPs are affected by the concentration of HAuCl<sub>4</sub>. The use of a 0.05 mM HAuCl<sub>4</sub> solution and subsequent reduction led to a SP band maximum of approximately 538 nm (Fig. 3.3(a), spectrum A). It decreased to 523 nm with an increase of HAuCl<sub>4</sub> concentrations from 0.05 to 1.0 mM, whereas a further increase in concentration (2.0 mM) caused a red shift to 528 nm.

The changes in the average size of colloidal AuNPs achieved in different HAuCl<sub>4</sub> concentrations are presented in Fig. 3.3(b). It is quite evident that the analysis of DLS gave supporting evidence and confirms the observations made from UV-Vis. These distribution curves obtained from DLS reveal that at low HAuCl<sub>4</sub> concentration (0.05 mM), the average particles size of AuNPs was 29 nm. Increasing the HAuCl<sub>4</sub> concentration to 0.1 mM, the average particle size decreased from 29 to 26 nm. Furthermore, an increase in gold precursor concentration from 0.1 to 0.5 mM leads to smaller particles with an average size of 17 nm. The smallest AuNPs were achieved with a concentration of 1.0 mM of HAuCl<sub>4</sub> solution with an average size of 14 nm. Highly concentrated HAuCl<sub>4</sub> (2.0 mM) formed somewhat larger Au particles with 15 nm size.

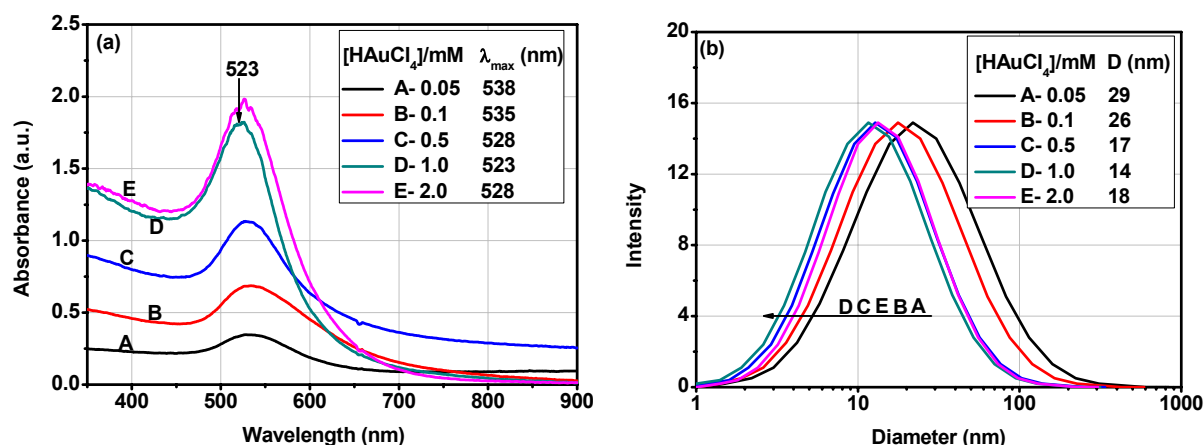


**Fig. 3.3.** UV-Vis spectra (a) and DLS distribution curves (b) of colloidal AuNPs prepared from 0.05, 0.1, 0.5, 1.0, and 2.0 mM HAuCl<sub>4</sub> solutions with 15 mM SC at 60 °C.

Furthermore, the initial concentration of Au precursor can also affect both the average size and shapes of colloidal AuNPs, which was thoroughly investigated by TEM. Fig. 3.4(a) shows that at low concentration of HAuCl<sub>4</sub> (0.05 mM) some of non-spherical particles such as irregular, triangular, hexagonal, rods, etc, were formed in addition to spherical AuNPs. Petroski et al. [95] gave two reasonable explanations for the formation of different shapes: (i) the growth rate of AuNPs at different planes of the particles and (ii) the particle growth competition with capping action of stabilizers. Regular and spherical-shaped AuNPs with a narrow size distribution were successfully obtained using a HAuCl<sub>4</sub> concentration of 1.0 mM with an average particle size of 12 nm (Fig. 3.4(b)). However, a further increase in the concentration to 2.0 mM led to the formation of bigger and non-spherical particles again with particle size between 17-25 nm (Fig. 3.4(c)).

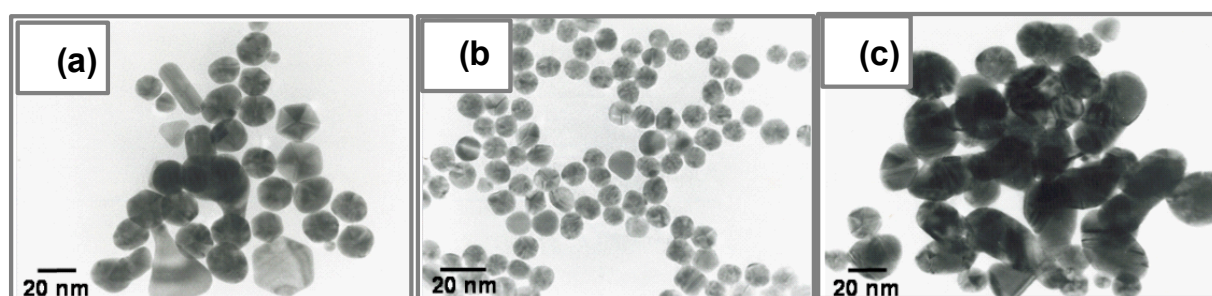


**Fig. 3.4.** TEM images of colloidal AuNPs obtained from different gold concentration (a= 0.05 mM) (b= 1.0 mM) and (c= 2.0 mM) using SC (15 mM) as reducing agent.

### 3.1.3. Influence of the reductants concentration

In order to investigate the influence of the reducing agent on the size of colloidal AuNPs, the HAuCl<sub>4</sub> solution was reduced with 7.0 mM, 15 mM, and 30 mM SC solutions. The effect of reducing agent concentration on AuNPs was measured by UV-

Vis and DLS as shown in Fig. 3.5(a) and (b). The position of the maximum absorption band was slightly blue shifted from 525 to 522 nm with increased concentration of SC, indicating the formation of smaller AuNPs. This result was further confirmed by DLS where the average particle size decreased from 25 to 17 nm with an increase in the reducing agent concentrations (Fig. 3.5(b)). This phenomenon indicated that the average size of AuNPs could be affected by higher concentration of citrate ions in the gold suspension, which avoid aggregation of small particles to bigger ones [96].

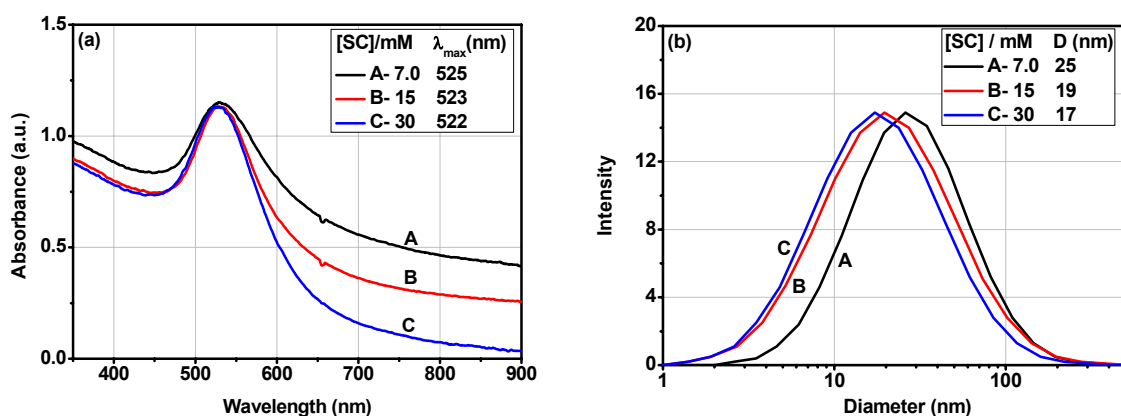


**Fig. 3.5.** UV-Vis spectra (a) and DLS distributions (b) of colloidal AuNPs prepared by reduction of 1.0 mM HAuCl<sub>4</sub> solution with 7, 15, and 30 mM solutions of SC at 60 °C.

### 3.1.4. Influence of initial pH-value of HAuCl<sub>4</sub> solution

After estimating the influence of temperature and reducing agent concentration, efforts were continued to check the effect of pH value on AuNPs size by UV-Vis and DLS. It is

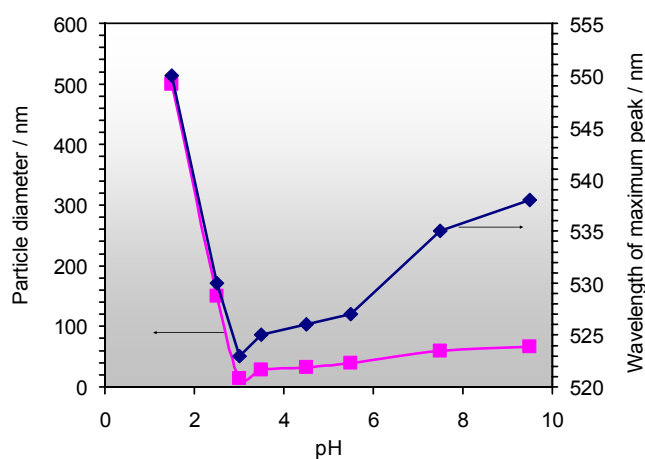


**Fig. 3.6.** UV-Vis spectra and DLS distributions of colloidal AuNPs prepared by reduction of 0.3 mM HAuCl<sub>4</sub> solution at different pH with 15 mM SC at 60 °C and [Au<sup>3+</sup>]/[SC] ratio of 1:4.

shown in Fig. 3.6 that the pH value of the reaction solution influences noticeably the particle size of the formed AuNPs. The particle size passed through a minimum of 14 nm at pH = 3.0. Lower pH-values of 1.5 and 2.5 led to considerably larger AuNPs of 500-150 nm whereas higher pH-values in the region between 5.5 and 9.5 induced only a moderate increase of the size (40-67 nm). In addition, the maximum of the SP band of resulting AuNPs prepared at low pH value (1.5) was blue shifted to a lower

wavelength from 550 to 523 nm when the pH value was raised to 3.0. However, further

increase in pH values of the reaction solution beyond 3.5 i.e., pH = 5.5, 4.5 and 9.5 induced a red shift on the position of the maximum of the SP band, and the size of AuNPs increased again. In addition, the stability of Au colloids dispersion was observed to be pH value dependent due to the fact that hydroxide can change the surface charges of nanoparticles [97].

### 3.1.5. Influence of gold precursor

Additional experiments showed that the size of Au particles can be slightly influenced by precursor materials. These experiments were done using sodium thiocyanate as reductant. Three different gold precursors such as (a)  $\text{HAuCl}_4 \cdot 3\text{H}_2\text{O}$  (commercial), (b)  $\text{HAuCl}_4 \cdot 3\text{H}_2\text{O}$  (lab prepared) and (c)  $\text{NaAuCl}_4 \cdot 2\text{H}_2\text{O}$  (commercial) were used in the preparation. First, ICP analysis was carried out to check the accurate concentration of samples (a-c) and found comparable (0.04-0.05 mg/l). It should be noted that colloidal AuNPs of larger than 4 nm a surface plasmon band in the visible region between 450 and 550 nm, whereas this band is damped for AuNPs with particle size less than 4 nm. Therefore, the UV-vis spectra (not shown) of the three preparation samples (a-c) showed no SP band indicating that the average particle size is below 4 nm since larger particles would show a narrow spectra and intense plasmon absorption band between 480 and 520 nm [98]. These results are slightly different from each other, indicating a considerable change for these results in size. In addition, dynamic light scattering exhibited a bimodal size distribution. The smallest particles were found from precursor-a (7 nm) while the biggest from precursor-b (13 nm). DLS showed pronounced differences in their size whereas no such drastic differences were observed from TEM analysis where the smallest one was around 3 nm (Fig. App. 2). Furthermore, the morphology and size of the AuNPs were examined using TEM. Fig. App. 2 shows a representative set of TEM micrographs for the colloidal AuNPs prepared using precursors a, b and c. As we observed from TEM image, the difference in the size of AuNPs is relatively small, and there is an insignificant change in the size of Au. The shape of colloidal AuNPs is found to be always spherical and is independent on the nature of precursor used.

## 3.2. Effect of nature of reductant on the size and shape AuNPs

The influence of the nature of reducing agents such as citric acid (CA), iso-ascorbic acid (IA), sodium borohydride (SB), tannic acid (TA), and sodium thiocyanate (ST) on the formation of colloidal AuNPs was also investigated under the optimized conditions.

### 3.2.1. Optical observation

Optically, colloidal AuNPs in solution display visible colors and surface plasmon (SP) resonance bands in the visible region between 500 and 550 nm. Fig. 3.7 shows a

representative set of colors of colloidal AuNPs prepared using different reducing agents under similar conditions. The characteristic color change was found to be strongly influenced by the nature of reductant. A colloidal mixture with the smallest observed particles (2-5 nm) was yellow-orange in color (F), and was obtained using ST as reducing agent. The color of the colloidal solution with a midrange size (12 nm) prepared by SC was rose-red (B), while large particles gave a red, red, pink, light red and light green color using CA (A), IA (C), SB (D) and TA (E), resp., as reductants. Such colors result from a SP resonance initiated by the interaction of the electric field of visible light with the confined electron gas within the particles, which caused collective oscillation of the conduction electrons with respect to the core [99].

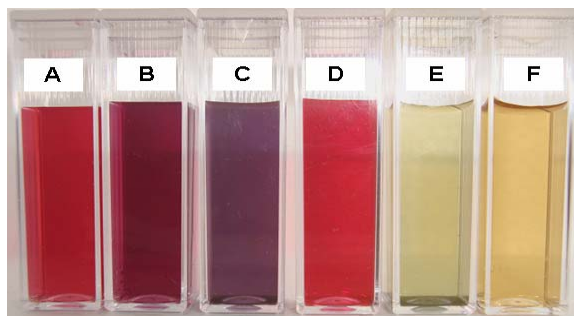


**Fig. 3.7.** Photo showing the colors of colloidal AuNPs prepared with different reducing agents: A-CA, B- SC, C- IA, D- SB, E- TA, and F- ST.

### 3.2.2. Zeta potential observations

Zeta potential can be used to get further insights on the stability of the obtained colloidal AuNPs. The magnitude of zeta potential gives an indication of potential stability of colloid. In general, the particles with zeta potential values more positive than +30 mV or more negative than -30 mV are considered stable. On the other hand, the colloids are least stable at isoelectric point, where the zeta potential is zero. In other words, the colloids with high zeta potentials (positive or negative) are electrically stabilized while the ones with low zeta potentials tend to coagulate. In the present study, the  $\zeta$  values varied in the range from -17 mV to -39 mV, depending upon the type of reducing agent / process applied. Thus, the different stability of AuNPs is also reflected by the changes in  $\zeta$  values. The zeta potential value confirmed that the highly stable colloidal mixture formed using either CA (-39.0 mV) and SC (-39.2 mV), whereas the less stable particles were obtained with TA (-17.4 mV).

### 3.2.3. UV-Vis spectroscopy

UV-Vis absorption spectra (Fig. App. 3) of colloidal AuNPs obtained by different reductants showed SP bands, which differ in their  $\lambda_{\max}$  and SP band intensities as well as in their FWHM, indicating a clear influence of the reductants on these parameters. The spectra were recorded when both the color and absorption intensity of the colloidal samples stayed constant. Among six different reducing agents used, application of IA and TA showed plasmon band positions with a lower wavelength (520 and 522 nm,

respectively) compared to others. These bands were also observed to be somewhat broad and less intense. However, colloidal AuNPs prepared by other reducing agents such as SC, SB, CT and CA showed comparable band position ( $528 \pm 1$  nm) with some deviations in their band intensities. Interestingly, in case of using ST as reductant, UV-Vis results confirmed that the SP resonance becomes weakened and shifts towards higher energy and even disappears sometimes, which indicates that the particle size of AuNPs decreased to  $\leq 4$  nm [100]. Such phenomenon might be due to the fact that the electrons of small AuNPs exist in discrete energy levels, and gold in bulk state has a continuous absorbance in the UV/Vis/IR regions, which effectively collapses into a single SP band in the case of AuNPs. Additionally, the nature of the reducing agent has shown a significant influence on the rate of reduction of the  $\text{HAuCl}_4$  solution. This means the formation of AuNPs by reduction of  $\text{Au}^{+3}$  to  $\text{Au}^0$  species took varying reaction times ranging from a few seconds to several minutes. For instance, the use of strong reducing agents such as IA, SB and TA revealed a complete reduction in some seconds (ranging from 3 to 8 sec), while the use of mild reductants such as SC and ST did not show complete reduction until 50 min and 15 min, respectively. In addition, the colloidal AuNPs formed using IA, SB and SB were relatively less stable compared to other reductants.

#### 3.2.4. DLS investigations

Average size distribution of colloidal AuNPs produced using different reducing agents was recorded by DLS (Fig. App. 4). The reduction using ST (f) produced the smallest Au particles with an average particle size of approximately 8 nm while the biggest particles were obtained by use of CA (a) with average size of 49 nm. Reduction using strong reducing agent such as SB (d), IA (c) and TA (e) produced particles with sizes of about 17, 42, 30 nm, respectively, with varying shapes of nanowires and spherical particles. The average particle size obtained with varying reductants changes in the following order:  $\text{CA} > \text{IA} > \text{TA} > \text{SB} > \text{SC} > \text{ST}$ . However, the stability order of such AuNPs was found to be somewhat different:  $\text{CA and SC (most stable)} > \text{SB} > \text{IA} > \text{ST} > \text{TA (not stable)}$ .

#### 3.2.5. TEM study

TEM images of colloidal AuNPs synthesized under similar conditions using various reductants are shown in Fig. 3.9. CA as reducing agent led to predominantly spherical AuNPs with an average particle size of 45 nm; Fig. 3.9(a), but most of the particles exhibited other structures such as hexagonal shapes. Applying SEM particle sizes of about 47 nm were measured for the same sample. This means SEM (not shown) measurement also gave comparable results with that of TEM, which is an indicative of



reliability and supporting evidence on the size of AuNPs in this sample. On the other hand, polyhedral AuNPs with an average particle size of  $3\pm 1$  nm and 12 nm were obtained using ST and SC, respectively, as shown in Fig. 9(f) and (b). In addition, strong reductants, such as IA and SB, have a noticeable influence on the morphology of the colloidal AuNPs as shown in Fig. 3.9(c) and 3.9(d). Most AuNPs produced using IA were spherical, tiny particles with an average diameter size of 38 nm, whereas SB produced wire-like networks with diameters of 11 nm. Moreover, SEM results are in line with TEM results as shown in Fig. App. 5.

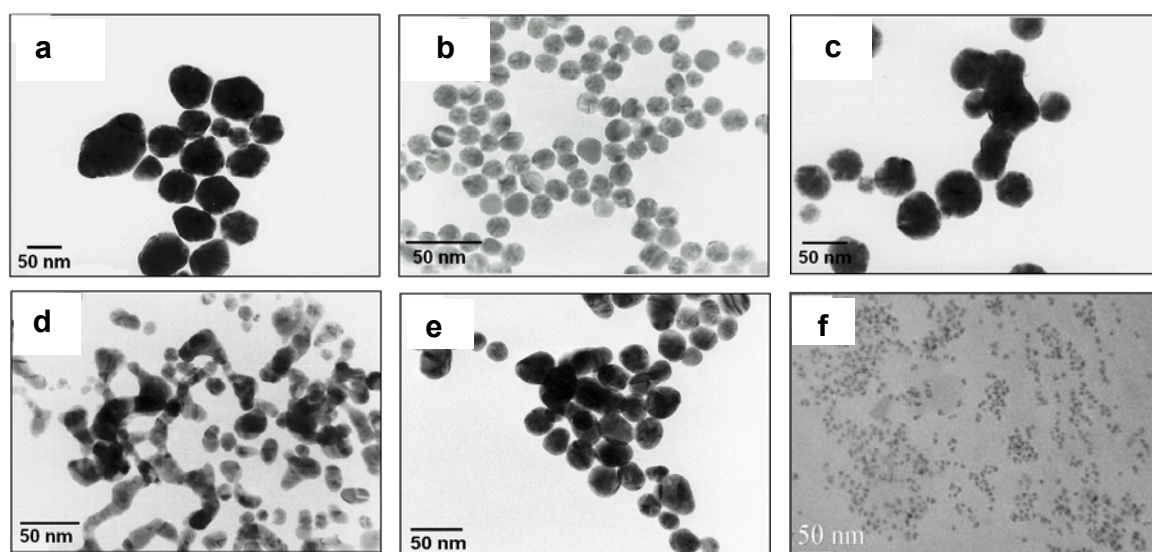


**Fig. 3.9.** Representative TEM images of colloidal AuNPs particles prepared by reduction of  $\text{HAuCl}_4$  solution using different reductant: (a) CA, (b) SC, (c) IA, (d) SB, (e) TA, (f) ST.

### 3.2.6. XRD and EDX analysis

Conclusive evidence for the formation of colloidal AuNPs prepared using SC (as a model) was also obtained from XRD and EDX analysis. The XRD patterns of the colloidal AuNPs prepared are presented in Fig. App. 6(a). XRD patterns showed two reflections at  $2\theta = 38.2$  and  $44.2$ , which can be assigned to Au (111) and (200) lattice planes, respectively. The crystallite size of AuNPs was also calculated according to the Scherrer Equation. The results revealed that crystallite sizes of 11 nm were observed at the final product. The other reflections located at  $2\theta = 26$ , 32, 45 and 56.5 correspond to NaCl (111), (200), (220) and (222) lattice planes, respectively. These reflections originate from NaCl formation through the interaction of sodium and chloride ions present in the reaction solution. In addition, an EDX spectrum was obtained from the same gold colloid sample as used for XRD. As shown in Fig. App. 6(b), it demonstrated the distinct presence of gold signals at 1.87, 2.12 keV (Au) and 9.89 keV (AuL). We also observed Cu peaks, which used to coat the AuNPs.

Table 3.1 gives an overview of the colloidal AuNPs sizes obtained with different reductants. In general, DLS measurements refer to the hydrodynamic diameter, whereas SEM and TEM are based upon the diameter of the Au core.

**Table 3.1.** Comparison of average size of AuNPs synthesized using different reducing agents (values are given in nm).

Reductant	UV-Vis	DLS	SEM	TEM	Reaction t.	Shape
CA	529	49	47	45	15 min	Multi
SC	527	13	12	12	50 min	Sphere
IA	520	42	40	38	6 sec	Sphere
SB	528	17	13	11	3 sec	Multi
TA	522	30	26	25	8 sec	Sphere
ST	no band	8	impossible	3	20 min	Sphere

### 3.3. Long-term stability of the colloidal AuNPs

The long-term stability of the colloidal AuNPs obtained was monitored over a longer time period by various techniques. The colloidal AuNPs were deliberately stored for this purpose in a closed glass vessel in dark environment. Afterwards, samples were taken at different pre-defined times (e.g. 2 days, 1 week, 4 weeks, and 8 weeks) and were analyzed by Zeta potential measurements, UV-Vis, DLS, and TEM to check the changes in Zeta potential values, SP bands, size distribution, morphology etc. The time-dependent changes using different reducing agents are described in the following section. Therefore, the resulting colloidal AuNPs in section 3.2 were examined with regard to monitor their stability. These experiments were realized in the absence of additional stabilizers. Table 3.2 provides information regarding the first examination of the fresh colloidal AuNPs samples using different methods.

**Table 3.2.** Results of long-term investigations: sizes of colloidal AuNPs

Reducing agents	Observation and Color		$\tau$ (day)	$\zeta$ (mV)	Peak <sub>max</sub>	Size of Au	
	fresh	storage			UV-Vis (nm)	DLS (nm)	TEM (nm)
CA	purple	+, no change	120	-39.0	529	49	45
IA	deep-red	-, colorless	2	-37.0	520	42	38
TA	light green	-, colorless	5 h	-17.4	522	30	25
SB	light red	±, no change	5	-38.4	528	17	12
SC	ruby-red	+, no change	90	-39.4	527	13	12
ST	yellow	±, no change	7	-28.3	no band	8	3

### 3.3.1. Optical observations

The formation of stable colloidal AuNPs was first checked optically by a color change and estimating the precipitation time ( $\tau$ ) (Table 3.2). Among of all reductants, CA and SC did not lead to any change in color nor appearance of agglomeration over a period of more than 3 months, while a precipitation of agglomerates using IA, SB and ST was observed after 2, 5 and 7 days, respectively. However, a precipitate from the colloidal AuNPs solution prepared using TA was observed within a few hours, which indicates instability. The color of the latter colloidal changed from colored to transparent. The colloidal AuNPs obtained by reduction using ST showed a short-term stability of 3 days.

### 3.3.2. Zeta potential measurements

The long-term stability of colloidal AuNPs was followed spectroscopically by zeta potential technique, which indicates the changes in surface charge with time. It has been long recognized that the zeta potential is a very good index of the magnitude of the interaction between colloidal particles and its measurement is widely used to control the stability of colloidal NPs. In case of colloidal particles having a large positive or negative zeta potential, these particles tend to repel each other and they do not show any disposition to come together. However, in case of low absolute zeta potential values, these particles aggregate and flocculate due to the absence of repulsive force which prevents such agglomeration. Zeta potential results ( $\zeta$ ) of the freshly prepared samples using different reductants are shown in Table 3.2. Fig. 3.10 depicts the changes on the zeta potential values of different colloidal AuNPs samples prepared using various reductants at definite points of storage time. We can clearly observe from this fig. that particles obtained using CA and SC were stable up to 14 days, and the zeta potential of these samples was relatively constant within this time frame. These nearly constant values of zeta potential indicate a long-term stability of the corresponding colloids, which could be due to the presence of citrate ions as stabilizers around the surface of AuNPs. On the other

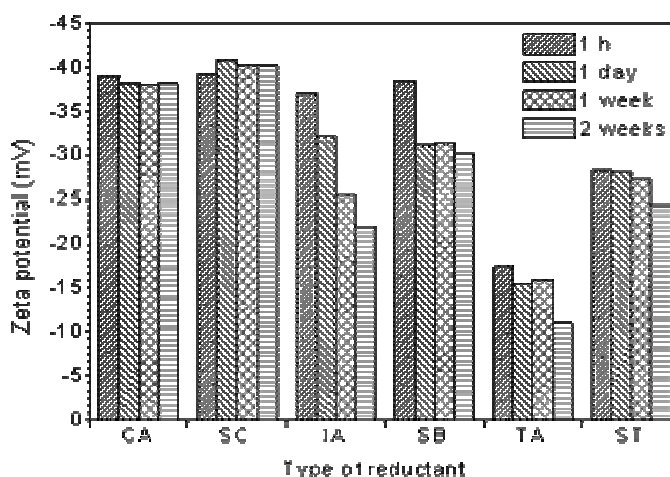


**Fig. 3.10.** Zeta potential of colloidal AuNPs prepared using CA, IA, TA, SB, SC and ST. The  $\zeta$  was recorded at different storage times.

hand, fresh colloidal AuNPs prepared using strong reducing agents (SB and IA) showed high zeta potential values, i.e. within -38.4 mV and -37.0 mV, respectively, which

dropped drastically to lower absolute values with time as shown in Fig. 3.10. In addition, the reduction using ST produced the smallest colloidal AuNPs with a zeta potential value of -28.3 mV. This value was constant up to 7 days and then it decreased to a value of -24.3 mV after 14 days. The reduction with TA resulted in the lowest value of zeta potential of -17 mV and produced unstable particles. These changes were found to be indications of instability, which were further confirmed by UV-Vis, DLS and TEM.

### 3.3.3. UV-Vis spectroscopy

UV-Vis absorption spectra have been proved to be quite sensitive to the formation of colloidal AuNPs due to their intense SP bands. It should be noted that the position of these bands are depended on different factors (e.g. size, shape, etc.) and also on the extent of colloidal aggregates [101,102,103]. Therefore, the stability of colloidal AuNPs can be also monitored by UV-Vis technique. It is well known that the typical SP band position of AuNPs is in the visible light region between 500 nm and 550 nm. Figs. App. 7(a-f) show the stability of colloidal AuNPs prepared using different reductants. Fig. App. 7(a) depicts UV-Vis spectra of the gold colloids prepared using CA, which in the range of 480-600 nm. It is noteworthy that no significant changes in the SP bands ( $530 \pm 1$  nm) could be observed even after 64 days. This observation indicates that no aggregation took place and hence the AuNPs formed using CA was quite stable within this period of time. However, the intensities of the absorption bands gradually increase with time, which might be due to an increase in the number of AuNPs. On the contrary, colloidal AuNPs synthesized by IA reduction did not form stable colloidal solutions, as could be proven with UV-Vis in Fig. App. 7(c). In this Fig., the SP band was broadened and red-shifted to longer wavelength maxima and finally it vanished completely in the sample (in 527-535 nm range), which was stored for 7 days onwards. In case of TA, the fresh prepared samples showed a SP band at 525 nm as can be seen in Fig. App. 7(e), which completely vanished the day after due to the huge agglomeration of Au particles. Moreover, the influence of SB as a reductant was tested on the stability of colloidal AuNPs and the results are given in Fig. App. 7(d). As expected, SB is not able to stabilize AuNPs, probably due to its stronger basic nature. If SC was used as a reducing agent, AuNPs did not show significant changes in the maximum wavelength of the SP band, but an increase of absorbance and of FWHM value was found after storage of 64 days, as shown in Fig. App. 7(b). The increasing of absorbance signifies the formation of new colloidal particles. These particles did not aggregate due to the presence of citrate ions, which caused repulsive forces and prevented aggregation. Furthermore, in case of ST, the UV-Vis spectra (Fig. App. 7(f)) of the samples taken after different storage time are not significantly different from each other after the first 2 days, indicating that changes of the average particle size might not be taken place. Notably,

these spectra indicate that the average particle size is below 5 nm since particle with particle sizes bigger than 5 nm would display sharp and intense SP band in the range of 500-550 nm [98]. However, 7 days afterward, UV-Vis spectra showed an appearance of a new shoulder of SP band at 530 nm. This might be pointed to the agglomeration of Au particles as long as we did not observe a SP in the earlier samples.

### 3.3.4. DLS investigations

In general, fine particles in the colloidal mixture were thermodynamically unstable due to the high energetic state. Therefore, these particles agglomerate to become thermodynamically stable by reducing their surface free energy if they are not hindered by stabilizing agents. In our study, particle size determined by DLS provides information on the size distribution of gold particles, which can aggregate in the colloidal mixture over time. Fig. 3.11 shows the average particle size of colloidal AuNPs prepared using various reductants at different storage time.

It is clear that the nature of reducing agent played a significant role with regard to size and stability of colloidal AuNPs. In case of CA and SC as reductant, DLS measurements showed more or less a constant size (ca. 50 nm and 14 nm, respectively) of AuNPs over a period of 64 days. However, a significant change on the average size of colloidal AuNPs was observed using IA and TA due to agglomeration of individual particles from 42 nm and 32 nm (freshly prepared) to reach approximately 950 nm and 980 nm, respectively, after the storage of 64 days.

Additionally, a slight increase in the average particle size was also observed with using SB and ST, where the particle size increased from 17 nm and 8 nm (an hour after preparation) to 51 nm and 63 nm (64 days later), respectively.

### 3.3.5. TEM study

The stability and the formation of aggregates caused by increasing the storage time can be also conveniently and more precisely confirmed by TEM, whose results are in good agreement with zeta potential, UV-Vis and DLS studies. Fig. App. 8 presents TEM images of colloidal AuNPs obtained using different reducing agents and the samples were taken from the colloidal solution stored for 8 h onward. We have also showed the

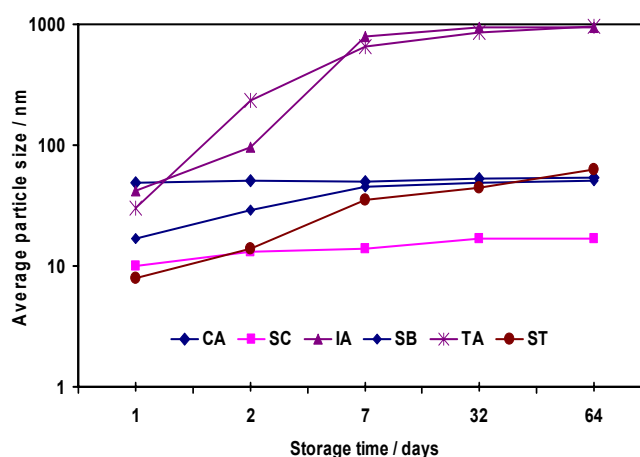


**Fig. 3.11.** Typical average particle size collected via DLS for colloidal AuNPs prepared using CA, IA, TA, SB, SC and ST, measured at various storage times.

TEM images of fresh samples for comparison (images F). The TEM image of the sample using CA and SC (Fig. App. 8(a) & (b)) gave corroborative evidence on the findings that CA- and SC-reduced gold colloids did not aggregate in solution, confirming the suitability of CA and SC not only as reducing agent but also as effective stabilizer. On the other hand, the particles aggregated with increasing ageing time and formed big clusters when the IA and TA was used as reductant. Such large areas of agglomeration of AuNPs could be seen Fig. App. 8(c) and e using IA and TA. As mentioned earlier, the reduction process of gold colloids using SB was finished within 3 sec, which is extremely fast. Hence, the network formed after 3 sec was immediately going to agglomerate to wire-like structures, which could be monitored by the broadening of the SP band and the TEM picture (Fig. App. 8(d)) confirmed the formation of Au nanowires networks. TEM imaging (Fig. App. 8(f), ST) further showed that in case of using ST, a significantly lower aggregation of Au particles was observed compared with IA and TA as reductants.

It can be concluded that weak reducing agents such as CA and SC showed a slow reaction rate with relatively good long-term stability of the prepared AuNPs in solution, whereas the stronger reducing agents like IA, TA and SB induced fast reaction rates with unstable particles. ST showed an insignificant change in the stability of AuNPs. In addition, the different coordinating abilities of such agents influenced notably the size, shape and dispersion of the AuNPs formed.

### **3.4. Effect of the reductants combination on the size and stability of AuNPs**

#### **3.4.1. Zeta potential measurements**

A part of this study is to investigate the effect of stabilizing agents (e.g. ligands) on the long-term stability of such colloidal AuNPs. The reduction of  $\text{HAuCl}_4$  solution using TA and ST in the presence of stabilizer (e.g., sodium citrate, polyvinylpyrrolidone (PVP), etc.) was taken as an example to attain our goal. We showed earlier in Table 3.2 that the stability of colloidal AuNPs using TA and ST as reductants in the absence of stabilizers was found to have poor zeta potentials (-17.4 and -28.3 mV). Fascinatingly, the combination (SC+TA) and (SC+ST) revealed not only for producing small particles but also for quite stable particles with a  $\zeta$  value of -32.4 and -38.3 mV. Therefore, it can be stated that the combination of two reducing agents has a clear positive influence on downsizing and stability of AuNPs. However, the possibility of appearance of other influencing factors such as i) repulsive electrostatic forces, which stabilize the particles, ii) attractive electrostatic forces between non-equivalent metal particles due to charge redistribution, iii) attractive size-dependent dispersive forces between identical particles,

iv) attractive dipole forces between in-plane magnetic or electric dipoles etc. cannot be ruled out. In addition, from chemical point of view it can be supposed that citric acid and/or citrate might be good chelating agents, their -OH and COO- groups are hard bases. Such compounds are well suited to trap and stabilize small colloidal particles. Otherwise, tannic acid as a very bulky molecule is not able to such effects; it rather seems that such compounds lead to immediate reduction due to large number of OH groups. As proven by the results wire-like materials were formed, no spherical-like particles were seen. Nevertheless, the combination of a strong fast reductant such as TA with a small particle stabilizer such as SC seems to be successful for formation of small and stable particles. However, further studies are necessary to clarify these aspects more in detail. Fig. 3.14 represents the changes in the zeta potential value of colloidal AuNPs in the presence of stabilizers at different storage time.

### 3.4.2. UV-Vis spectroscopy

UV-Vis results proved the stability of colloidal AuNPs in the presence of stabilizers as shown in Fig. App. 10(a &b). We clearly observed that the maximum peak position of the SP band was unchanged over the storage time when SC was used with TA, which verifies the effect of SC as stabilizer; whereas the SP band vanished with increasing storage time using TA alone, as shown earlier (Fig. App. 7(e)),. In case of ST, we showed earlier (Fig. App. 7(f)) that the UV-vis spectrum of colloidal AuNPs demonstrated their instability since a new band appeared which indicated the agglomeration of particles.

### 3.4.3. DLS investigations

Monitoring the stability of colloidal AuNPs formed using stabilizers was also followed by DLS (Fig. 3.15a and b, insert). The average size of the particles prepared with the mixture of TA with SC slightly increased from 9 nm to approximately 10 nm within 14 days, whereas using ST with SC particles gave 7 nm in size with no notable changes in the size of AuNPs after 14 days.

### 3.4.4. TEM study

TEM images confirmed that very stable colloidal AuNPs were obtained using the TA/SC or ST/SC combination. A typical TEM image of using TA and ST as reducing agents in the presence of SC can be seen in Fig. 3.12(a) and (b). No considerable change in size and morphology between the fresh and stored samples can be observed in both images. Therefore, we can conclude that the application of mixing these two reducing agents leads to an increase in the stability of gold particles in colloidal mixture compared to those prepared using single reductant, either with TA or ST.



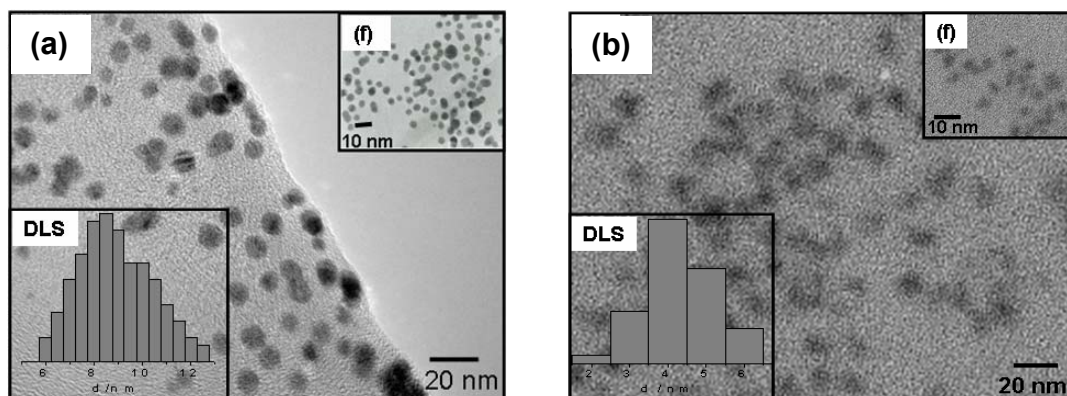


**Fig. 3.12.** TEM images of colloidal AuNPs synthesized (storage for 14 days) (a) using TA and (b) ST as reducing agent in the presence of SC. Images (e) show the fresh samples of AuNPs. The insets illustrate the size distribution histogram of the respective colloidal AuNPs achieved by DLS.

### 3.5. Formation growth mechanism of colloidal AuNPs

#### 3.5.1. Formation of colloidal AuNPs with sodium citrate

- Optical observation

The simultaneous mixing of  $\text{HAuCl}_4$  and SC solutions led to the formation of colloidal AuNPs by the appearance of the typical ruby-red color of the final slurry. During the course of AuNPs growth, a succession of color changes in the reaction solution was observed passing from pale yellow to colorless, grey, light blue, purple, ruby and finally to red (Fig. 3.13). No further change in the color was observed after 60 min of reduction indicating completion of reaction. The applied preparation method is similar to those reported previously [104] and their results should not be repeated here in detail.



**Fig. 3.13.** Color changes of the reaction solution during the course of colloidal AuNPs formation with SC as reducing agent.

- UV-Vis spectroscopy

UV-Vis spectroscopy was applied as an effective method to illustrate the evolution of metallic species during the formation of colloidal metal clusters [105]. Absorbance or wavelength of surface plasmon (SP) band provides information on particles size,



concentration, and dielectric medium properties [106,107], in general. Fig. 3.14 depicts the time-resolved UV-vis spectra obtained during the reduction of  $\text{HAuCl}_4$  with SC. The *in situ*-measurement of SP band during the origination of AuNPs certainly

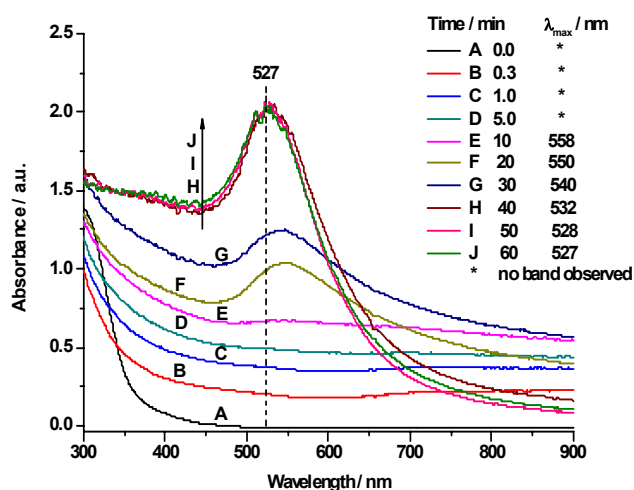


**Fig. 3.14.** Time-resolved UV-vis spectra during the reduction of 1.0 mM  $\text{HAuCl}_4$  solution with 15 mM SC solution at 60 °C.

provides useful information of assessing the reaction kinetics. Colloidal AuNPs are known to exhibit a strong absorption in the visible range (380-780 nm) and localized bands at 520-560 nm due to surface plasmon resonance, which is caused by collective oscillations of the conduction electrons upon excitation with visible light [108]. Mie first described the theoretical basis of this behavior [109]. Besides, changes in the wavelength and bandwidth of this SP band depend significantly on various factors such as particle size [102,110], shape [111],

dielectric environment [112], and the sign and size of the core charge [113,114]. The formation kinetics was followed by measuring changes in the absorption bands of resulting NPs at the maximum absorption wavelength ( $\lambda_{\text{max}}$ ). As reported elsewhere [98,115], the position of the absorption band of metal species strongly depends on the size and length of the nanoclusters.

- TEM study

Fig. 3.15 displays TEM images showing various steps involved during the course of AuNPs formation. Four main stages of AuNPs development were observed: (i) in the very initial stage (Figure 3.15(a), after 1 min, colorless solution), the formation of large nanocrystals having flower-like morphology was observed. Individual flower- or flake-like nanoclusters reached sizes between 80-100 nm with irregular shape. Such type of AuNPs shape has also been reported elsewhere [116]. This result undeniably supports the UV-vis results. At initial stages of reduction, large nanocrystals were formed, i.e. no clear SP bands could be detected in UV-Vis (see Fig. 3.15). (ii) Subsequently, wire-like networks with a smaller diameter ranging from 10-20 nm were observed when the reaction time was prolonged to 10 min (Fig. 3.15(b), light blue solution). These wire-like networks exhibited a face-centered cubic (fcc) lattice with distinct facets that mostly showed Au(200) lattice planes. However, such wire-like structures could not be verified

again with UV-vis (see Fig. 3.14) but some indirect hints from the spectra shape could be realized. Wang and co-workers [117] reported that the corresponding absorption band of gold nano-wires gave an extremely broadened band in the range of 650-1000 nm due to the longitudinal mode of the SP absorption and depending on the aspect ratio of the nanochains. Link and El-Sayed [118] also observed a strong longitudinal SP absorption band in the range of 700-1000 nm in the case of AuNPs with cylindrical shape and various aspect ratios. Nevertheless, no such bands were observed in the present experiments. (iii) When the reaction solution started becoming purple after 30 min, these nano-wires began to breakdown to form NPs with a diameter ranging from 12 to 16 nm (Fig. 3.15(c)). (iv) The final stage was observed after a period of 60 min where TEM images showed highly uniform NPs with an average diameter of 12 nm and a polyhedral, spherical-like morphology with obviously spherical-like particles exhibiting Au(111) and Au(200) lattice planes, as shown in Fig. 3.15(d). Interestingly, no further change in the morphology of the particles was observed after 60 min. The large aggregates of gold flower-like nanocrystals observed in the first stage may be later compartmentalized due to the absorption of citrate ions on the surface of the gold particles, which may effect a strong repelling layer preventing the NPs from coming into close contact and further growth [104,119]. Additionally, SEM results displayed similar information to those obtained from Tem as shown in Fig. App. 11.

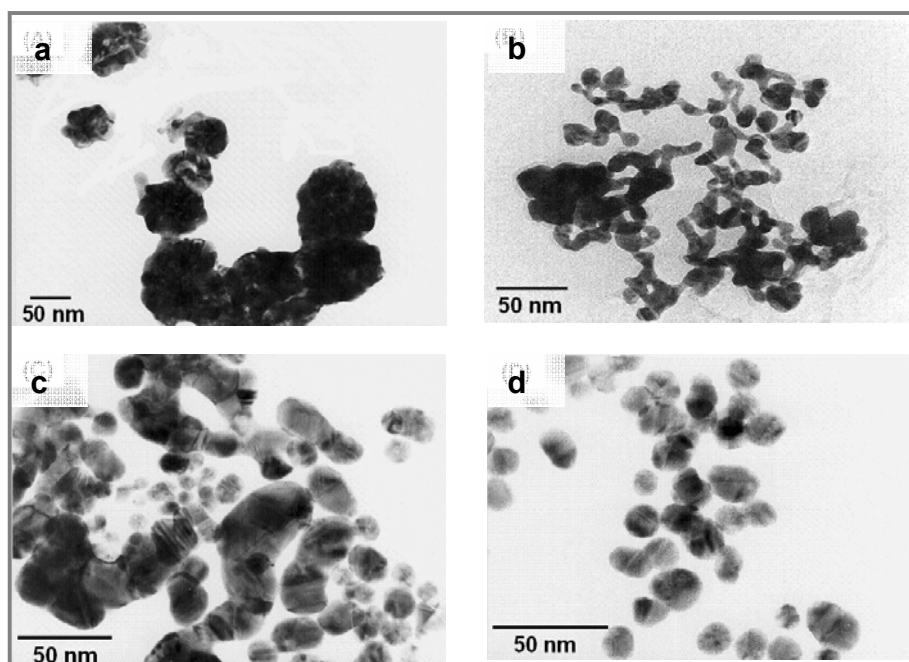


**Fig. 3.15.** TEM images taken during the formation of colloidal AuNPs obtained by reduction of 1.0 mM  $\text{HAuCl}_4$  solution with 15 mM SC solution at 60 °C and an  $[\text{Au}^{3+}]/[\text{SC}]$  ratio of 1:4 at reaction time of (a) 1 min, (b) 10 min, (c) 30 min, and (d) 60 min.

- XRD analysis

Conclusive evidence for the formation of colloidal AuNPs was also obtained from XRD analysis. The XRD patterns of the gold colloids are presented in Fig. 3.16. XRD patterns showed two reflections at  $2\theta = 38.2$  and  $44.2$ , which can be assigned to Au (111) and (200) lattice planes, respectively. Moreover, The crystallite size of AuNPs is calculated based on the Scherrer equation:  $t = 0.9\lambda / B \cos\theta$ , where  $t$  corresponds to the particle size in Å,  $\lambda$  is the X-ray wavelength,  $\theta$  is the Bragg angle, and  $B$  corresponds to the full width at half maximum (fwhm, in radians) of the peak under consideration. The results revealed that crystallite sizes of 20 nm, 12 nm and 11 nm were observed at different sampling times of 1 min, 10 min and 60 min, respectively. The other reflections located at  $2\theta = 26, 32, 45$  and  $56.5$  correspond to NaCl (111), (200), (220) and (222) lattice planes, respectively. These reflections originate from NaCl formation through the interaction of sodium and chloride ions present in the reaction solution. The unusual KCl pattern observed at  $2\theta = 28^\circ$  might be caused by an impurity of the reducing agent.

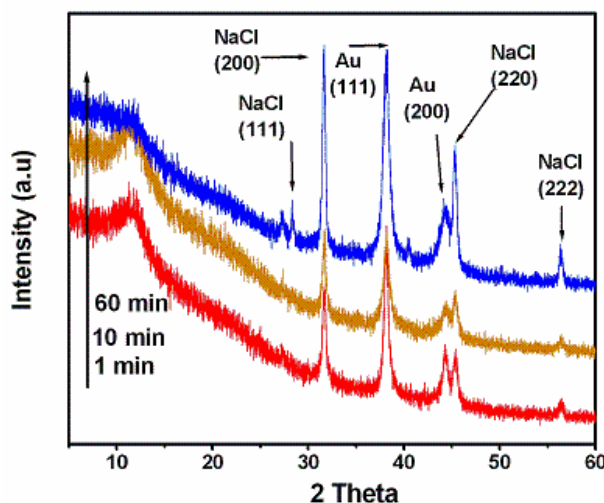


**Fig. 3.16.** XRD patterns of colloidal AuNPs using SC at different reaction time of 1, 10, and 60 min.

- DLS investigations

Supporting investigations regarding the formation of such colloidal AuNPs were also conducted using DLS technique, which provide a more direct measurement of colloidal AuNPs in solution. Fig. App. 12 portrays time-resolved size distribution curves recorded by DLS during the reduction of a  $\text{HAuCl}_4$  solution (1.0 mM) with SC (15 mM) over a period of 60 min. Initially, the average diameter of the gold cluster amounted to 220 nm immediately after the addition of SC to  $\text{HAuCl}_4$  solution. The most significant changes occurred during the first minute of the AuNPs formation where the average particle size decreased considerably from an initial value of 220 nm to 120 nm. When the reaction progressed, the average particle diameter rapidly decreased, indicating disaggregation of the Au nano-clusters flakes to a size of about 30 nm after 10 min. As the reaction progressed, the average particle size decreased from 30 to 25 nm after 20 min. Finally, the smallest AuNPs with an average size of ca.10 nm appeared after 60 min.

Interestingly, these small nanoparticles did not change further even after 2 hours of reaction time.

**Table 3.3.** Variation of average size of AuNPs at different time intervals during the reduction of HAuCl<sub>4</sub> with SC at 60 °C (process-I). <sup>a</sup>: maximum wavelength, <sup>b</sup>: particle size from XRD.

Time (min)	Color of solution	$\lambda_{\max}^a$	AuNPs Size (nm)		
			XRD <sup>b</sup>	DLS	TEM
1	colorless	no band	20	122	80-100
10	light blue	558	12	31	15-25
30	purple	540	n.d.	18	15-20
60	red	527	11	13	12

### 3.5.2. Formation of colloidal AuNPs with tannic acid

- Optical observation

Colloidal AuNPs were also synthesized using other type of single reducing agent such as tannic acid (TA). Fig. App. 13 shows a typical example of the variation of suspension color when the reductant was added to the gold chloride solution. Upon the addition of TA, the initial yellow solution became light blue within 2 sec indicating the first stage of the reduction. Subsequently, the solution turned from light blue to blue, which finally transferred to dark blue within 9 sec. No further change was observed afterwards, which indicates the completion of the reaction. In addition to the physical observation of color changes at different time intervals, the corresponding changes in the morphology and size distribution were also proven by various characterizations.

- UV-Vis spectroscopy

UV-vis spectra (Fig. App. 14) only reveal broad absorption behavior in the range from 500-900 nm that might point to the formation of large nanocrystals and/or nanowires. SP bands, actually appearing at ca. 520-560 nm were not seen probably due to the wire-like morphology of the particles. No further change in the spectrum was observed even after 9 sec.

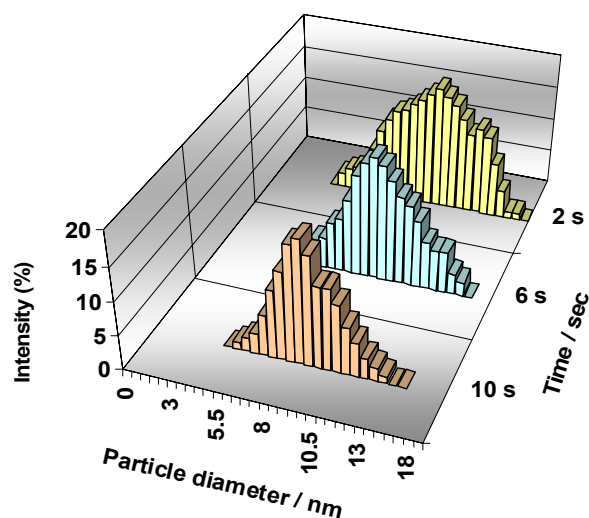
- TEM study

Fig. App. 15 depicts the corresponding TEM images confirming that gold particles are in nanowires shape. At the early stage (Fig. App. 15(a), after 2 sec, light blue solution), Au nanowires extended from a big nanostructure. After 5 sec (blue solution), a clear nanowires shape was observed with wire diameter of approximately 15-20 nm and up to some hundred nanometers in length as shown in Fig. App. 15(b). At final stage (Fig. App. 15(c), 9 sec, dark blue), large aggregates of Au nanowires were observed due to

an assumed instability of the parent structures. Afterwards, the nanowires network remained stable without changes after 5 min of reaction, which however still corresponded to the broad absorption spectrum. Interestingly, such nanowires structure was also discovered in the very early stage using SC as reductant (see Fig. 15b). Another interesting observation is that the formation process of colloidal AuNPs was extremely fast, which was completed within 9 sec.

- DLS investigations

Furthermore, the histogram obtained from DLS (Fig. 3.17) depicts the evolution of gold colloids of average sizes between 16 and 45 nm vs. reaction time. Another interesting observation is that the formation process of colloidal AuNPs using TA was extremely fast, which was completed within 9 sec. Such quick reduction is expected from the stronger nature of reducing agent. At first stage, a broad size distribution with an average particle size of 35 nm was recorded in the suspension. After that, the average size was slightly decreased from 35 to 31 nm.



**Fig. 3.17.** Time-resolved plot of the size distribution of colloidal AuNPs obtained by DLS. reaction conditions: 1.0 mM  $\text{HAuCl}_4$ , 15 mM TA, 60 °C,

The final stage showed a better distribution with average size of 27 nm.

### 3.5.3 Formation of colloidal AuNPs by combination of SC and TA

- Optical observation

The application of a mixture of SC+TA surprisingly caused an extremely faster reduction compared to SC while comparable time with that of TA was found. Some changes in the color of the solution were also observed as shown in Fig. App. 16. The light yellowish solution of starting materials turned to yellow-orange immediately after the addition of the mixture of SC+TA, which then turned to orange-red, and the final colloidal solution exhibited a ruby-red color within 10 sec. The stirring of the solution was continued for another 5 min, but no further change in color was observed.

- UV-Vis spectroscopy

The samples were also collected at different stages of reduction and characterized by UV-vis, TEM and DLS techniques with a view to follow the growth steps. Fig. App. 17

shows the UV-vis spectra monitoring the formation of AuNPs at different reaction times. Interestingly, the maximum of SP band position was recorded in the region of around 520 nm (even after 2 sec), which is a characteristic for the formation of AuNPs. This result points to the fact that the formation of AuNPs with spherical-like morphology is occurring within the very first stage (2 sec). Moreover, this observation completely differs from the usage of any of single reducing agents. In the subsequent stages (6 and 10 sec), no considerable shift in the band position could be noticed.

- TEM observation

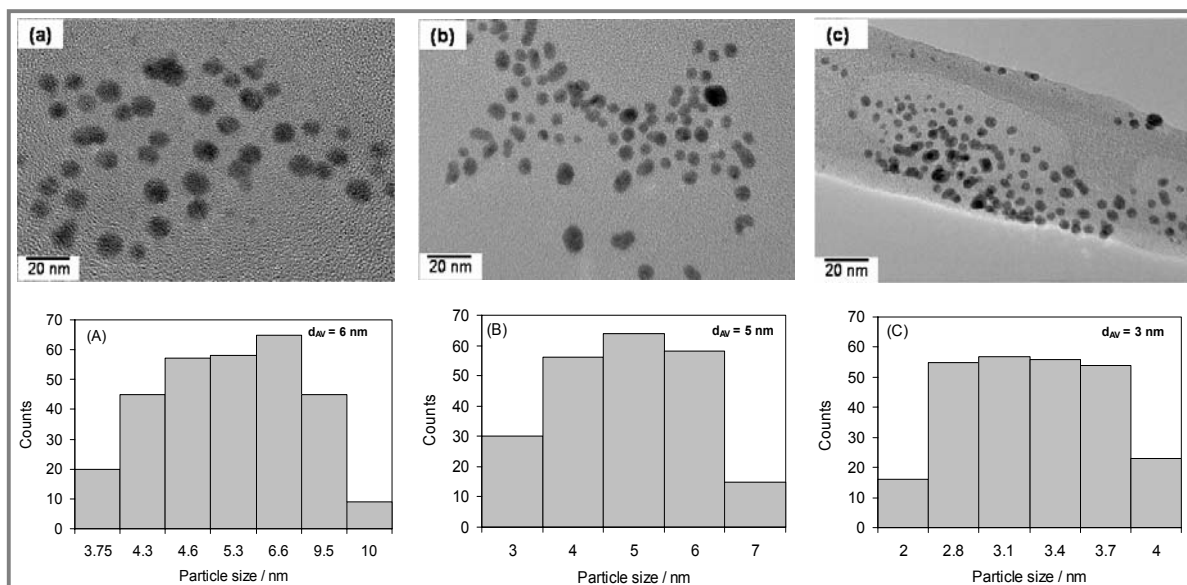


**Fig. 3.18.** TEM images taken during the formation of colloidal AuNPs obtained by reduction of 1.0 mM HAuCl<sub>4</sub> solution with 15 mM SC solution in the presence of TA at 60 °C and an [Au<sup>3+</sup>]/[SC] ratio of 1:4 at reaction time of (a) 2 sec, (b) 6 sec, (c) 10 sec.

Fig. 3.18 shows a time succession of TEM images. After 2 sec, monodispersed AuNPs were formed mostly with spherical-like morphology; however, a few percentages of particles with irregular shapes were also present (Fig. 3.18(a)). The particle size distribution revealed an average size of 6 to 7 nm. With increasing reaction time (6 sec), the average particle size slightly decreased to ca. 5 nm (Fig. 3.18(b)), and finally to ca. 3 nm after 10 sec (Fig. 3.18(c)). No further change whether in the morphology nor in the size of AuNPs was noticed by TEM even after 5 min, which further supports the results of UV-vis that the reaction was completed in short time (10 sec). However, it has to be noticed that larger error margins have to be taken into account due to such fast reduction. Nevertheless, this result proves that the usage of a combination of two reductants, i.e. SC and TA, leads to smaller particles compared to reactions using single reductants. Furthermore, it can be easily seen by independent characterization techniques that the application of two reductants reveal very small particles already in

first stage of the particle formation. In addition, all reported processes show larger particles in the beginning of the reduction vs. larger particles at the end of the respective process. The probable reason for obtaining different morphology of rather spherical-like particles in case of SC and TA+SC use vs. wire-like network might be due to differences in the charge and binding affinity of the reductants to colloidal mixture

- DLS investigations

The histogram (Fig. App. 18) shows the evolution of gold colloids of average sizes between 3.5 and 15 nm vs. reaction time. It can also be seen that the formation process of colloidal AuNPs was extremely fast, which was completed within 10 sec. Initially, after an addition of the SC+TA mixture to  $\text{Au}^{3+}$  solution, a broad size distribution with an average particle size of 11 nm was characterized in the suspension. After 6 sec, the average particle size slightly decreased to 9.5 nm with a more narrow size distribution, indicating that the most considerable change in this process was obtained. At final stage after 10 sec, the mean average size of AuNPs reached 8.5 nm with a very narrow size distribution. In addition, another sample was tested after 1 min but no further changes occurred.

**Table 3.5.** Variation of average size of AuNPs at different time intervals during the reduction process of  $\text{HAuCl}_4$  with combination of SC and TA at 60 °C (process-III).

Time (sec)	Color of solution	$\lambda_{\text{max}}^*$	AuNPs Size (nm)	
			DLS	TEM
2	yellow-orange	520	11.5	6.3
6	orange-red	521	9.5	4.9
10	ruby-red	521	8.5	3.2

Moreover, comparison of average size of AuNPs obtained from different techniques at different time intervals during the reduction process of  $\text{HAuCl}_4$  with reductant combination of SC and TA is presented in Table 3.6. Interestingly, all analytical methods gave complementary evidence and hence no significant change in the values of AuNPs size could be observed at various stages of reduction process. Furthermore, all applied techniques also showed similar tendencies but with certain variations on the absolute size of Au particles.

Based on the above results, the different steps involved in the formation processes of colloidal AuNPs, using a single reducing agent (process-I), (process-II), and a combination of two reducing agents (process-III), can be schematically depicted in Fig. 3.19. This imagination is mainly depending on the results from TEM analysis. In



comparison, processes I, II and III differ considerably in particle morphology as well as growth steps involved during AuNPs formation. Process-I shows three distinct particle shapes during the reduction steps, namely: large Au flower/flake-like nanocrystals (after 1 min), wire-like networks (after 10 min), and spherical Au particles (almost polyhedrons) after 60 min. Process-II gives different steps which includes some nanocrystals (after 2 sec), nanowires structures after 5 sec which then aggregated at the end of the reaction. However, such considerable differences in particle morphology were not found in case of process-III where the reduction was achieved in a single step and quickly. In addition, the color of colloidal suspensions colors was also found to depend upon the nature of reductant used.

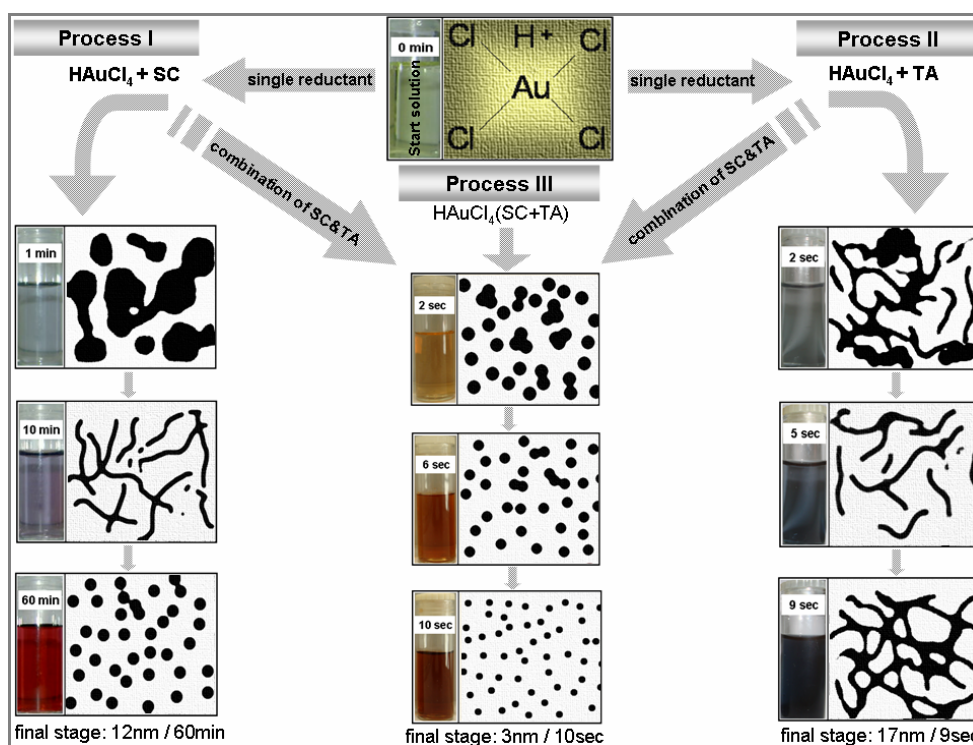


**Fig. 3.19.** Scheme of the formation mechanism of colloidal AuNPs in solution. Process I shows the different steps of AuNPs formation using single reductant. Process II represents the steps of AuNPs formation using a combination of two reductants.



---

## 4. Characterization of Supported, Promoted, Bimetallic and Spent Au Catalysts

---

*The as-prepared solid gold catalysts supported on different oxides carriers (CaO, MgO, ZrO<sub>2</sub>, TiO<sub>2</sub>, Al<sub>2</sub>O<sub>3</sub>) and also on their corresponding metal oxy-fluorides powders have been characterized by means of different techniques such as ICP, XRF, TGA, DTA, BET-SA, Pore size distribution, XRD, FTIR, HRTEM, EDX, SEM, XPS & solid state NMR and the results are presented in this chapter. In addition, the characterization results of bi-metallics, gold promoted vanadia solids and also some selected spent samples mainly from the group of supported catalysts are included in this chapter.*

---

## 4.1. Supported gold catalysts

### 4.1.1. XRF and ICP results

- Gold catalysts supported on different oxide carriers

The data shown in Table 4.1 compare the results of XRF and ICP measurements on the composition of supported catalysts. The results obtained XRF & ICP show some deviations. However, ICP is more reliable than XRF, which can also be realized by summing up the values of individual components present in the catalysts. In general, XRF results on Au loading showed somewhat higher values compared to ICP results. In contrast, ICP showed higher values for support contents compared to XRF. The contents of Na and Cl in case of MgO, CaO and ZrO<sub>2</sub> supports are found to be in higher concentration compared to TiO<sub>2</sub> and Al<sub>2</sub>O<sub>3</sub>. The nominal content of Au was 1 wt%, which is in good agreement with the estimated values.

**Table 4.1.** Comparison between XRF and ICP results for Au catalysts on different metal oxides.

Catalyst	Catalyst composition by XRF			Catalyst composition by ICP		
	Au	Support	Na <sup>+</sup> , Cl <sup>+</sup>	Au	Support	Na <sup>+</sup> , Cl <sup>+</sup>
Au/MgO	1.1	90.9	0.4	0.7	97.9	0.7
Au/CaO	1.1	95.8	0.3	0.8	97.8	0.6
Au/ZrO	1.2	95.6	0.4	0.9	98.6	0.6
Au/TiO <sub>2</sub>	1.1	95.8	0.1	0.9	98.8	0.1
Au/Al <sub>2</sub> O <sub>3</sub>	1.1	92.7	0.1	0.8	98.7	0.2

- Gold catalysts supported on metal oxy-fluorides

The Au catalysts supported on different oxy-fluorides carriers are also examined using XRF and ICP-OES methods. The data obtained are summarized in Table 4.2. The resulting values did differ considerably between the theoretical and the experimentally observed ones. Nevertheless, the most considerable observation is again the high concentration of Na<sup>+</sup> and Cl<sup>+</sup>, which in turn might affect the catalytic performance of the catalysts. Here also the nominal content of Au was fixed at 1 wt%.

**Table 4.2.** Comparison between XRF and ICP results for gold catalysts supported on different metal oxy-fluorides.

Catalyst	Catalyst composition by XRF			Catalyst composition by ICP		
	Au	Support	Na <sup>+</sup> , Cl <sup>+</sup>	Au	Support	Na <sup>+</sup> , Cl <sup>+</sup>
Au/MgF <sub>2-x</sub> (OH) <sub>x</sub>	1.0	95.9	1.1	0.6	97.9	1.4
Au/CaF <sub>2-x</sub> (OH) <sub>x</sub>	0.9	95.8	1.2	0.7	97.8	1.1
Au/ZrF <sub>4-x</sub> (OH) <sub>x</sub>	1.3	95.6	1.2	0.6	98.6	1.4
Au/TiF <sub>4-x</sub> (OH) <sub>x</sub>	1.1	95.8	1.3	0.9	98.8	1.3
Au/AlF <sub>3-x</sub> (OH) <sub>x</sub>	1.0	95.7	1.2	0.8	98.7	1.5

### 4.1.2. EDX analysis

The EDX results for the selected samples (Au/TiO<sub>2</sub> and Au/Al<sub>2</sub>O<sub>3</sub>) showed that these catalysts are composed of various elements (e.g. Au, support (Ti or Al), O and Cl). The electron beam of EDX apparatus hits merely on the surface of the catalysts, hence the results depend on the surface area struck by the electron beam. As shown in Fig. 4.1, expected elements appeared in EDX for the prepared catalyst. The biggest portion corresponds to the support (Ti or Al) as expected followed by gold. Such observation is also confirmed from the results of XRF and ICP. Some other elements present in the catalysts (e.g. C, Cl, etc.) are detected to be in very low amounts.

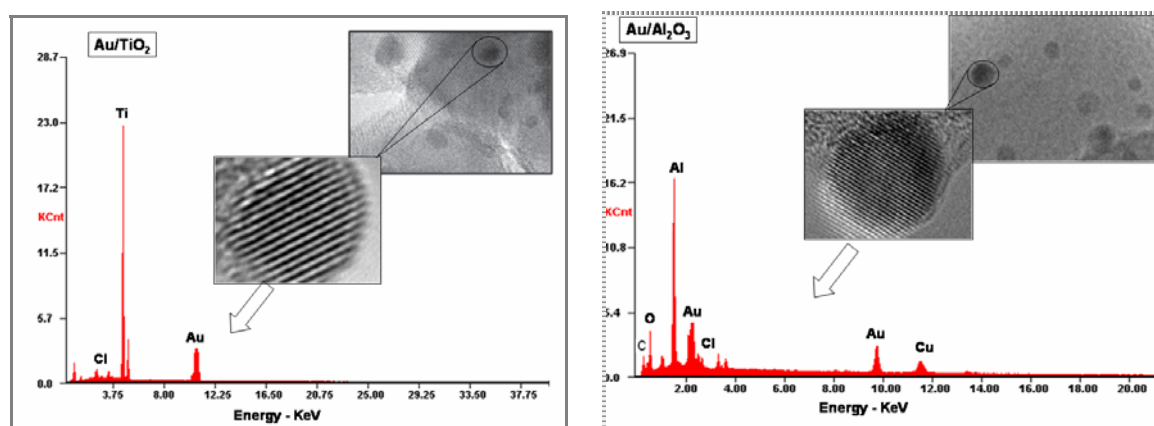


Fig. 4.1. EDX spectra of gold catalysts supported on TiO<sub>2</sub> and Al<sub>2</sub>O<sub>3</sub>.

### 4.1.3. Thermal analysis

The thermal analysis is used to examine the changes in thermal stability of gold catalysts, changes in phase composition and to determine the weight loss of the material upon heating. The total weight loss of gold catalysts upon the heating of samples in the range of temperature from 25 °C to 900 °C is studied.

#### TGA analysis

- Gold catalyst supported on oxide carriers

TGA plots of uncalcined Au catalysts supported on different metal oxides (e.g. MgO, CaO, ZrO<sub>2</sub>, TiO<sub>2</sub>, Al<sub>2</sub>O<sub>3</sub>, etc.) are presented in Fig. 4.2(a). It is clear from the figure that the stability of Au catalyst is depended on the nature of the supports used. It should be noted that the precursors of MgO and CaO are Mg(OH)<sub>2</sub> and Ca(OH)<sub>2</sub>. All the studied catalysts have shown that the weight loss mainly occurs in two stages. First stage occurred in the temperature range from r.t. to 150 °C, which is due to the loss of water molecules weakly bound to the material. Second stage observed between 150 and 350 °C, seems to be due to dehydroxylation and also to the decomposition of reducing

agents used. The weight loss observed on the whole temperature range from 5 to ~20%, which however depends on the type of support used. Among all catalysts, alumina supported one is losing weight continuously with rise in temperature, while all others except CaO supported one showed only a marginal weight loss in the temperature range from 350 to 900 °C. The sudden weight loss observed in case of MgO supported catalyst at around 330 °C can be attributed to the conversion of  $\text{Mg}(\text{OH})_2$  into MgO [120]. Interestingly, CaO supported solid displayed quite stable behavior up to ca. 630 °C and then showed abruptly ca. 20% wt. loss at this temperature. This is undeniably due to transformation of  $\text{Ca}(\text{OH})_2$  into CaO. Holgado et al. [121], also observed different stages of weight loss in case of  $\text{Ca}(\text{OH})_2$  decomposition to CaO, the first one at 323 °C (3% wt. loss) and the second one at 623 °C (wt. loss of 17%) and the third one at 880 °C (wt. loss of 7%). Our results are in good agreement with those reported by Holgado et al. [121]. In addition, AuNPs supported on reducible carriers (e.g.  $\text{ZrO}_2$ ,  $\text{TiO}_2$ ) are found to have the lowest weight loss in the whole temperature range among all investigated samples, which is about 6 and 11 %, respectively.

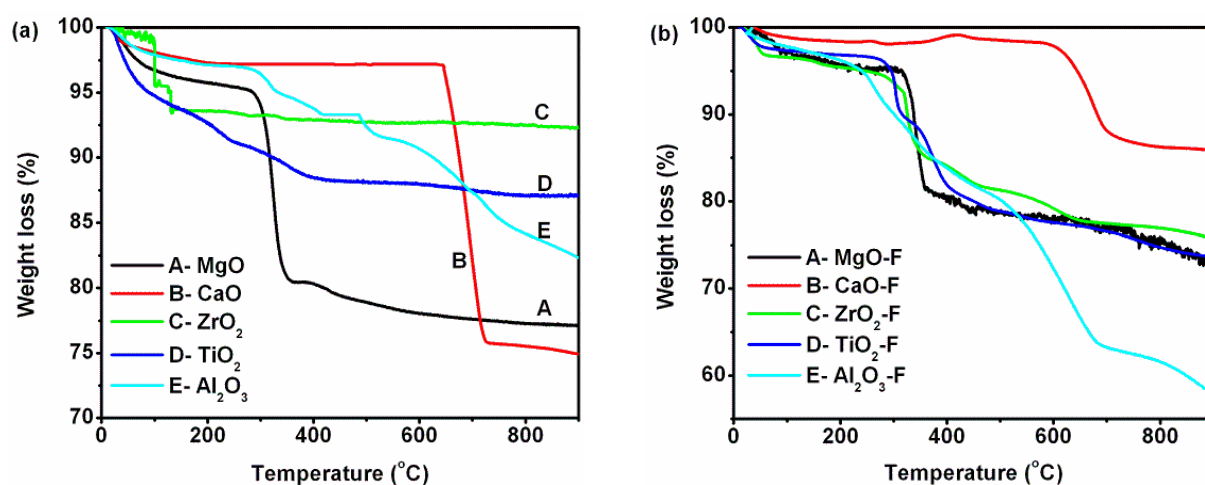


**Fig. 4.2.** TGA profiles of Au catalysts supported on different (a) metal oxide carriers and their corresponding (b) oxy-fluorides carriers.

- Gold catalyst supported on metal oxy-fluorides

Thermal analysis results of AuNPs supported on oxy-fluorides carriers are shown in Fig. 4.2(b). All catalysts showed slight weight loss ( $\leq 5\%$ ) up to 300 °C and then there is a sudden weight loss ( $\geq 15\%$ ) in almost all solids except  $\text{CaF}_{2-x}(\text{OH})_x$  supported one. It is evident that  $\text{Au}/\text{CaF}_{2-x}(\text{OH})_x$  displayed no significant weight loss even up to 600 °C. However the weight loss increased suddenly to 14 % (the lowest among all catalysts) when the temperature is further raised to 900 °C. The highest weight loss (40%) is

occurred for gold catalyst supported on  $\text{Al}_2\text{O}_3$ -oxy-fluorides. Nevertheless, a comparable weight loss ( $\sim 25\%$ ) is observed in the case of  $\text{Au}/\text{MgF}_{2-x}(\text{OH})_x$  and  $\text{Au}/\text{TiF}_{4-x}(\text{OH})_x$ . Interestingly, this weight loss for both solids is more or less occurred at the same temperature ( $\sim 300^\circ\text{C}$ ).

### DTA analysis

DTA detects the release or absorption of heat, which is associated with chemical and physical changes in materials as they are heated or cooled. Such information is necessary to understand the thermal properties of materials. DTA values are also measured in the same range as that of TGA (i.e.  $25^\circ\text{C}$  to  $900^\circ\text{C}$ ) under air atmosphere and the heating rate of temperature was  $10^\circ\text{C}/\text{min}$ .

- Gold catalyst supported on metal oxide

DTA patterns of the gold catalysts are given in Fig. 4.3(a). The initial weight loss observed by TGA for the all catalysts from  $20$  to  $300^\circ\text{C}$  are also evidenced by a small endothermic transition in the DTA curve. Such endothermic effect is observed from  $300$  to  $450^\circ\text{C}$  on the whole in almost all samples, which can be ascribed to the loss of water by dehydroxylation, decomposition of metal precursors to form oxides and also due to decomposition of organic reductants. Almost all catalysts, exhibited a broad exothermic peak in the range of  $470$  to ca.  $700^\circ\text{C}$ , which seems to be due phase transformation of supports (e.g.  $\text{TiO}_2$  (anatase) to  $\text{TiO}_2$  (rutile), monoclinic  $\text{ZrO}_2$  to tetragonal  $\text{ZrO}_2$  etc. It is also more likely that such exothermic peaks are due to the formation of metal oxide phase of the used support. XRD analysis of these also gave some supporting information on such assumption, which will be discussed later on.

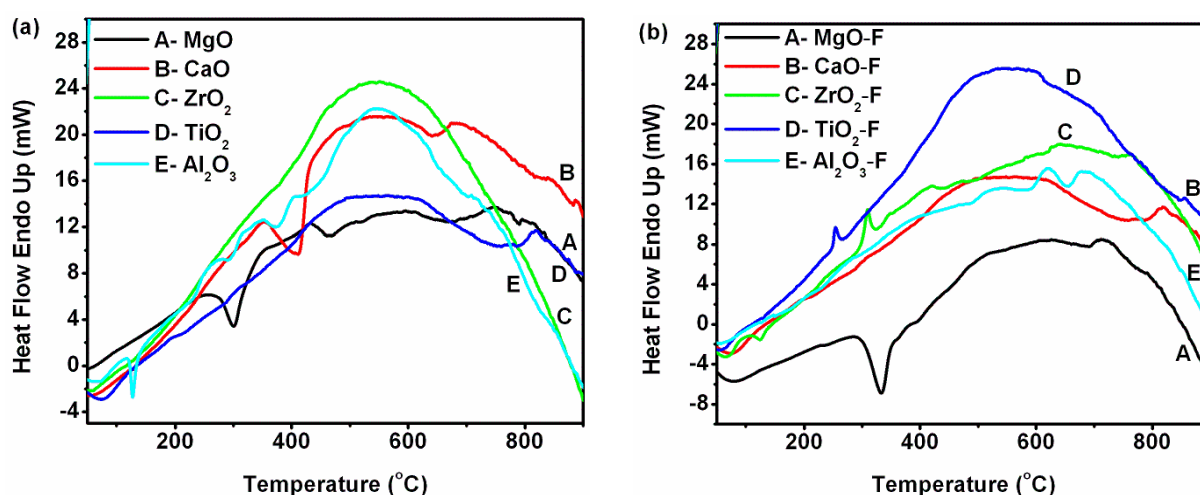


**Fig. 4.3.** DTA profiles of Au catalysts supported on different (a) metal oxide carriers and their corresponding (b) oxy-fluorides carriers.

- Gold catalyst supported on metal oxy-fluorides

Fig. 4.3(b) shows the DTA curves of the AuNPs supported over various metal oxy-fluorides powders. DTA curves of oxy-fluorides showed somewhat different patterns compared to the cases of metal oxides. In the temperature range of 250 to 350°C, the Ti- & Zr-O<sub>x</sub>-F solids showed exothermic effect, while Mg-O<sub>x</sub>-F displayed sharp endothermic effect. On the other hand, CaO<sub>x</sub>-F and Al-O<sub>x</sub>-F are silent in this temperature range and hence did not show any such effect. However, both type of supports showed a broad exothermic peak in the DTA pattern between 400 and 600 °C.

#### 4.1.4. Solid state NMR investigations

In NMR, magic angle spinning (MAS) is used for selected sample to determine the local environment of fluorine and aluminum species in the prepared catalysts. <sup>19</sup>F and <sup>27</sup>Al MAS NMR spectra are recorded at 202.32 MHz using an excitation pulse of 2.4 μs with 60 s repetition time.

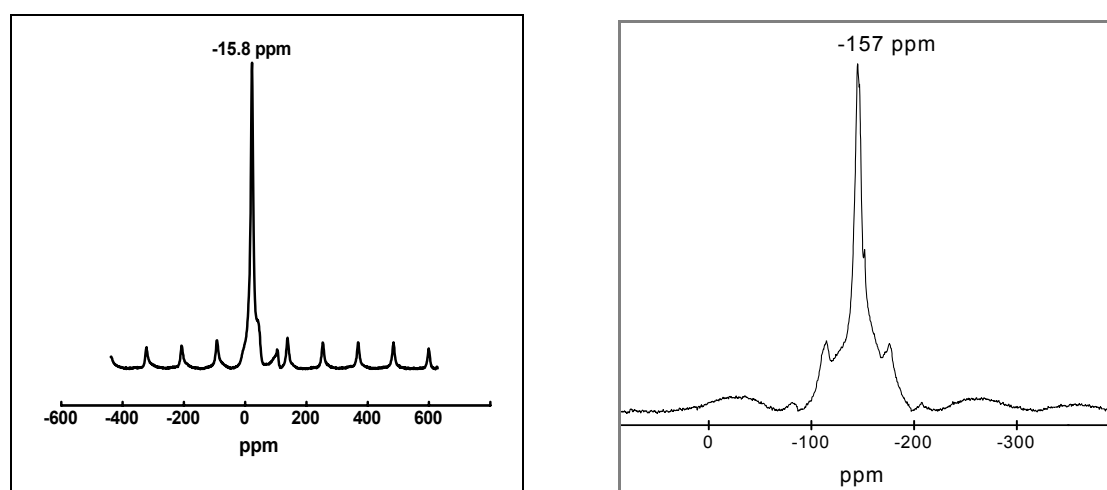


Fig. 4.4. <sup>19</sup>F (a) and <sup>27</sup>Al (b) MAS NMR of gold catalyst supported on aluminum oxy-fluoride.

#### <sup>27</sup>Al and <sup>19</sup>F MAS-NMR

The <sup>27</sup>Al and <sup>19</sup>F MAS NMR spectra of Au catalysts supported on fluorides carriers are shown in Fig. 4.4(a & b). It is reported elsewhere [122] that the chemical shift position of fluorine compound is found to be occurred at  $\delta_F = -172$  ppm and  $\delta_{Al} = -16$  ppm in <sup>19</sup>F and <sup>27</sup>Al MAS NMR spectroscopy, respectively. The spectra of our Au catalyst supported on aluminum oxy-fluoride showed the main signal at -157 ppm (Fig. 4.4(a)), which is consistent with an octahedral AlF<sub>6</sub> environment and also observed for amorphous and crystalline phases [123]. Moreover, the asymmetric line shapes of the

$^{27}\text{Al}$  peaks (Fig. 4.4 (b)) illustrate the contribution of  $^{27}\text{Al}$  quadruple parameters in the Au catalyst supported on Al-oxy-fluoride.

#### 4.1.5. BET surface areas

- Gold catalyst supported on metal oxides

The specific surface areas and pore volumes of different pure supports and gold catalysts supported on different metal oxides are presented in Table 4.3. It is clear from the table that the surface areas and pore volumes are observed to change significantly by changing the nature of support materials. It is obvious that the surface area of most supports were drastically decreased after impregnation into the AuNPs. Nevertheless, for both  $\text{TiO}_2$  and  $\text{Al}_2\text{O}_3$ , an addition of AuNPs did not show a noticeable effect on the values of BET surface areas. These results indicate that the AuNPs are highly dispersed on the support without any sintering effect. Such good dispersion is also confirmed by XRD and TEM, which will be shown later.

**Table 4.3.** BET-SA and pore volumes of gold catalysts on various oxide supports

Entry	Catalyst	BET-SA ( $\text{m}^2/\text{g}$ )		Pore vol. of cat. ( $\text{cm}^3/\text{g}$ )
		Pure Support	Catalyst	
1	Au/MgO	59	34	0.09
2	Au/CaO	37	27	0.07
3	Au/ZrO <sub>2</sub>	53	39	0.1
4	Au/TiO <sub>2</sub>	47	43	0.12
5	Au/Al <sub>2</sub> O <sub>3</sub>	265	261	0.80

- Gold catalyst supported on metal oxy-fluorides

The surface areas, pore volume of pure supports and the catalysts are presented in Table 4.4. BET surface areas of pure supports are varied in the range from 112 to 670  $\text{m}^2/\text{g}$ . However, the surface areas of these supports noticeably decreased after impregnation of Au followed by calcination. Such decrease is, however, depended on the type of support used. The Au/MgF<sub>2-x</sub>(OH)<sub>x</sub> catalyst showed the highest surface area and pore volume among all investigated catalysts.

**Table 4.4.** BET-SA and pore volumes of 1% gold catalysts on various oxy-fluoride supports.

Entry	Catalyst	BET-SA ( $\text{m}^2/\text{g}$ )		Pore vol. of cat. ( $\text{cm}^3/\text{g}$ )
		Support	Catalyst	
1	Au/MgF <sub>2-x</sub> (OH) <sub>x</sub>	670	364	0.61
2	Au/CaF <sub>2-x</sub> (OH) <sub>x</sub>	117	43	0.18
3	Au/ZrF <sub>4-x</sub> (OH) <sub>x</sub>	112	78	0.11
4	Au/TiF <sub>4-x</sub> (OH) <sub>x</sub>	175	106	0.19
5	Au/AlF <sub>3-x</sub> (OH) <sub>x</sub>	279	251	0.42

#### 4.1.6. XRD analysis

Catalysts studied by XRD were calcined at 350 °C for 5 h in air. It should be noted that XRD is not able to identify the gold signal, i.e. when very small Au crystallites (< 5nm) or amorphous phases are present. In addition, the strong sharp reflections indicate that relatively large particles feature in the support, whereas the broad reflections mean the Au size is relatively small.

- Gold catalyst supported on metal oxide

The XRD patterns of the fresh Au catalysts are displayed in Fig. 4.5(A). Different oxide supports have been used such as MgO, CaO, ZrO<sub>2</sub>, TiO<sub>2</sub> and Al<sub>2</sub>O<sub>3</sub>. In general, the XRD pattern of Au shows the typical diffraction pattern of metallic Au by the presence of two diffraction lines one at  $2\theta = 38.2^\circ$  ( $d = 2.35 \text{ \AA}$ ) and the other at  $2\theta = 43.4^\circ$  ( $d = 2.03 \text{ \AA}$ ). Among all studied catalysts, Al<sub>2</sub>O<sub>3</sub> powder supported Au catalysts is found to be X-ray amorphous, which is in agreement with BET surface area data (261 m<sup>2</sup>/g). The XRD of the fresh Au/TiO<sub>2</sub> sample also showed no patterns due to Au, indicating that the gold particle size is less than 3 nm or Au has been doped into TiO<sub>2</sub> lattice. This observation lent good support to the observations occurred by TEM that confirmed the size of Au found to be less than 3 nm. However, the sample reveals reflections that corresponding to TiO<sub>2</sub>. In contrast, the XRD results of the ZrO<sub>2</sub> supported Au catalysts showed that a weak reflections correspond Au phase besides the typical zirconia reflections (e.g. monoclinic phase). Moreover, gold catalysts supported on MgO and CaO exhibited the gold metal phases in addition to intense reflections that corresponding to MgO and CaO. Hints on the formation of bigger AuNPs are also provided by TEM and SEM.

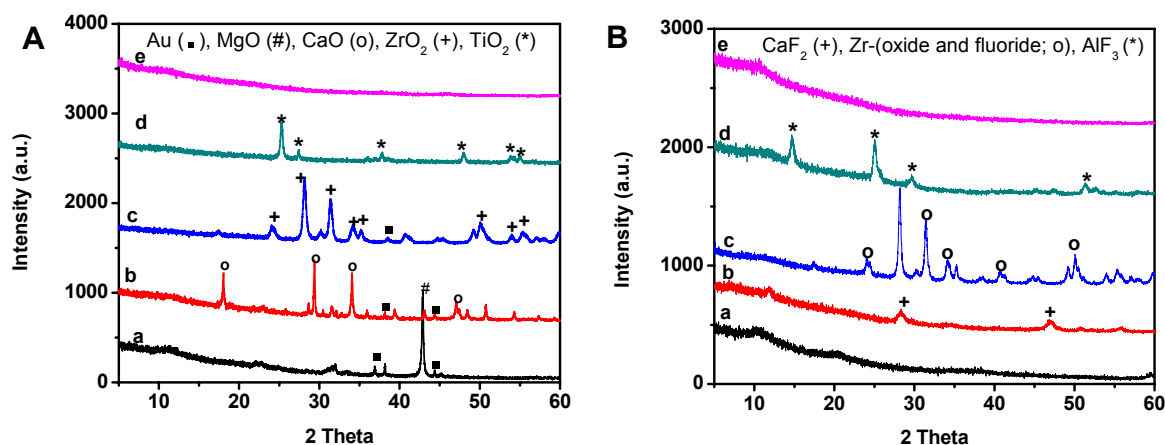


**Fig. 4.5.** XRD patterns of fresh 1% Au catalysts with different supports **A-** (a: MgO , b: CaO, c: ZrO<sub>2</sub>, d: TiO<sub>2</sub>, e: Al<sub>2</sub>O<sub>3</sub>); **B-** (a: MgO-F , b: CaO-F, c: ZrO<sub>2</sub>-F, d: TiO<sub>2</sub>-F, e: Al<sub>2</sub>O<sub>3</sub>-F).

- Gold catalyst supported on metal oxy-fluorides



XRD patterns of gold catalysts over metal oxy-fluorides are shown in Fig. 4.5(B). Unlike metal oxide supports, none of five oxy-fluoride supported solids showed reflections correspond to Au metallic phase, which gives indications that the crystallite size of Au in all these samples is < 5nm. It is also possible that the loading of gold metal was probably rather low to obtain large crystallites and for this reason, XRD did not identify their presence. Of all the five supports,  $\text{MgF}_{2-x}(\text{OH})_x$  and  $\text{TiF}_{4-x}(\text{OH})_x$  supported Au catalysts are completely X-ray amorphous probably due to their very high specific surface areas (see Table 4.4). However, in case of  $\text{Au}/\text{AlF}_{3-x}(\text{OH})_x$  catalyst, only a single phase of  $\text{AlF}_3$  was detected at  $2\theta = 16.8, 25.9, 29.9$  and  $52.1$ . On the other hand, XRD patterns of the materials showed the formation of mixed phases, i.e. two phases (oxy-fluoride and oxide phases) in the case of  $\text{CaF}_{2-x}(\text{OH})_x$  and  $\text{ZrF}_{4-x}(\text{OH})_x$  solids.

#### 4.1.7. XPS study

The summary of XPS results such as binding energy (B.E.), atomic ratios obtained from supported gold catalysts are given below in Table 4.5. It can be seen that the B.E. values of Au  $4f_{7/2}$  and  $4f_{5/2}$  spectral lines of Au are varied over a narrow range from 83.3 to 83.7 eV, and 87.4 to 87.6, respectively. These values clearly indicate that the gold in the catalysts is present mainly in metallic form, i.e. Au (0). This is good agreement with reported in the literature [124,125]. The most striking feature here is the clear enrichment of Au in the near-surface-region particularly in the  $\text{Au}/\text{TiO}_2$  solid compared to others as evidenced by the Au/metal ratios. The values of spectral lines correspond to other components of the catalysts, e.g. supports, O as well as C are also summarized for better comparison in Table 4.5. Furthermore, Au supported on metal-oxy fluoride catalysts were also characterized by XPS. However, these results are not shown here due to their poor performance in the investigated reactions.

**Table 4.5.** Binding energy and the surface atomic ratio of supported gold catalysts

Catalyst	Binding energy (eV)				Au/M atomic ratio
	Au ( $4f_{7/2}, 4f_{5/2}$ )	M	O	C	
Au/MgO	83.3,	458.8	531.5	286.9	0.009
	87.4	472.0	538.9	288.2	
Au/CaO	83.5,	350.5	534.4	285.2	0.008
	87.6		538.7	287.4	
Au/ZrO <sub>2</sub>	83.6,	182.2	529.8	285.3	0.011
	87.6	184.9	531.2	289.1	
Au/TiO <sub>2</sub>	83.4,	458.9	529.9	285.7	0.016
	87.6	472.0	532.5	289.2	
Au/Al <sub>2</sub> O <sub>3</sub>	83.7,	74.5	523.3	285.4	0.012
	87.6		531.1	288.3	

M: Ca, Mg, Zr, Ti and Al

#### 4.1.8. TEM study

- Gold catalyst supported on metal oxides

TEM studies were used to explore such properties since the catalytic activity of gold catalyst is strongly depended on its particle size. It reported the nature of the support can affect the size, morphology and dispersion of Au particles via metal-support interactions [e.g. 126]. Representative TEM images of Au catalysts supported on different metal oxides carriers (e.g. MgO, CaO, ZrO<sub>2</sub>, TiO<sub>2</sub>, Al<sub>2</sub>O<sub>3</sub>) are presented in Fig. 4.6. It is obvious that the resulting Au particles show almost spherical shape dispersed on the supports and the nature of support has considerable influence on the particle size. Hence, in order to check clearly such effect on the size of gold particles, the particle size distribution curves corresponding to the TEM images is given in the Fig. 4.6 (inset). Note that the size distribution was calculated using equation (2.4) by measuring more than hundred individual gold particles. Among all catalysts, TiO<sub>2</sub> and Al<sub>2</sub>O<sub>3</sub> carriers found to give particles size with a narrow size distribution in the range from 1-5 nm. However, in case of non-reducible supports (e.g. MgO, CaO), there is a considerable increase in the Au particles, which varies in the range from 1 to 10 nm, while the morphology of the particles remained unaltered. The sequence of increasing mean Au particle size for the gold catalysts supported on different carriers are Au/TiO<sub>2</sub> < Au/Al<sub>2</sub>O<sub>3</sub> < Au/ZrO<sub>2</sub> < Au/CaO < Au/MgO, suggests a dependency on the reducibility of the carrier. Nevertheless, in terms of activity, Au/TiO<sub>2</sub> and Au/Al<sub>2</sub>O<sub>3</sub> are found to be the best catalysts. Therefore, these supports are much considered in our discussion.

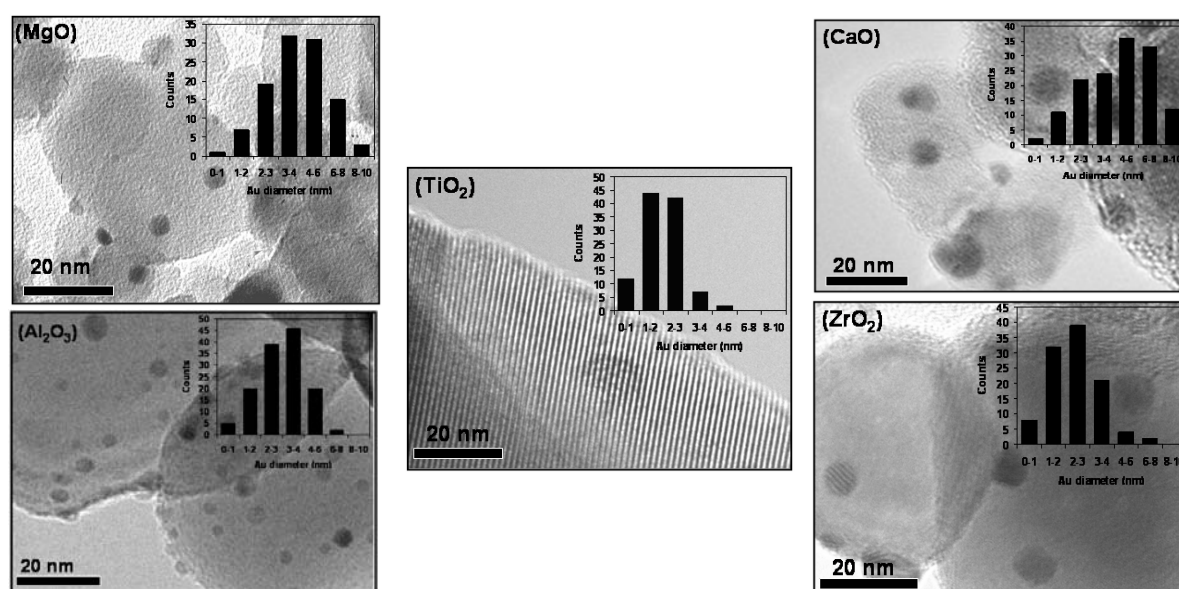


**Fig. 4.6.** TEM images of gold catalysts supported on different metal oxide carriers. The size distribution curves correspond to the TEM micrographs are presented in the insert.

- Gold catalysts supported on metal oxy-fluorides

We have previously showed that the particle size of AuNPs over different oxides carriers are depended on the nature of support used and the smallest Au particles obtained on Au/TiO<sub>2</sub>. For better comparison, the corresponding metal oxy-fluorides have also been used as novel supports for gold nanoparticles and such electron micrographs are shown in Fig. 4.7. It is clear from TEM images that there is a notable change in the gold particle size could be noticed when we shift from metal oxide to metal oxy-fluorides as support materials. To be brief, metal oxy-fluorides as carriers showed considerably bigger Au particles in the range from 4 to 15 nm compared to oxide carriers. The biggest Au particles were found in case of CaO-oxy-fluorides support, while the smallest one by Ti-oxy-fluoride. The activity and selectivity were found to be very much dependent on the size of Au particles, which will be discussed later on. Moreover, the shape of most of the gold particles in both types of carriers (oxides and oxy-fluorides) was found to be almost unchanged and remain relatively spherical. On the contrary, in few cases the oxy-fluorides as supports displayed irregular shapes of Au particles in addition to spherical ones, as shown in Fig. 4.7. Summarizing the TEM results, it can be stated that the nature of support showed a considerable effect on the size, shape and distribution of Au particles.

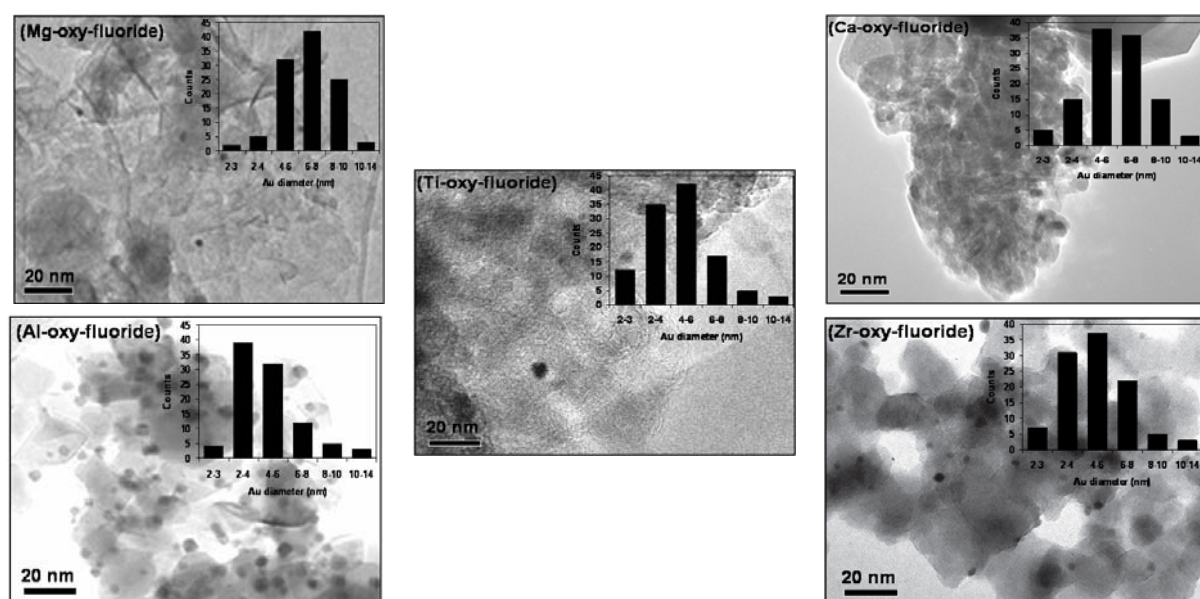


**Fig. 4.7.** TEM images of gold catalysts supported on different metal oxy-fluoride carriers. The curves correspond to the TEM micrographs are presented in the insert.

### High-resolution TEM

In order to control the nanocrystal shape of Au and further to understand the growth mechanism, high-resolution TEM (HRTEM) was performed. This technique has

provided us information regarding the nature of the crystal faces. HRTEM images of AuNPs supported on  $\text{TiO}_2$  and  $\text{Al}_2\text{O}_3$  are selected as examples and shown in Fig. 4.8a and 4.8b, respectively. These images obviously revealed that the metal particles are almost spherical and most of them are highly diffused into the matrix of the both supports. However, some of them are also located on the surface of the support. From HRTEM image of AuNPs supported on Au/ $\text{TiO}_2$  (a) and Au/ $\text{Al}_2\text{O}_3$  (b) solids, one can clearly observe the crystal planes of Au. The lattice plane fringes of the AuNPs are used to calculate the d-spacing values, and were compared with those of bulk Au (the values in Tables 4.5 and 4.6. correspond to images of Au/ $\text{TiO}_2$  and Au/ $\text{Al}_2\text{O}_3$  of Fig. 4.8), indicating the formation of Au nanocrystals with spherical lattice. These results confirmed that precursor of  $\text{HAuCl}_4$  was reduced to  $\text{Au}^0$ .

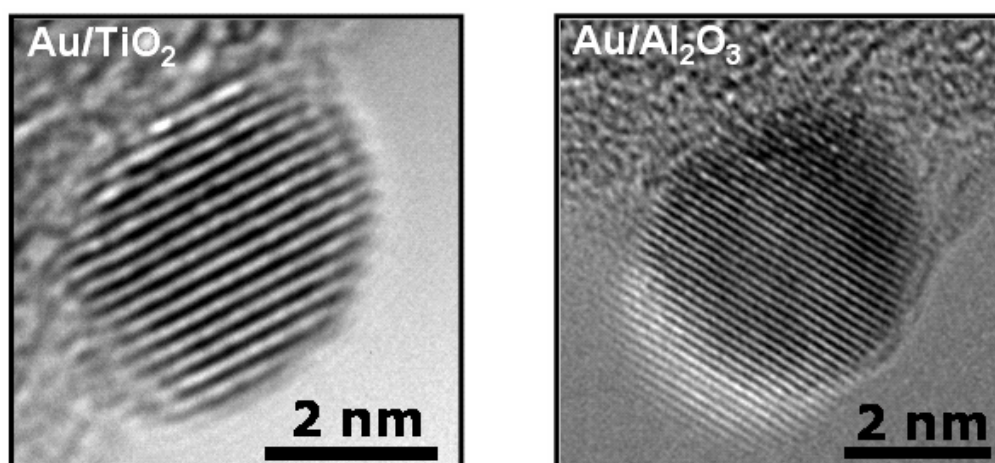


Fig. 4.8. HRTEM images of the AuNPs catalysts supported on  $\text{TiO}_2$  and  $\text{Al}_2\text{O}_3$  carriers.

**Table 4.5.** The inter planar spacing and diffraction planes of AuNPs supported on  $\text{TiO}_2$  carrier

d-spacing calculated from HRTEM, (Å)	d-spacing in bulk Au, (Å)	Miller indices ( <i>hkl</i> ) assignment
2.35	2.35	111
2.06	2.04	200
1.43	1.44	220
1.18	1.17	222

**Table 4.6.** The interplanar spacing and diffraction planes of AuNPs supported on  $\text{Al}_2\text{O}_3$  carrier

d-spacing calculated from HRTEM, (Å)	d-spacing in bulk Au, (Å)	Miller indices ( <i>hkl</i> ) assignment
2.38	2.35	111
1.41	1.44	220
1.16	1.17	222

### Other parameters calculated from TEM and XRD

It is possible to calculate the gold metallic surface area and metal dispersion of the catalysts from the TEM and XRD results. The results concerning such calculation of the gold-based catalysts with metal oxides and their corresponding oxy-fluorides were estimated based on the equations (2.3, 2.5 and 2.6); and summarized in Table 4.7 and 4.8. The metallic surface area of AuNPs over oxides carriers, which estimated from TEM varies between  $0.3 \text{ m}^2\text{g}^{-1}$  (Au/MgO) and  $1.1 \text{ m}^2\text{g}^{-1}$ , while from 0.2 and  $0.6 \text{ m}^2\text{g}^{-1}$  over their corresponding oxy-fluorides. It is also clear from Table 4.7 and 4.8 that there is a good agreement between the results obtained using TEM and XRD. However, one should note that these determinations made using both the techniques might be considered only as a relative measure of the metallic surface area of the catalysts. A dispersion of 45% was obtained for Au/TiO<sub>2</sub>, which considerably exceeds the estimated dispersion of Au/Al<sub>2</sub>O<sub>3</sub> (30 %). In some catalysts, XRD was not able to determine the particle size due to that contain very small gold crystallites, below the XRD detection limit (~3 nm) or the metal loading is very low. From, table 4.7, the largest metallic gold surface area calculated from the HRTEM measurements was found to be  $1.1 \text{ m}^2\text{g}^{-1}$  on AuTiO<sub>2</sub> catalyst. However, other samples, the Au metallic surface areas are relatively much smaller.

**Table 4.7.** AuNPs supported on oxide carriers characterization by means of ICP, XRD and HRTEM

Catalyst	Au (wt.%)	$d_{\text{Au}}$ (nm) <sup>a</sup>	$S_{\text{Au}}$ ( $\text{m}^2\text{g}^{-1}$ ) <sup>b</sup>	$d_{\text{Au}}$ (nm) <sup>c</sup>	$S_{\text{Au}}$ ( $\text{m}^2\text{g}^{-1}$ ) <sup>d</sup>	$d_{\text{Au}}$ (%) <sup>e</sup>
Au/MgO	0.7	5.9	0.3	4.7	0.4	16.9
Au/CaO	0.8	7.1	0.3	5.7	0.4	14.0
Au/ZrO	0.9	3.9	0.6	3.9	0.6	25.6
Au/TiO <sub>2</sub>	0.9	2.2	1.1	amorphous	n.d.	45.4
Au/Al <sub>2</sub> O <sub>3</sub>	0.8	3.1	0.7	amorphous	n.d.	30.3

<sup>a</sup>: mean diameter of Au particles, HRTEM; <sup>b</sup>: Au surface area, HRTEM; <sup>c</sup>: mean diameter of Au particles, XRD; <sup>d</sup>: Au surface area, XRD; <sup>e</sup>: Au dispersion, HRTEM; nd.: not determined.

**Table 4.8:** AuNPs supported on oxy-fluoride carriers characterization by means of ICP, XRD and HRTEM

Catalyst	Au (wt.%)	$d_{\text{Au}}$ (nm) <sup>a</sup>	$S_{\text{Au}}$ ( $\text{m}^2\text{g}^{-1}$ ) <sup>a</sup>	$d_{\text{Au}}$ (nm) <sup>b</sup>	$S_{\text{Au}}$ ( $\text{m}^2\text{g}^{-1}$ ) <sup>b</sup>	$d_{\text{Au}}$ (%)
Au/MgF <sub>2-x</sub> (OH) <sub>x</sub>	0.6	8.1	0.2	n.d.	n.d.	12.3
Au/CaF <sub>2-x</sub> (OH) <sub>x</sub>	0.7	7.6	0.23	n.d.	n.d.	13.1
Au/ZrF <sub>4-x</sub> (OH) <sub>x</sub>	0.6	6.3	0.24	4.3	0.2	15.9
Au/TiF <sub>4-x</sub> (OH) <sub>x</sub>	0.9	4.1	0.6	n.d.	n.d.	24.4
Au/AlF <sub>3-x</sub> (OH) <sub>x</sub>	0.8	4.3	0.5	n.d.	n.d.	23.2

<sup>a</sup>: mean diameter of Au particles, HRTEM; <sup>b</sup>: Au surface area, HRTEM; <sup>c</sup>: mean diameter of Au particles, XRD; <sup>d</sup>: Au surface area, XRD; <sup>e</sup>: Au dispersion, HRTEM; nd.: not determined.

### 4.1.9. SEM study

To understand the surface morphology and to provide more information about the dispersion of AuNPs over the different oxide and oxy-fluorides supports, SEM investigation was performed on various samples calcined at 350 °C. We have showed earlier that the AuNPs supported on oxide carriers gave small Au particles of less than 5 nm. However, the lower resolution of SEM compared to TEM is main reason to select catalysts having the particle size bigger than 5 nm. Therefore, AuNPs supported on the different metal carriers are selected (MgO, CaO, TiO<sub>2</sub>, ZrO<sub>2</sub>, Al<sub>2</sub>O<sub>3</sub>) as shown in Fig. App. 19. It should be noted that SEM results are usually showed bigger particles compared to TEM results for the similar samples. The analyses showed that there were also some differences in the morphologies of the samples. In general, most of the examined contain agglomerations of irregular-shaped crystals. SEM images showed the formation of agglomerates with various dimensions.

## 4.2. Characterization studies of promoted gold catalysts

### 4.2.1. XRF and ICP results

Table 4.9 presents the data of XRF and ICP-OES results of different gold promoted vanadia catalysts. In addition, gold alone and V<sub>2</sub>O<sub>5</sub> alone supported on TiO<sub>2</sub> are also given. It should be noted that the nominal values of Au and V<sub>2</sub>O<sub>5</sub> are fixed at 1 wt% and 10 wt%, respectively. It can be seen that the content of V<sub>2</sub>O<sub>5</sub> in all the catalysts estimated from ICP is slightly higher than the ones from XRF. On the other hand, the content of Au is marginally higher in XRF analysis than ICP. Nevertheless, the values are within error margins. The presence of small amounts of NaCl from both the techniques gives hints that some residues from HAuCl<sub>4</sub> precursor and sod-citrate reductant are still remained in the catalysts even after calcination.

**Table 4.9.** Comparison between XRF and ICP results of selected promoted V<sub>2</sub>O<sub>5</sub>-Au catalysts.

Catalyst (1 wt% Au)	Catalyst composition by XRF			Catalyst composition by ICP		
	Au	V <sub>2</sub> O <sub>5</sub>	Na <sup>+</sup> , Cl <sup>+</sup>	Au	V <sub>2</sub> O <sub>5</sub>	Na <sup>+</sup> , Cl <sup>+</sup>
AuV <sub>2</sub> O <sub>5</sub> /CaO	1.1	7	1.4	0.8	8.5	0.6
AuV <sub>2</sub> O <sub>5</sub> /Al <sub>2</sub> O <sub>3</sub>	1.2	7.5	1.6	0.7	9	0.2
AuV <sub>2</sub> O <sub>5</sub> /AlF <sub>3-x</sub> (OH) <sub>x</sub>	0.8	8	1.5	0.8	9	1.4
AuV <sub>2</sub> O <sub>5</sub> /TiO <sub>2</sub>	1.1	9	1.1	0.9	10.5	1.3
Au/TiO <sub>2</sub>	1.0	-	1.2	0.9	-	0.1
V <sub>2</sub> O <sub>5</sub> /TiO <sub>2</sub>		8	-	-	9	-



### 4.2.2. XRD analysis

From XRD results (Fig. 4.9), it is surprising to note that no reflections correspond to  $V_2O_5$  are present in any of these samples. This fact shows that the 10 wt%  $V_2O_5$  used during preparation seems to be X-ray amorphous. Similarly, no gold reflections can be seen, as expected. In other words, neither crystalline  $V_2O_5$  nor crystalline Au is present in these solids, probably they are finely dispersed on the surface of the supports. However, intense reflections correspond to supports except Alumina could be observed.  $Al_2O_3$  has shown very weak reflections due to small crystallite size and high surface area.

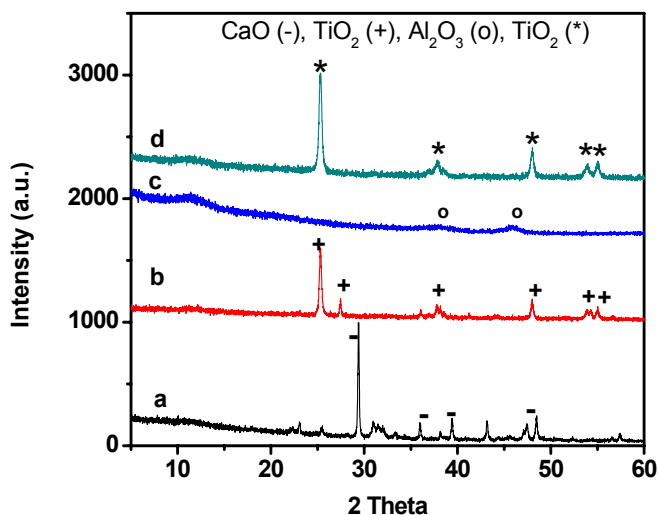


**Fig. 4.9.** XRD patterns of fresh promoted gold catalyst ( $Au-V_2O_5$ ) with different supports (a:CaO, b:  $TiO_2$ , c:  $Al_2O_3$ , d:  $V_2O_5/TiO_2$ ).

### 4.2.3. BET surface areas

Among several promoted  $V_2O_5$ -Au catalysts, four catalysts have been selected based on their catalytic activity and the surface areas estimated from these samples are presented in Table 4.10. It is clear from the Table that after the impregnation of vanadia to the supported gold catalysts, the BET surface area are decreased, as expected. Such decrease more prominent in the case of  $Al_2O_3$  supported catalyst. For better comparison of surface areas of different types of gold catalysts, one may check Tables 4.3, 4.4 and 4.10. It should be noted that, for ammoxidation reactions, somewhat low surface area catalysts (50 to 100  $m^2/g$ ) are preferred to minimize the development of hot spots and run away temperatures during the course of reaction.

**Table 4.10.** BET-SA and pore volumes of gold-vanadia catalysts on different supports.

Catalyst	Au content (wt.%)	$V_2O_5$ content (wt.%)	BET-SA ( $m^2/g$ )	$VO_x$ surface density ( $nm^{-2}$ )
$AuV_2O_5/CaO$	0.8	8.5	22	2.3
$AuV_2O_5/Al_2O_3$	0.7	9	178	3.0
$AuV_2O_5/AlF_{3-x}(OH)_x$	0.8	8	145	3.3
$AuV_2O_5/TiO_2$	0.9	10.5	40	1.5
$Au/TiO_2$	0.9	-	43	-
$V_2O_5/TiO_2$	-	9	37	1.2

#### 4.2.4. TEM and EDX studies

The TEM/EDX images of promoted gold catalysts by vanadia are shown in Fig. 4.10. It is clear from this Fig. that the surface of  $V_2O_5$ -Au catalysts are remarkably dependent on the metal oxide support material. For un-promoted catalysts, the X-ray and TEM data pointed to an average gold particle size below 5 nm and a uniform deposition of gold on the supports (Fig. 4.6, Au/TiO<sub>2</sub>). However, notable changes on the gold catalysts are observed with vanadia addition in case of using CaO as carrier. Particularly, the morphology and the dispersion of AuNPs on the supports are relatively not homogeneously dispersed with some varying shapes. Interestingly, a notable change in the size of Au particles has been noted after deposition of vanadia into the supported Au catalysts (e.g. Au/TiO<sub>2</sub> and Au/Al<sub>2</sub>O<sub>3</sub>). Among all catalysts, vanadia-gold catalyst supported over CaO showed a kind of agglomeration (Fig. 4.10(a)). Vanadia nanostructured particles are observed to have different shapes (e.g. nanorods, needles etc.), which have typical lengths of about 20 nm and diameters ranging from 1 to 4 nm (Fig.4.10(d)). The corresponding EDX analysis of TEM images is shown in Fig. 4.10 (insert Figs.) and confirmed the expected composition of the catalysts.

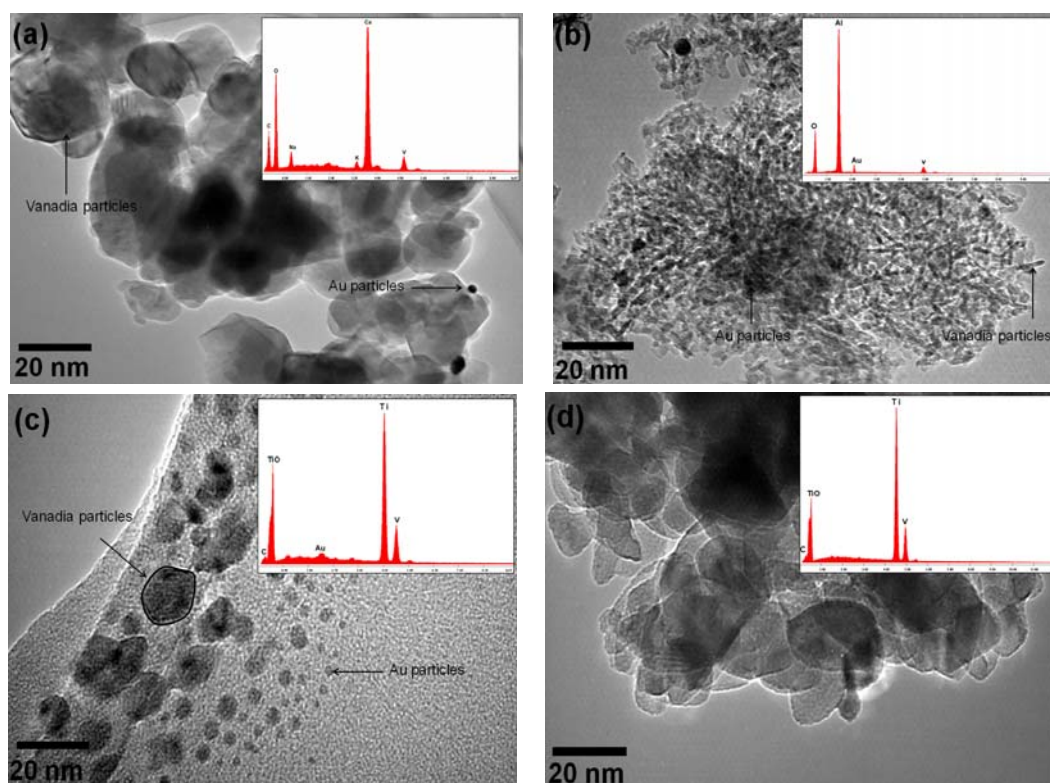


**Fig. 4.10.** TEM images and EDX-(insert) results of different catalysts Au- $V_2O_5$ /CaO-(a), Au- $V_2O_5$ /Al<sub>2</sub>O<sub>3</sub>-(b), Au- $V_2O_5$ /TiO<sub>2</sub>-(c),  $V_2O_5$ /TiO<sub>2</sub>-(d).



### 4.3. Characterization studies of bi-metallic catalysts

Gold nanoparticles supported on TiO<sub>2</sub> are found to be the best catalysts among all tested catalysts in terms of catalytic activity. Therefore, this catalyst containing other metals (e.g. Pd, Ag) has been selected for further studies.

#### 4.3.1. BET surface areas and ICP results of bi-metallic

Gold-(Pd or Ag) bimetallic catalysts loaded on different supports (TiO<sub>2</sub>, CeO<sub>2</sub>, and ZnO) are studied with the same metal contents, i.e. 1 wt % Au and 1 wt% second metal. BET-SA, pore volumes and ICP values of these catalysts are presented in Table 4.11. As shown in this table, nominal and actual loading of bimetallic catalysts showed comparable values. The surface area and pore volumes are varied in the range from 14 to 38 m<sup>2</sup>/g depending upon the nature of metal carriers. Of all the three carriers used, the surface area of the TiO<sub>2</sub> supported bimetallic catalysts (Au/Pd and Au/Ag) showed the high surface area and pore volume compared to all other catalysts.

**Table 4.11.** BET and ICP results of Au-bimetallic (1 wt% each) catalysts over different carriers.

Bimetallic catalyst	Catalysts composition (ICP)			BET-SA (m <sup>2</sup> /g)	Pore volume (cm <sup>3</sup> /g)
	Au	Pd / Ag	Cl		
Au-Pd / TiO <sub>2</sub>	1.1	1.2	0.2	38.2	0.071
Au-Ag / TiO <sub>2</sub>	1.2	1.2	0.1	31.1	0.057
Au-Pd / CeO <sub>2</sub>	0.9	0.8	0.4	14.2	0.012
Au-Pd / ZnO	0.9	1.0	0.3	28.3	0.051

#### 4.3.2. XRD analysis

The XRD patterns of the bimetallic catalysts are shown in Fig. 4.11. Of all the four catalysts, only in the TiO<sub>2</sub> supported 1%Au-1%Ag catalyst, showed very weak reflections correspond Au metallic phase can be seen besides the typical anatase reflections. In contrast, Au-Pd catalysts supported on TiO<sub>2</sub>, CeO<sub>2</sub> and ZnO did not show any reflections corrected to either Au or Ag metallic phases. This result

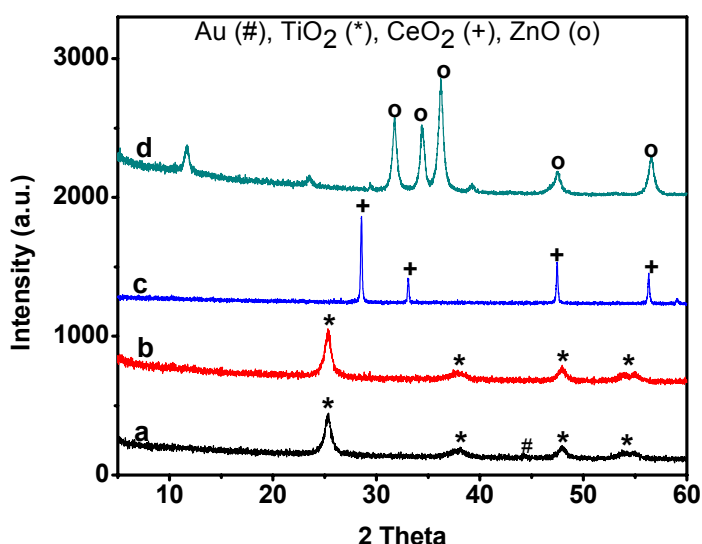


**Fig. 4.11.** XRD patterns of different bimetallic (a: AuAg/TiO<sub>2</sub>, b: AuPd/TiO<sub>2</sub>, c: AuPd/CeO<sub>2</sub>, d: AuPd/ZnO).

suggests that the metallic particle size of the prepared catalysts seemed to be too small to be detected by XRD. Similar such observation is also made with those of monometallic catalyst systems (not shown in this thesis). This observation lent reasonable support to the observations made by TEM that the particle size of metals is found to be relatively small. In addition, Au-Pd catalysts reveal only reflections that correspond to TiO<sub>2</sub>, CeO<sub>2</sub> and ZnO. A difference in peak intensity of all catalysts may originate from the different degrees of crystallinity of the supports.

### 4.3.3. TEM and EDX studies

Electron micrograph of the Au-Pd and Au-Ag catalysts on different carriers are depicted in Fig.4.12 (a-d). All these bimetallic systems showed a narrow size particle distribution but varying size of the noble metal particles, which again depended on the type of carrier used. TEM image in the case of Au-Pd catalyst indicate that the particles supported on TiO<sub>2</sub> are nearly spherical (Fig. 4.12(a)) and the average particle size ranges between 1 nm and 5 nm with the maximum close to 2.5 nm. The (111) lattice spacing is also determined to be  $0.234 \pm 0.01$  nm. Bulk Au and Pd have lattice spacing of 0.236 and 0.225 nm, respectively.

On the other hand, the size of Au-Ag bimetallic particle supported again on TiO<sub>2</sub> exhibit somewhat bigger particles compared to Au-Pd catalyst, which vary between 2 nm and 9 nm, as shown in Fig. 4.12 (b). Additionally, the lattice spacing calculated from the HRTEM for Au-Ag/TiO<sub>2</sub> solid has shown the value of about 0.230 nm, which lies between the Ag (111) plane (0.226 nm) and the Au (111) plane (0.235 nm), and such value provide some hints for a probable alloy state. However, such alloying is not confirmed from XRD patterns. Furthermore, Au and Pd nanoparticles are detected within the pore of ceria support at a magnification of 800 k (Fig.4.12 (c)). The size of the contrasted particles measured from TEM ranged between 1 and 4 nm. The spherical lattices of these particles are identified from their d-spacing values, which corresponding well to both the metals. In the case of supporting AuPd nanoparticles with ZnO, the Au and Pd particles are uniformly distributed on the support with the size ranging from 2 to 6 nm and the shape of the particles is nearly spherical, as shown in Fig. 4.12 (d).

Furthermore, the corresponding EDX patterns for some representative particles are shown in the insert images of Figs. 4.12 (a) and (b) of the Au-Pd and Au-Ag catalysts supported on TiO<sub>2</sub>. The results clearly show that the presence of both Au-Pd and Au-Ag in the particles, thus indicating a close interaction between the two metals.

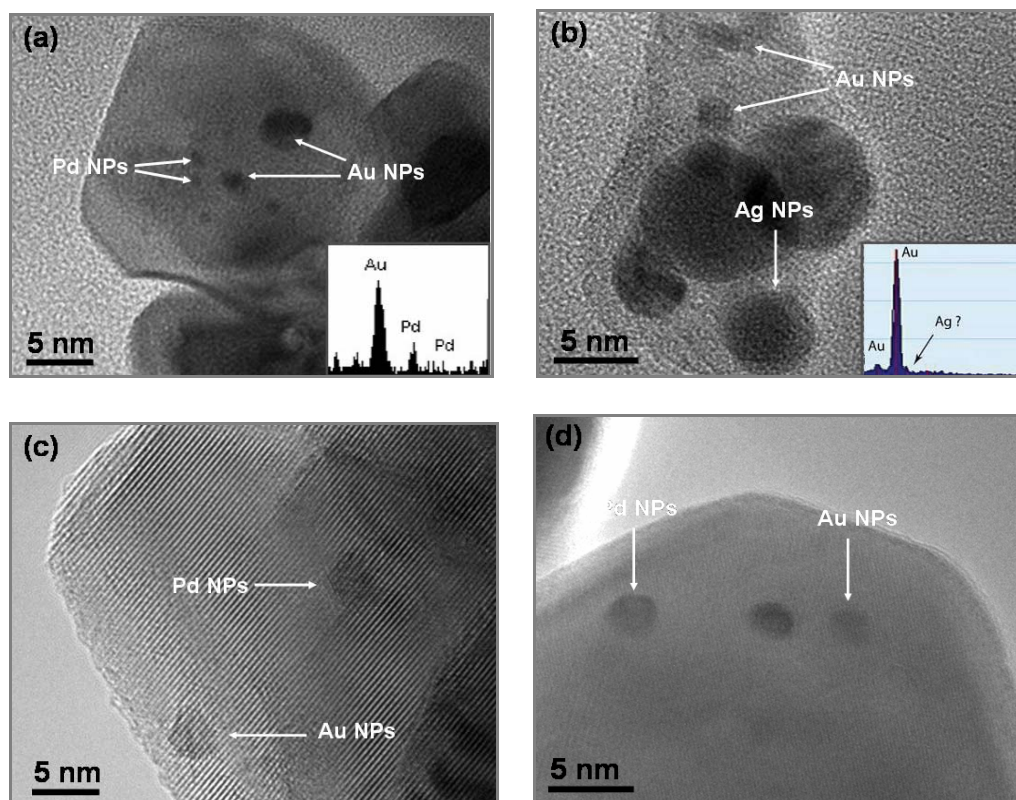


Fig. 4.12. TEM images of Au-Pd and Au-Ag catalysts supported on different supports (a & b: TiO<sub>2</sub>, c: CeO<sub>2</sub>, d: ZnO). Insert images show the EDX spectrum of the catalysts.

#### 4.4. Characterization of spent mono-metallic Au solids

It should be noted that only two catalysts such as i) Au/TiO<sub>2</sub> and ii) Au/Al<sub>2</sub>O<sub>3</sub> are selected based on their better performance and checked various aspects of these two solids before and after the reaction.

##### 4.4.1. Optical observations

In the first instance, the color of the spent catalyst is checked. The color of two selected above-mentioned catalysts are changed considerably after the catalytic testing from grey to black and from purple to dark purple in the case of supporting gold on TiO<sub>2</sub> and Al<sub>2</sub>O<sub>3</sub>, respectively. Such changes in the color might be due to a change either in the oxidation state of Au or due to some structural changes.

##### 4.4.2. BET surface areas

Au/Al<sub>2</sub>O<sub>3</sub> displayed a considerable decrease in the value of BET surface area in the spent sample (after 4 h of reaction) compared to its corresponding fresh one. Here, the surface area decreased from 261 to 210 m<sup>2</sup>/g. In contrast, the Au/TiO<sub>2</sub> showed only a marginal decrease from 43 m<sup>2</sup>/g (fresh) to 40 m<sup>2</sup>/g (spent).

#### 4.4.3. XRD analysis

XRD patterns of the used gold catalysts are shown in Fig. 4.13. Au/Al<sub>2</sub>O<sub>3</sub> (fresh) catalyst is found to be X-ray amorphous, while its corresponding used one showed a very weak reflection corresponds to Au (111). On the other hand, the Au in Au/TiO<sub>2</sub> solid seemed to be remained in amorphous state even after the reaction, i.e. no reflection corresponds to Au could be seen in both fresh and spent samples. In addition, some hints on the increased intensity of TiO<sub>2</sub> reflections in the spent sample is observed.

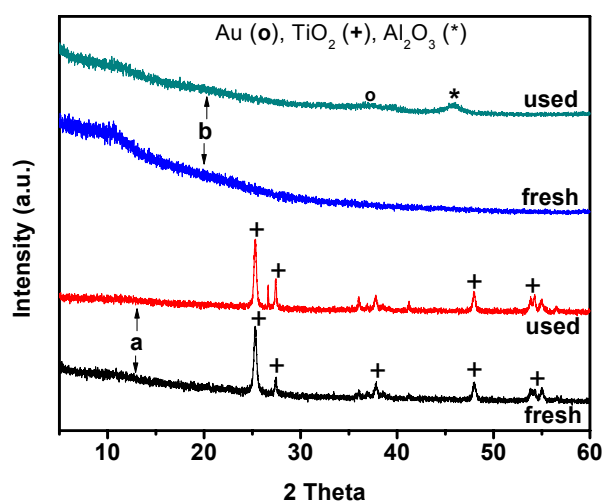


Fig. 4.13 XRD patterns of fresh and used Au catalysts supported on TiO<sub>2</sub> (a) and Al<sub>2</sub>O<sub>3</sub> (b).

#### 4.4.4. TEM study

A notable change in the Au particle size in case of used catalyst compared to their fresh one was observed as shown in Fig. 4.14. In the case of fresh Au/TiO<sub>2</sub> (Fig.4.14 (a)), the mean particle size was only 2 nm, which is observed to grow partly to 4 nm and in some instances a few particles even up to 10 nm are also found. The majority of the small Au particles, which observed in the fresh catalyst, are disappeared. In contrast to this observation, the used Au/Al<sub>2</sub>O<sub>3</sub> catalyst (Fig.4.14 (b)) exhibited considerably less growth in the size of gold particles. The size of Au particles is found to be varied in a small range compared to Au/TiO<sub>2</sub> catalyst.

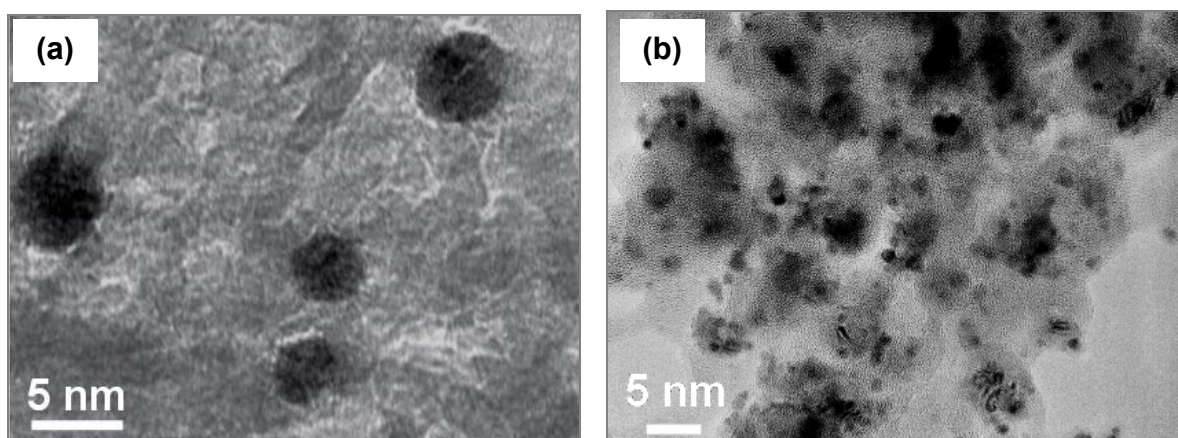


Fig. 4.14. TEM images of used 1% Au catalysts supported on (a) TiO<sub>2</sub> and (b) Al<sub>2</sub>O<sub>3</sub>.

The summary of various parameters between the fresh and spent Au/TiO<sub>2</sub> and Au/Al<sub>2</sub>O<sub>3</sub> solids are compared in Table 4.12. As mentioned above, the gold catalyst on irreducible carrier (Al<sub>2</sub>O<sub>3</sub>) displayed a significant decrease in the BET surface area of the catalysts after reaction compared to corresponding fresh one. In contrast, the gold catalyst over reducible carrier (TiO<sub>2</sub>) showed more or less constant surface area values both in the fresh and used catalysts. XPS showed that Au/M values are decreased in the spent samples compared to their corresponding fresh ones in both Au/TiO<sub>2</sub>, and Au/Al<sub>2</sub>O<sub>3</sub> samples. However, such decrease is more pronounced in case of Au/Al<sub>2</sub>O<sub>3</sub> solid. Overall, it can be concluded from these results that there is a strong influence of the support on growth of particle size of Au.

**Table 4.12.** Comparison between fresh and used catalysts using analytical methods.

Catalyst	Color of catalyst	BET-SA	XRD (nm)	TEM (nm)	Au/M ratios*
Au/TiO <sub>2</sub> -fresh	Grey	43	amorphous	2.2	0.016
Au/TiO <sub>2</sub> -used	Black	40	amorphous	4.1	0.008**
Au/Al <sub>2</sub> O <sub>3</sub> -fresh	Purple	261	amorphous	3.5	0.012
Au/Al <sub>2</sub> O <sub>3</sub> -used	dark purple	210	Weak refn.	4.1	0.0**

\* Surface ratios estimated from XPS; \*\* after four cycles

---

## 5. Catalytic Activity of Colloidal, Supported, Promoted and Bimetallic Au Catalysts

---

*Colloidal, supported and promoted gold nanoparticles have been used as catalysts for homocoupling of phenylboronic acid to biphenyl, the oxidation of benzyl alcohol to benzaldehyde, oxidation of cyclohexane to adipic acid and ammoxidation of 2-methylpyrazine to 2-cyanopyrazine, respectively.*

---

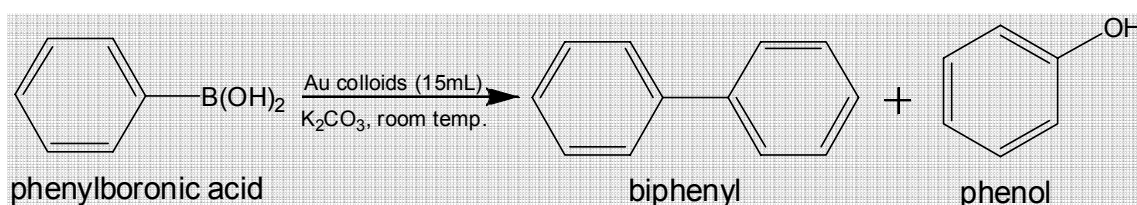
## 5.1. Application of colloidal AuNPs in liquid-phase reaction

### 5.1.1. Colloidal gold nanoparticles as catalysts

It has been reported elsewhere [127,128] that colloidal metal nanoparticles are effective as catalysts due to their high surface-to-volume ratio compared to bulk materials. Such type of catalysts have been tested mainly for homogeneous reactions such as cross-coupling reactions [129], Suzuki reactions [130] and oxidations reactions [131]. In the present study, homocoupling of phenylboronic acid (scheme 5.1) to biphenyl has been selected as model reaction to check the catalytic performance of some selected colloidal AuNPs with varying Au size.

### 5.1.2. Homocoupling of phenylboronic acid to biphenyl

As mentioned above, preliminary catalytic activity of colloidal AuNPs is examined towards homocoupling of phenylboronic acid in water under aerobic conditions. It should be noted that the AuNPs used were prepared using a-(SC+TA), b-(SC) and c-(TA), which gave Au size of 3 nm, 12 nm, and 17 nm, respectively. This particle size was analyzed by TEM. After the reaction at ambient temperature for 20 h, biphenyl with yield of 26, 41 and 60 % has obtained as a major desired product using c, b, a as catalysts, respectively. In addition, phenol is also observed as a minor product. All the tests were conducted under identical reaction conditions.



**Scheme 5.1.** Homocoupling of phenylboronic acid catalyzed by gold colloid.

The reaction conditions applied are: amount of catalyst: 15 mL, T: 25 °C, stirring speed: 1000 rpm under air, t: 20h, solvent ( $\text{H}_2\text{O}$ ): 10 mL, amount of phenylboronic acid: 0.11 g. It can be clearly seen from the results that the particle size of Au has a strong influence. The bigger the Au size the poorer the catalytic performance. In other words, the colloidal AuNPs prepared using the combination of reductants (SC + TA) gave the smallest particles (3 nm) and hence the best performance.

## 5.2. Application of supported AuNPs in liquid-phase reactions

### 5.2.1. Supports used and their roles in general

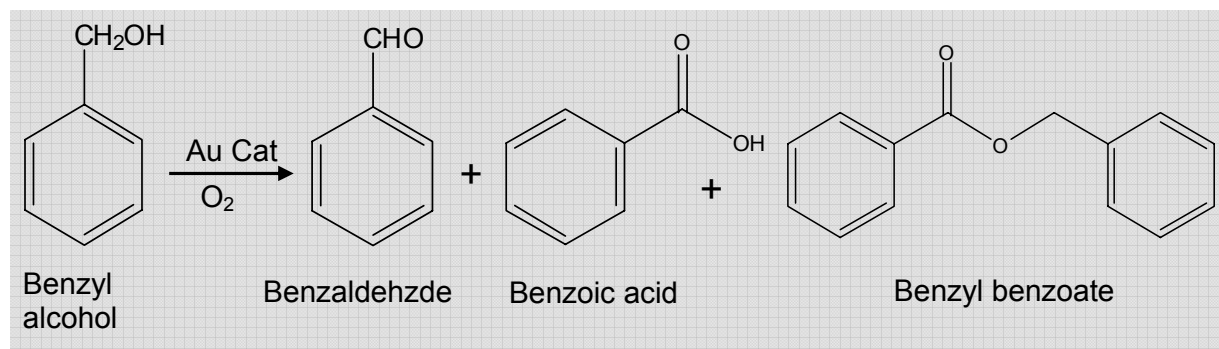
In heterogeneous reactions, the catalyst is generally carried out on supported metal catalysts [132]. The support can stabilize the small metal particles with high dispersion degrees and also provide high metal surface areas [133]. It is also reported elsewhere [e.g. 134,135] that the nature of support material can be significantly affected the catalytic performance of heterogeneous reactions, along with other factors such as the extent of metal loading, catalyst preparation, particle size, etc. Particularly, the catalytic properties of supported noble metals (e.g. gold) are known to be strongly dependent on the nature and kind of support materials. Previous studies [136,137] showed that the acidic support usually enhances the electron deficiency on the noble metal than the basic ones. For instance, metals supported on reducible oxides (e.g.  $\text{TiO}_2$ ,  $\text{CeO}_2$ ) exhibit a strong metal-support interaction (SMSI) [138,139]. Such catalysts exhibit a strong synergy between the two metallic components, which in turn leads to significantly higher catalytic activities compared to the single metal catalysts. In contrast, irreducible oxides (e.g.  $\text{Al}_2\text{O}_3$ ,  $\text{SiO}_2$ ) are assumed to be relatively inert. Additionally, metal fluoride based materials are also being reported in recent times as effective supports in catalysis [140,141]. Such materials can be used in different forms such as simple binary, oxy-hydroxyl doped fluorides etc. Metal fluorides possess the strongest electronegative element, which generates a higher Lewis acidity on the metal center compared to their corresponding oxides. In the present study, we have also used 10 different types of supports, which showed considerably different influences on the particle size, size distribution as well as the performance. Among these 10 different supports, 5 supports are oxide based and the other 5 are their corresponding oxy-fluorides. The influence of all these 10 supports were tested for two different reactions such as oxidation of benzyl alcohol and oxidation of cyclohexane and again both in liquid phase conditions. One should note that oxy-fluorides are used for the first time as novel supports particularly for these two reactions. More details on the influence support on the performance are detailed below.

### 5.2.2. Oxidation of benzyl alcohol to benzaldehyde using supported Au catalysts

In this study, the applications of AuNPs supported over metal oxides and their corresponding oxy-fluorides have been investigated in the oxidation of benzyl alcohol (BA) to benzaldehyde (BAI) (scheme 5.2). Gold catalysts have been tested in the oxidation of BA under mild solvent free conditions (0.15 g catalyst, 140 °C, 5 bar  $\text{O}_2$ , 4 h), in an autoclave. Prior to perform the real catalysts, some blank tests were conducted initially under the similar reaction conditions but in absence of catalyst to determine



whether the oxidation can occur in the absence of a catalyst. In addition, such tests also give information on the thermal effects. From such experiments, it is noticed that the small amounts of BA can be converted into products, mainly to BAI. The conversion of BA achieved in blank test was about 10 %.



**Scheme 5.2.** Oxidation of benzyl alcohol with  $\text{O}_2$  in presence of Au catalyst.

- AuNPs supported over metal oxide carriers

Results showing the performance of Au catalysts supported on 5 different metal oxide carriers under the solvent-free oxidation of BA using oxygen as an oxidant are presented in Fig. 5.1. It is quite clear from this Fig. that the catalytic performance of Au catalysts is depended strongly on the nature of the support applied. BAI is the major product, however, some side-products such as benzyl benzoate, benzoic acid and acetal were also observed in small amounts. The formation of benzoic acid is expected from the over-oxidation of benzaldehyde, while the formation of benzyl benzoate is due to the further esterification reaction of the benzoic acid and benzyl alcohol. On the other hand, acetal formation is expected from the reaction of unreacted benzyl alcohol and the product benzaldehyde that initially leads to the formation of hemiacetal, which in turn undergoes protonation and deprotonation reactions and finally forms the acetal. However, the concentration of acetal in the product stream only in traces. Among all catalysts tested, the  $\text{TiO}_2$  supported AuNPs are highly active ( $X\text{-BA} = 81\%$ ) and selective ( $S\text{-BAI} = 95\%$ ) while  $\text{MgO}$  supported one is least active ( $X\text{-BA} = 16\%$  &  $S\text{-BAI} = 17\%$ ). The higher activity and selectivity of  $\text{Au/TiO}_2$  is undeniably due to some facts as summarizing here: i) smaller Au size, ii) higher dispersion of Au and iii) high surface enrichment of Au compared to other catalysts. On other hand, the opposite is true in the case of  $\text{MgO}$  supported gold catalyst and others (e.g.  $\text{Au/MgO}$ ,  $\text{Au/ZrO}_2$ ,  $\text{Au/Al}_2\text{O}_3$ ). Good supporting evidence for such claims is observed from both TEM and XPS. The decreasing order of conversion of BA with changing supports is in the following order:  $\text{TiO}_2 > \text{Al}_2\text{O}_3 > \text{ZrO}_2 > \text{CaO} > \text{MgO}$ .

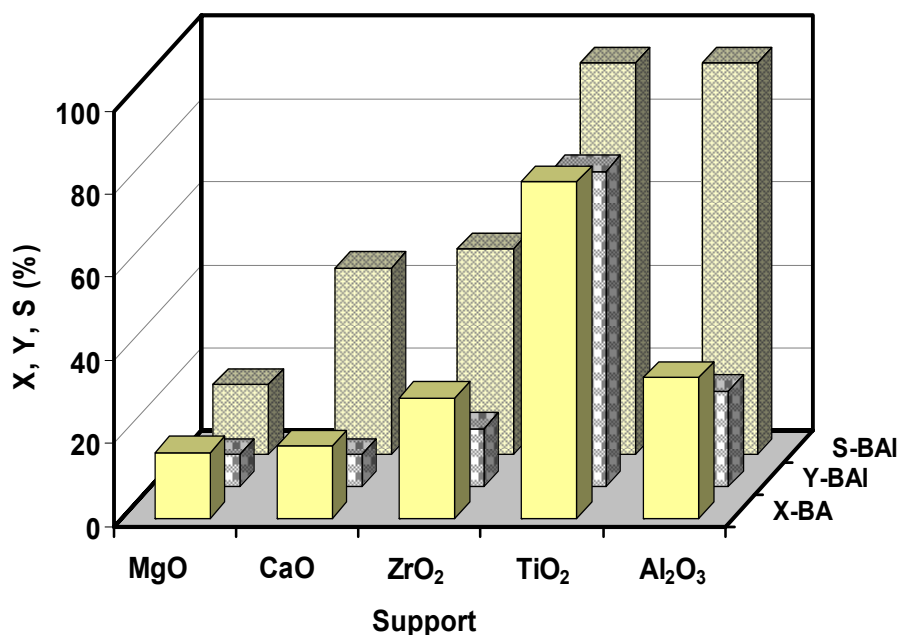


**Fig. 5.1.** Influence of support on oxidation of benzyl alcohol to benzaldehyde over 1% Au/M catalysts (M= MgO, CaO, ZrO<sub>2</sub>, TiO<sub>2</sub>, Al<sub>2</sub>O<sub>3</sub>). Reaction conditions: 30 mL BA, 0.15 g catalyst, 140 °C, 5 bar O<sub>2</sub>, 4 h. (X= Conversion; Y= Yield; S=Selectivity).

- AuNPs supported over metal oxy-fluorides

Further catalytic tests were carried out under similar conditions as above but using their corresponding oxy-fluoride supports. The results on the influence of various metal oxy-fluoride supports on the performance of AuNPs are depicted in Fig. 5.2. In comparison of these catalysts with those of metal oxides supported ones (see Fig. 5.1), it can be clearly seen that the catalytic performance of oxy-fluorides is inferior to the oxide carriers. However, the trend of change in the activity and selectivity is more or less comparable with that of oxide carriers. To be brief, the Au/TiF<sub>4-x</sub>(OH) displayed the superior performance (X-BA = 33%; Y-BAI = 67%) compared to all other oxy-fluoride supports. The poorest catalytic activity of BA oxidation using gold catalyst was found to be obtained again using magnesium oxy-fluoride supports. Such differences in the catalytic performance are again related to the size of Au particles. For instance, if we compare the Au size between TiO<sub>2</sub> and its corresponding oxy-fluoride supported catalyst, the oxide support (TiO<sub>2</sub>) possesses smaller AuNPs and hence higher activity, as expected. Similar is the case with other supports of this study. The decreasing order of conversion of BA with changing oxy-fluoride support is exactly similar to the oxide carriers, which is in the following order: TiF<sub>4-x</sub>(OH) > Au/AlF<sub>3-x</sub>(OH)<sub>x</sub> > Au/ZrF<sub>4-x</sub>(OH)<sub>x</sub> > Au/CaF<sub>2-x</sub>(OH)<sub>x</sub> > Au/MgF<sub>2-x</sub>(OH)<sub>x</sub>. However, we have shown for the first time that AuNPs supported on novel metal oxy-fluorides carriers can be used for the oxidation of

BA to BAI. Nevertheless, further investigations are needed to improve the catalytic activity of such fluorides.

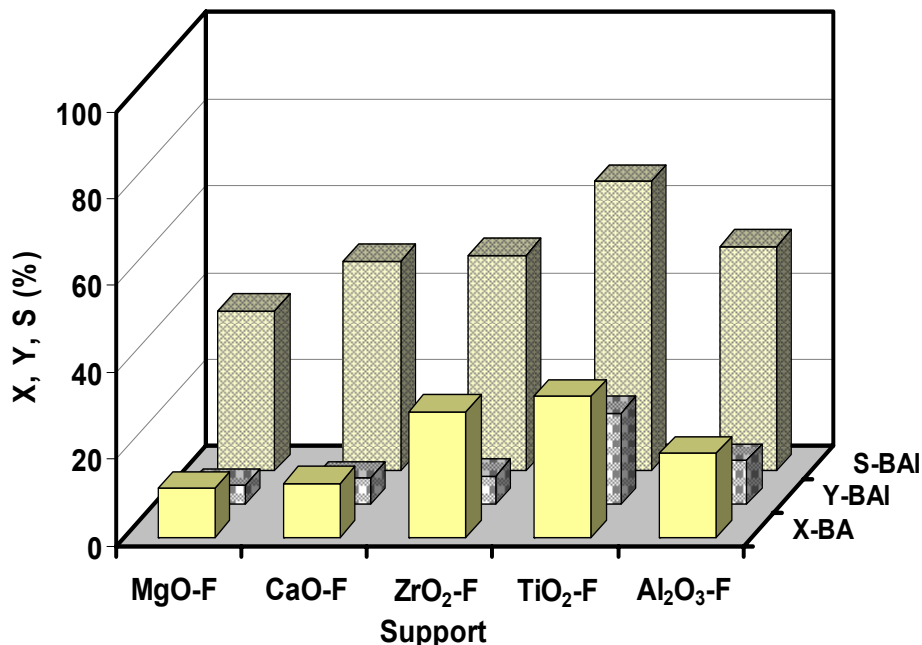
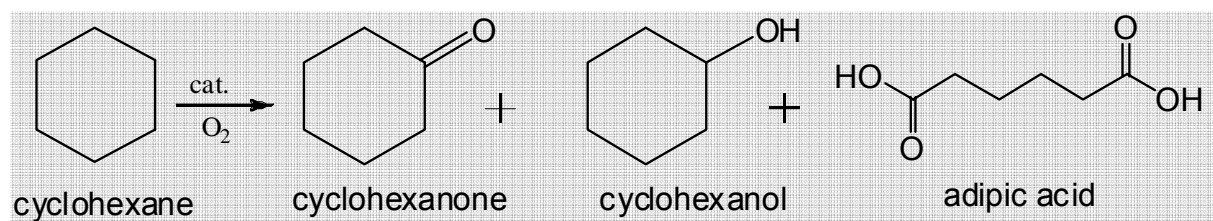


**Fig. 5.2.** Influence of nature oxy-fluoride support in oxidation of benzyl alcohol to benzaldehyde over 1% Au/M catalysts (M= MgO, CaO, ZrO<sub>2</sub>, TiO<sub>2</sub>, Al<sub>2</sub>O<sub>3</sub>). Reaction conditions: 30 mL BA, 0.15 g catalyst, 140 °C, 5 bar O<sub>2</sub>, 4 h. (X= Conversion; Y= Yield; S=Selectivity).

### 5.2.3. Oxidation of cyclohexane using supported Au catalysts

This section describes the conversion of cyclohexane (CH), selectivity of products during catalytic oxidation reaction using different catalysts. The primary objective of this study is first to check the influence of both types of supports (i.e. oxide supports and oxy-fluoride supports) on the catalytic performance in the direction of finding suitable catalyst carrier and then to check the effect of various reaction conditions for identifying optimum reaction conditions taking the best support. With these objectives, 10 different catalysts as mentioned above were prepared and tested in CH oxidation (Scheme 5.3).



**Scheme 5.3.** Oxidation of cyclohexane with O<sub>2</sub> in presence of catalyst.

A blank experiment was also executed by treating CH with oxygen and TBHP at 150 °C in the absence of catalyst. The aim of such experiment is to check the thermal effects and further to confirm whether there is a notable oxidation occurs under those conditions. This blank test showed a conversion of CH approximately 0.4 % in the first 1 h. Subsequently, the conversion is gradually increased to ca. 2 % after 4 h of reaction time. Comparing this result with that of a catalyzed reaction, it can be clearly observed that the blank test in absence of catalyst has exhibited only a very low and negligible conversion and hence presence of a catalyst is essential and plays a key role on the performance. Following the initial experiments, the influence of metal oxide and metal (oxy) fluoride supported on CH oxidation is investigated.

- AuNPs supported on metal oxide carriers

The influence of support on the oxidation of CH was carried out under the following conditions (10 ml CH, 20 ml solvent (acetonitrile), 0.3 g catalyst, 0.1 g TBHP,  $p_{O_2} = 10$  bar,  $t = 4$  h, 1500 rpm,  $T = 130$  °C). The main products of the reaction are adipic acid (AA), cyclohexanone (-One) and cyclohexanol (-Ol). These two ketone and alcohol products together referred to as "KA", which is the well-known denotation raised from the commercial production of AA from cyclohexanone and cyclohexanol. In addition, some other by-products such as glutaric acid, succinic acid, cyclohexylhydroperoxide, CO and CO<sub>2</sub> are also expected in very small amounts, whose concentration however depends upon the reaction conditions and type of catalyst used. Nevertheless, AA is the desired product among all other products.

The influence of oxide supports on the oxidation activity of CH to AA is presented in Fig 5.3. It is obvious that the nature of support has a significant influence on the conversion of CH as well as the selectivity of products. TiO<sub>2</sub> supported AuNPs exhibited the superior activity compared to all other catalysts, which is quite similar to the observation made above in the oxidation of benzyl alcohol (see Fig. 5.1.). In addition, these results provide further evidence that the smaller size of Au particle is necessary and is also a crucial parameter for improving the performance of the catalysts. Again in this case, the MgO & CaO supported catalysts gave the poorest performance. Over these two catalysts, the highest amount of undesired side-products such as CO and CO<sub>2</sub> (S = up to 35 %) is observed. Therefore, it can be concluded that MgO and CaO are not really suitable supports for this reaction. The conversion of CH and the selectivity of AA obtained over TiO<sub>2</sub> supported catalyst is 16.4 % and ca. 21.6%, respectively. Several efforts were also made in the literature by different research groups to use gold-based

catalysts for the direct oxidation of cyclohexane to adipic acid, but not even 1 % yield of adipic acid could be achieved from those investigations [84,85].

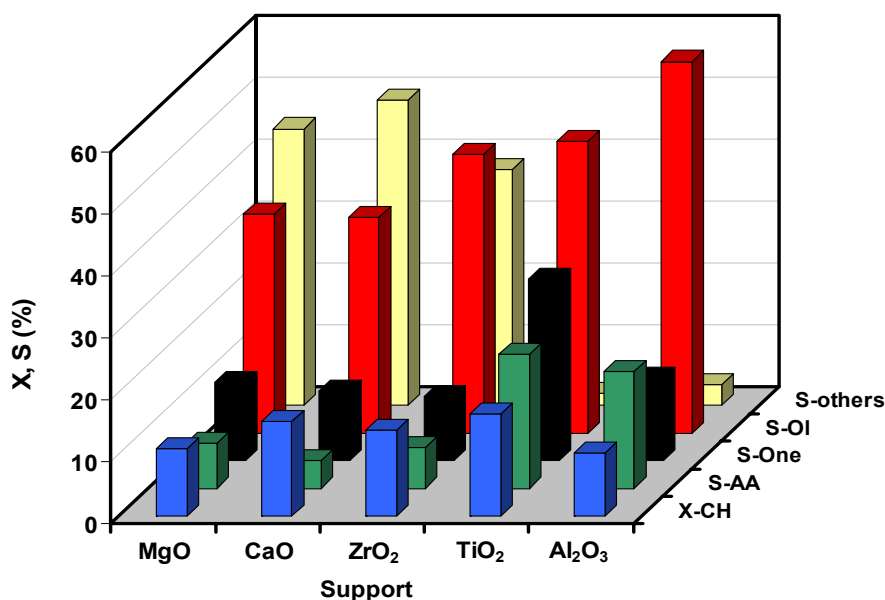


**Fig. 5.3.** Effect of different oxide support on the oxidation of cyclohexane over Au/X catalysts (X = MgO, CaO, ZrO<sub>2</sub>, TiO<sub>2</sub>, Al<sub>2</sub>O<sub>3</sub>). Reaction conditions: (10 ml CH, 20 ml solvent (acetonitrile), 0.3 g catalyst, 0.1 g TBHP, pO<sub>2</sub> = 10 bar, t = 4 h, 1500 rpm, T = 130 °C). X-CH = conversion of cyclohexane; S-AA = selectivity of cyclohexane; S-One = selectivity of cyclohexanone; S-OI = selectivity of cyclohexanol; S-Others = yields of glutaric acid, succinic acid, cyclohexylhydroperoxide, CO and CO<sub>2</sub>.

- Oxidation using AuNPs supported on oxy-fluorides

After investigating the influence of oxide carriers, further experiments were focused on testing the effect of various oxy-fluorides as novel supports in the direct oxidation of CH to AA. The catalytic tests were performed under the similar reaction conditions as above. The results obtained on the influence of oxy-fluorides are illustrated in Fig. 5.4. These results clearly indicate that the nature of support has a strong influence on the activity and selectivity. Interestingly, among all catalysts tested, AuNPs supported on titanium (oxy)-fluoride is found to give better performance ( $X_{CH} = 11\%$ ,  $S_{AA} = 10\%$ ,  $Y_{AA} = 3.5\%$ ) compared to others. More over, small amounts of CO and CO<sub>2</sub> are also found from these investigations. In terms of AA production, the decreasing order of the performance is:  $TiF_{4-x}(OH)_x > AlF_{3-x}(OH)_x > ZrF_{2-x}(OH)_x > MgF_{2-x}(OH)_x > CaF_{2-x}(OH)_x$ . It can be said from these results that oxy-fluoride supports exhibit poor performance compared to oxide carriers and this observation is quite similar to that of the results obtained from benzyl alcohol oxidation.

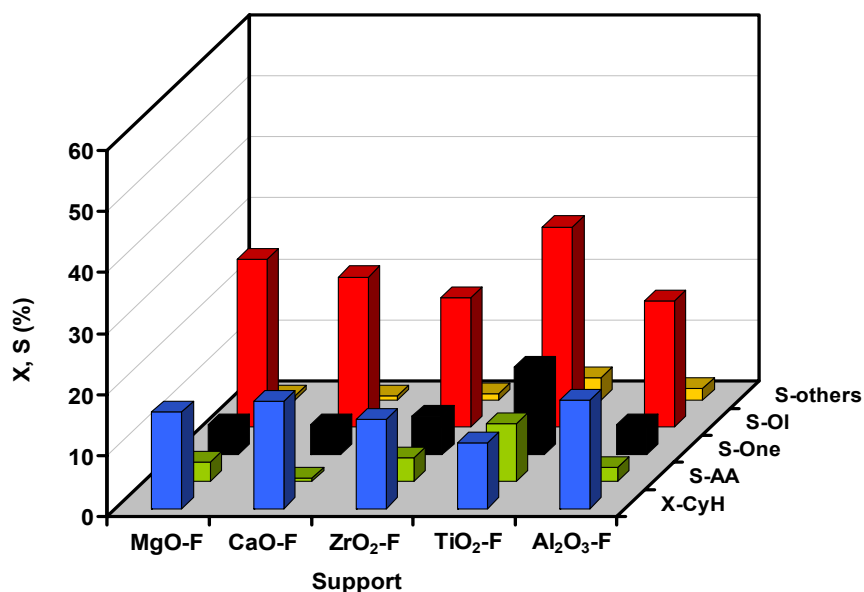


**Fig. 5.4.** Effect of different metal oxy-fluorides support on the oxidation of cyclohexane over Au/X catalysts ( $X = \text{MgF}_{2-x}(\text{OH})_x$ ,  $\text{CaF}_{2-x}(\text{OH})_x$ ,  $\text{ZrF}_{4-x}(\text{OH})_x$ ,  $\text{TiF}_{4-x}(\text{OH})_x$ ,  $\text{AlF}_{3-x}(\text{OH})_x$ ). (for all other denotations and conditions one can refer to Fig. 5.3).

#### 5.2.4. Optimization of the reaction conditions

From the above investigations, it has been clearly noticed that the  $\text{TiO}_2$  is the best support among all 10 different supports applied. Taking this observation as a basis, the  $\text{TiO}_2$  supported one is chosen for further investigations particularly for optimising the reaction conditions in the direction of enhancing the yield of AA. The results obtained on such investigations are shown below one after the other.

- Effect of catalyst amount

The catalyst amount can kinetically and mechanistically be affected the oxidation of CH. In general, the higher the amount of added catalyst the higher reactant conversion rates and product formation rates. However, such study is useful to avoid the effect of mass transfer limitations. Fig. 5.5 displays the affect of catalyst amount on the catalytic activity of CH oxidation. It is evident that the conversion of CH and the selectivity of AA are found to be increased from 7 to 26 % and 11 to 26 % with increase in catalyst amount from 200 to 400 mg. The yield of AA obtained is ca. 8 %, which is the remarkable outcome of this study [142]. Subsequently, the selectivity of AA remained relatively constant with further increase in catalyst amount. Interesting observation is that the selectivity of AA increased at the expense of selectivity of cyclohexanone. This result indicates that the formation of AA seems to occur from the over oxidation of

cyclohexanone. Besides, the selectivity of cyclohexanol is varied in the range from 46 to 58 % with increase in catalyst amount from 200 to 400 mg. Another important thing is that at high catalyst amounts (500 mg), the selectivity of “-OI” is decreasing while the selectivity of “-one” is increasing. This means, the “-one” is forming from “-OI” by simple oxidation. Nevertheless, it is clear that a high catalyst amount of 500 mg led to adverse effects on the performance, which resulted in the decreased selectivity of desired products and increased selectivity of by-products. Summing up all effects it can be said that the catalyst amount of 400 mg is optimum for better performance of the direct oxidation of CH to adipic acid and hence this amount is used for further investigations.

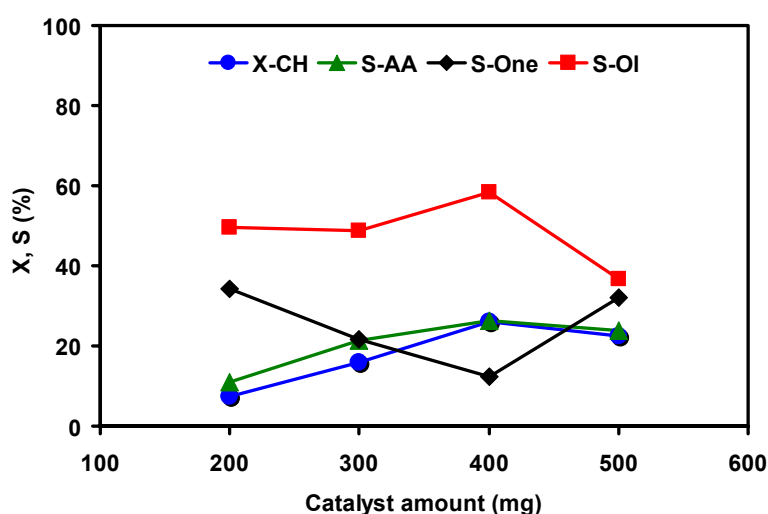


**Fig. 5.5.** Effect of catalyst dosage ( $\text{Au/TiO}_2$ ) on the oxidation reaction of cyclohexane. Reaction conditions: 5 ml CH, 25 ml solvent (acetonitrile), 0.1 g TBHP,  $p\text{O}_2 = 10$  bar,  $t = 4$  h, 1500 rpm. (for all other denotations one can refer to Fig. 5.3).

- Effect of reaction time

The changes in catalytic performance with time-on-stream using  $\text{Au/TiO}_2$  catalyst are presented in Fig. 5.6. It is evident that the catalyst showed a very low initial conversion of CH (ca. 2 %), which is observed to increase up to 4 h (ca. 26 %) and then decrease with further increase in reaction time. The reaction proceeds through the free radical mechanism, which is initiated by TBHP [143]. The conversion of CH is slightly decreased beyond 4 h reaction time and seems to be stabilized at this level, which might be due to a possible attainment of steady state conditions. The selectivity of AA is also observed to change in the same way as that of CH conversion and reaches the maximum selectivity of 26 % at 4 h (yield ca. 7 %). Again, S-AA increased at the expense of S-One up to 4 h, which gives further confirm that AA is formed from “-one”.

Some hints can be obtained if one carefully observes the results, that the reaction products gradually converted from “-OI” to “-One” particularly at longer reaction times of 6 and 8 h. It is known from the literature that the “-One” and “-OI” could be the first oxygenated products in the reaction mechanism [144]. It can be stated that the catalyst exhibited good performance at 4 h and hence this reaction time is further used.

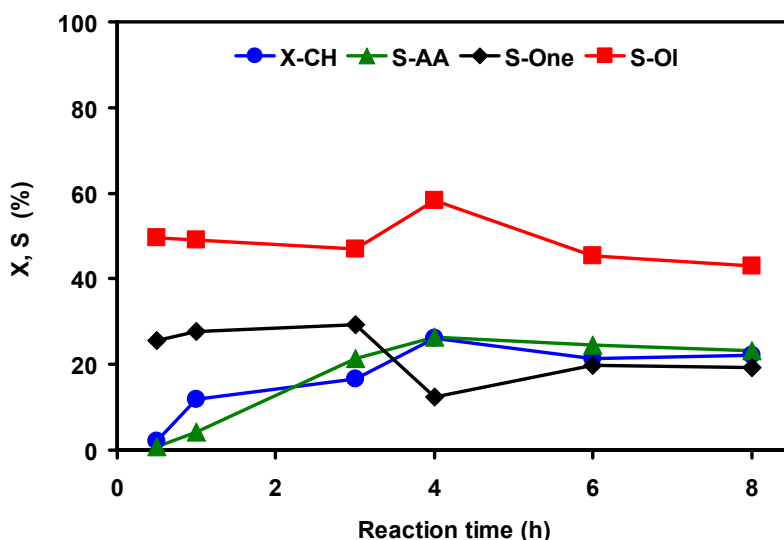


**Fig. 5.6.** Time-on-stream behavior of Au/TiO<sub>2</sub> catalyst for the oxidation reaction of cyclohexane. Reaction conditions: 5 ml CH, 25 ml solvent (acetonitrile), 0.4 g catalyst, 0.1 g TBHP, pO<sub>2</sub> = 10 bar, 1500 rpm, T = 150 °C. (for all other denotations one can refer to Fig. 5.3).

- Effect of reaction temperature

Effect of reaction temperature on the catalytic performance is depicted in Fig. 5.7. It is clear from this Fig. that the temperature has a promotional effect on the conversion of cyclohexane, which progressively increased from 2.4 to 28 %, with increase in temperature from 100 to 170 °C. The selectivity of AA is also increased from ca. 6 to 26 % with rise in temperature up to 150 °C and then slightly decreased with further rise in temperature to 170 °C. Interesting thing here is that “-OI” is the major product at low reaction temperatures (S-OI = 66.5 % at 100 °C), which hints to the fact that “-OI” is the primary product of the reaction. However, with rise in temperature promotes the rate of oxidation process, which in turn speeds up the conversion of “-OI” to “-one” and then to AA. Therefore, the selectivity of AA increased with temperature up to 150 °C. However, further rise in temperature to 170 °C has shown a detrimental effect on the formation of desired products but promotional effect on the formation of unwanted products mainly total oxidation products. From these results, it appears that a reaction temperature of 150 °C seems to be optimum for better selectivity of desired products at reasonably good conversion and hence this temperature is used in further investigations.



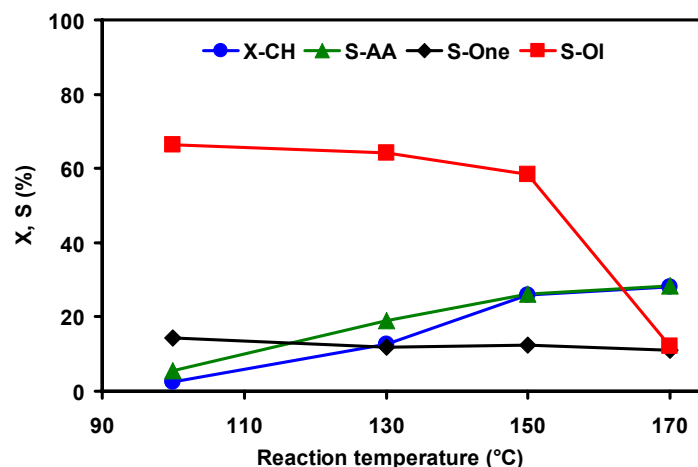


Fig. 5.7. Effect of reaction temperature on the oxidation of cyclohexane. Reaction conditions: 5 ml CH, 25 ml solvent (acetonitrile), 0.4 g catalyst, 0.1 g TBHP,  $pO_2 = 10$  bar,  $t = 4$  h, 1500 rpm. (for all other denotations one can refer to Fig. 5.3).

- Effect of solvent to CH ratio (v/v)

The investigation of solvent/CH ratio on the catalytic activity of 1% Au/TiO<sub>2</sub> catalyst was carried out in order to determine the optimum ratio. Fig. 5.8 illustrates the effect of such ratio on the performance in the CH oxidation. The solvent used is acetonitrile. It is clear from Fig. 5.8 that the conversion of CH is observed to decrease from 37 to 26 % with increase in the ratio from 1 to 5. It is also apparent that the selectivity of AA and “-One” are gradually increased from ca. 5 to 26 % and from ca. 6 to 12 %, respectively, with increase in the solvent/CH ratio. Among different solvent/CH ratios investigated, a ratio of 5 is giving the better results.

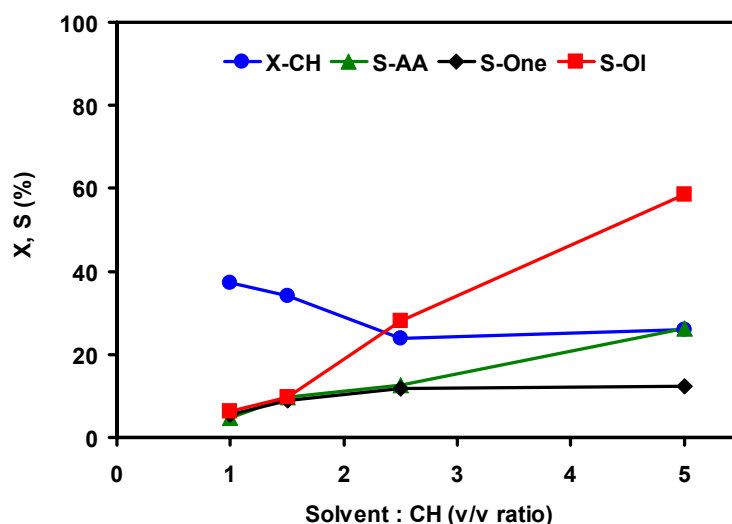
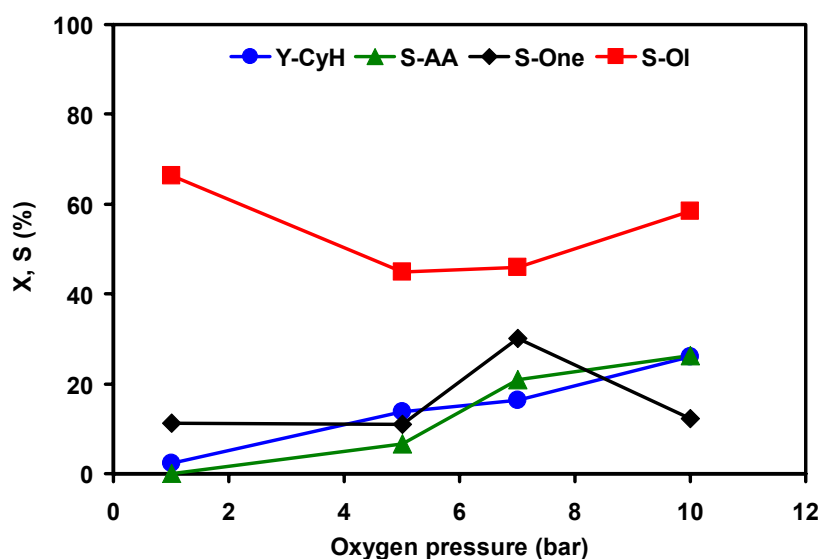


Fig. 5.8. Effect of acetonitrile to cyclohexane amount ratio on the oxidation of cyclohexane. Reaction conditions: 0.4 g catalyst, 0.1 g TBHP,  $pO_2 = 10$  bar,  $t = 4$  h, 1500 rpm,  $T = 150$  °C. (for all other denotations one can refer to Fig. 5.3).

- Effect of reaction pressure

After optimizing solvent/CH ratio, the effect of O<sub>2</sub> pressure on the conversion and products distribution of CH oxidation has been studied in the range of 1-10 bar under the similar reaction conditions as those used in previous tests. Fig. 5.9 shows that the conversion of CH is increased continuously from ca. 3 to 26 % with an increase in the O<sub>2</sub> pressure from 1 to 10 bar. This means higher O<sub>2</sub> pressure in the reaction system accelerates the reaction rate and hence promote the formation of products. The selectivity of AA is found to be more or less zero at 1 bar. However, it has been increased drastically from zero to 26 % with increase in pressure. This phenomenon might be due to the fact that “-OI” oxidized to “-One” at higher O<sub>2</sub> pressure. Interestingly, the selectivity of “-One” is also found to decrease remarkably from ca. 30 to 12 % with increase in oxygen pressure. A potential reason for such decrease in the selectivity of “-One” when O<sub>2</sub> pressure reaches 10 bar is that “-One” oxidized to AA and also perhaps to other side-products. In conclusion, a reaction pressure of 10 bar is better for improved performance.



**Fig. 5.9.** Effect of the initial oxygen pressure on the oxidation reaction of cyclohexane. Reaction conditions: 5 ml CH, 25 ml solvent (acetonitrile), 0.4 g catalyst, 0.1 g TBHP, t = 4 h, 1500 rpm, T = 150 °C. (for all other denotations one can refer to Fig. 5.3).

- Effect of stirring speed

Fig. 5.10 illustrates the changes in the conversion of CH and selectivity of products with change in stirring speed. The conversion is notably increased with increase in stirring speed and reached a value of 26 % at 1500 rpm. After that, it increased marginally to

27% at 2000 rpm, which is clearly no significant improvement. In addition, the selectivity of AA also increased continuously from 18 to 27 while the s-one decreased from 22.5 to 12.7 with rise in stirring speed from 500 to 2000 rpm. On the whole, the stirring speed of 1500 rpm is better optimum.

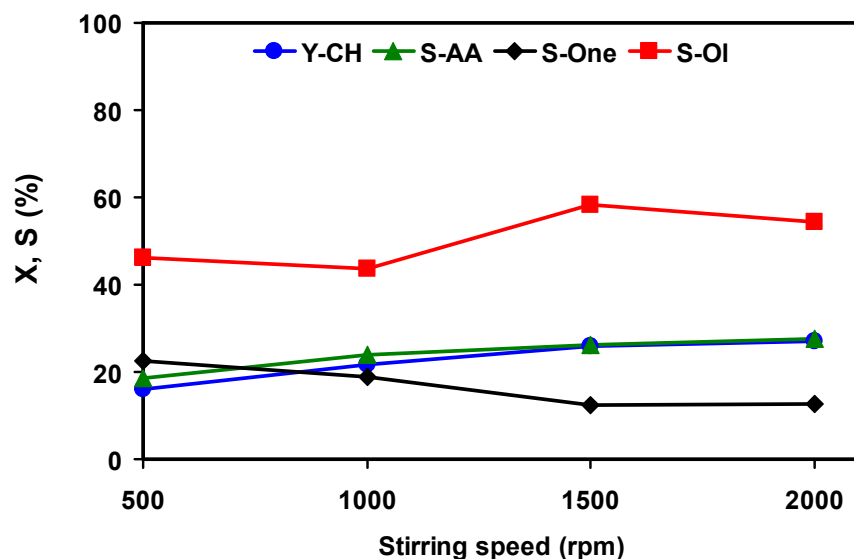


**Fig. 5.10:** Effect of stirring speed on the oxidation reaction of cyclohexane to AA. Reaction conditions: 5 ml CH, 25 ml solvent (acetonitrile), 0.4 g catalyst, 0.1 g TBHP,  $pO_2 = 10$  bar,  $t = 4$  h,  $T = 150$  °C. (for all other denotations one can refer to Fig. 5.3).

- Effect of catalyst reuse

To check the reusability and stability of the catalyst, recycling and washing experiments were carried out using 1% Au/TiO<sub>2</sub>, and the results are given in Fig. 5.11. After the first run, the catalyst was separated by filtration, washed, dried at 120 °C and then subjected to the second run under the same reaction conditions. In a similar way, the catalyst was used for four such cycles. It is observed that a slight decrease in the conversion of CH and the selectivity of products is observed after four runs. Interestingly the S-OI decreased from first run to second run and then remained more or less constant. On the whole, it can be said the catalyst performance decreased to some extent after four runs, which might be due to either leaching or deactivation or due to marginal loss of catalyst weight during the process of recovery of the catalyst. It is also observed that there is a slight decrease in the weight of recovered catalyst sample from run to run. However, the former one seems to be appropriate when XPS results are considered. XPS analysis of fresh and spent (after 4 cycles) gave some indications on the loss of Au from the catalyst due to leaching (see Table 4.5.).

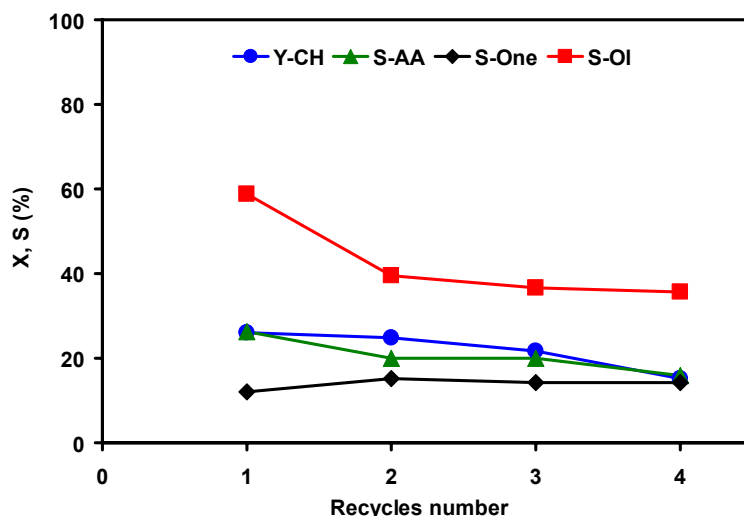


**Fig. 5.11.** Recycling results of Au/TiO<sub>2</sub> catalyst for the oxidation reaction of cyclohexane. Reaction conditions: 5 ml CH, 25 ml solvent (acetonitrile), 0.4 g catalyst, 0.1 g TBHP, pO<sub>2</sub> = 10 bar, t = 4 h, T = 150 °C. (for all other denotations one can refer to Fig. 5.3).

#### 5.2.4.8. Effect of reactor type

In order to check the effect of the type of reactor on cyclohexane oxidation, a systematic study was carried out using glass reactor and autoclave reactor under optimum reaction conditions. The results of autoclave reactor are already presented above. The present run was performed in glass reactor using 1% Au/TiO<sub>2</sub> catalyst at 1 bar. In this case, the selective oxidation products are mainly cyclohexanone and cyclohexanol. Surprisingly, no adipic acid is found, which might be due to low reaction pressure. The conversion of CH obtained from this run is only 5 %, while the combined selectivity of KA is about 33 % and the balance are unwanted by-products. In a similar way, the tests performed in autoclave at 1 bar also did not give any adipic acid in the product stream. From this comparison, it can be concluded that the type of reactor (glass or autoclave) has no remarkable effect on the performance.

#### 5.2.5. Oxidation of cyclohexane using bi-metallic catalysts

In general, it is expected that bimetallic systems (e.g. Au–Pd and Au–Pt) show high activity and high resistance towards deactivation due to synergistic effects. However, the system is often too complex to correlate the activity with the specific catalyst feature.

- Au-Pd bimetallic system

To investigate the influence of second-metallic element (i.e. bimetallic system) in the catalytic performance for the oxidation reaction of cyclohexane, a set of experiments were also performed under identical reaction conditions. For these tests, different

catalysts such as pure  $\text{TiO}_2$  support, monometallic systems (e.g. 1%  $\text{Au}/\text{TiO}_2$  and 1%  $\text{Pd}/\text{TiO}_2$ ) and bimetallic system (1%  $\text{Au}$ -1%  $\text{Pd}/\text{TiO}_2$ ) were used. The results of these investigations are portrayed in Fig. 5.12. The pure  $\text{TiO}_2$  is found to show the poorest performance, while the  $\text{Au}/\text{TiO}_2$  displayed improved catalytic activity as mentioned above (i.e.  $X\text{-CH} = \text{ca. } 25\%$ , and  $S\text{-AA} = 26\%$ ). In addition, the monometallic Pd catalyst (i.e.  $\text{Pd}/\text{TiO}_2$ ) exhibit somewhat inferior performance ( $X\text{-CH} = 16\%$ ,  $S\text{-AA} = 18\%$ ) compared to  $\text{Au}/\text{TiO}_2$  solid. Interestingly, the combination of Au and Pd ( $\text{Pd-Au}/\text{TiO}_2$ ) markedly improved the selectivity of AA from 26 to ca. 34 %, which is almost double to the  $S\text{-AA}$  obtained on  $\text{Pd}/\text{TiO}_2$  and also remarkably higher even to compared to monometallic  $\text{Au}/\text{TiO}_2$  catalyst. However, the conversion of CH ( $X = 21\%$ ) obtained on bimetallic  $\text{Pd-Au}/\text{TiO}_2$  is significantly higher than monometallic  $\text{Pd}/\text{TiO}_2$  but slightly lesser than monometallic  $\text{Au}/\text{TiO}_2$  sample. Considering all these effects, it can be claimed that the addition of second metallic component has a clear promotional effect on the selectivity of AA, which might be due to expected synergistic effects between Pd and Au. However, the precise role of the second metal is still a matter of discussion and hence further studies are necessary for better understanding of the properties of bimetallic catalysts.

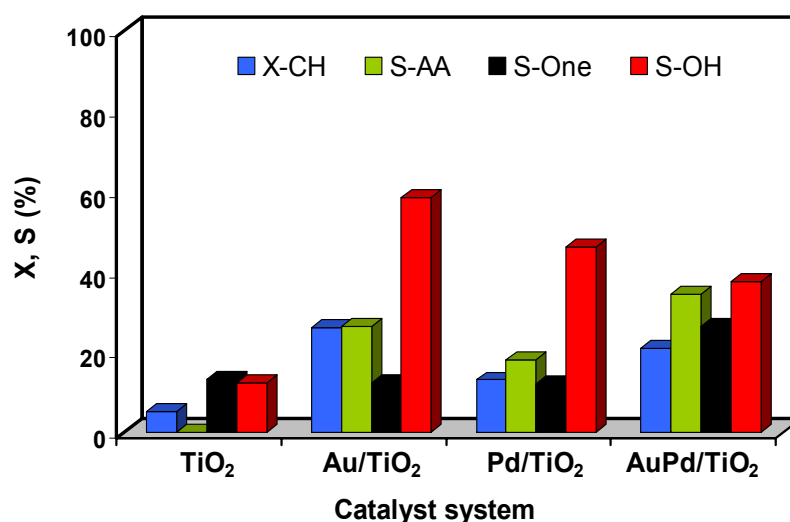


**Fig. 5.12.** Comparison on the catalytic activity of the mono-metallic (Au, Pd) and bi-metallic (Au- Pd) catalysts on the oxidation of cyclohexane. (X= Conversion; Y= Yield; S=Selectivity). (for all other denotations one can refer to Fig. 5.3).

- Au-Ag bimetallic system

In addition to Pd as second metal, some tests were also performed using Ag as a second metal. This means the bi-metallic system here is  $\text{Ag-Au}/\text{TiO}_2$ . The influence of monometallic (e.g. 1 % Ag) and bi-metallic catalysts in the cyclohexane oxidation is

shown in Fig. 5.13. The catalytic activity of both pure support and Au/TiO<sub>2</sub> were already discussed earlier. Fig. 5.13 showed that the reaction performed using 1% Ag/TiO<sub>2</sub> catalyst has no appreciable influence on the activity and selectivity behavior compared to Au/TiO<sub>2</sub>. Nevertheless, the catalytic performance of using Au-Ag/TiO<sub>2</sub> suggest that the presence of Ag has a clear influence on the performance but in different direction compared to Pd. Using Ag as second metal, not only the selectivity of KA (S = 82 %) is significantly improved compared to all mono-metallics (both Ag/TiO<sub>2</sub>, Pd/TiO<sub>2</sub> and Au/TiO<sub>2</sub>) but also the conversion of CH increased. Nevertheless, the influence of Ag addition on the selectivity of AA is not that bad (S-AA = 14.3%), which leads an yield of ca. 4 %. Considering the effects on the whole, it can be stated that both these metallic components (Pd, Ag) have shown different influences and thereby different distribution of products.

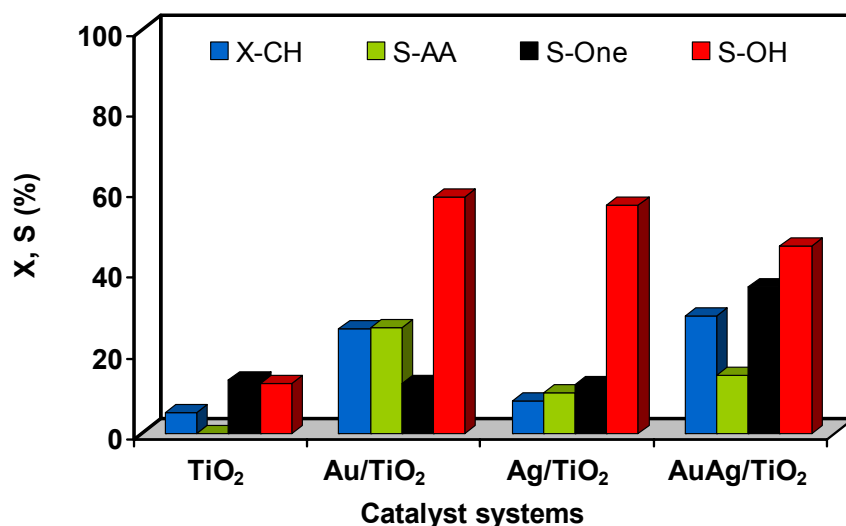


**Fig. 5.13.** Comparison on the catalytic activity of the mono-metallic (Au, Ag) and bi-metallic (Au- Ag) catalysts on the oxidation of cyclohexane, (X= Conversion; Y= Yield; S=Selectivity). (for all other denotations one can refer to Fig. 5.3).

### 5.2.6. Correlation between activity and particle size on the performance of catalyst

The correlation between the particle size and catalytic performance of various supported Au catalysts is portrayed in Figs. 5.15 (a) and (b). It is quite obvious that the activity results are in good agreement with the particle size and hence the conversion of CH and yield of AA are observed to change more or less in a similar fashion as that of Au size. As expected, the smallest AuNPs exhibit the best performance. The conversion of CH decreased from 26 % on TiO<sub>2</sub> supported one to 4 % on CaO supported solid, while the Au size increased from ca. 2 nm (TiO<sub>2</sub>) to 9 nm. Furthermore, the XPS results

also revealed strong evidences that the performance increases with enrichment of Au in the near-surface region. As can be seen from Fig. 5.14(a), TiO<sub>2</sub> supported solid displayed the highest surface Au/M values compared to others, which is similar to the performance. On the other hand, Fig. 5.14(b) also provides additional supporting evidence on the dispersion of Au and active Au metal areas. Again, from this figure it is clear that the TiO<sub>2</sub> exhibit high dispersion and high active metal area and hence the superior performance compared to other supports. On the whole, it can be stated that the better performance of TiO<sub>2</sub> is undeniably due to small Au size, high Au enrichment on the surface, high dispersion and high active metal area. Nevertheless, the influence of other parameters such as acidity characteristics, reducibility etc. cannot be ruled out.

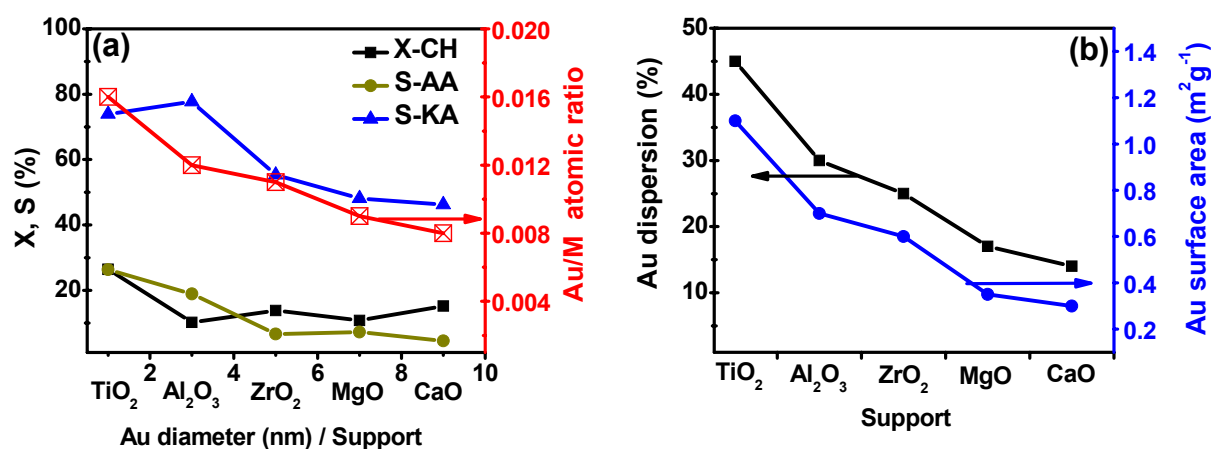
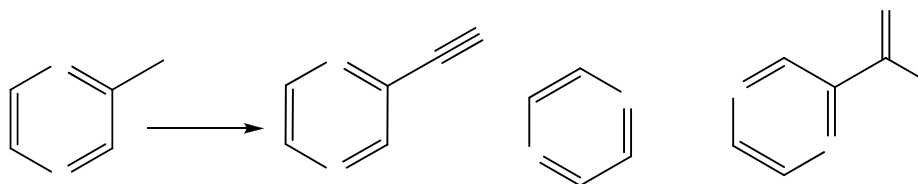


**Fig. 5.14.** The correlations between activity against Au size, Au/M ratio, dispersion and active Au area. a) activity & Au/M surface ratio against Au size (support) and b) dispersion and active metal area of Au against varying supports.

### 5.3. Application of promoted Au catalysts in gas-phase ammoxidation

The promoting effect of gold in vanadia catalysts used for the ammoxidation of 2-methylpyrazine to 2-cyanopyrazine (scheme 5.4), has been reported in this study. The ammoxidation reaction was carried out in a vertical fixed bed, continuous down flow micro-reactor under the reaction conditions shown in chapter 2 (see 2.3.2.).



**Scheme 5.4.** Overall reaction pathway of ammoxidation of 2-methylpyrazine

### 5.3.1. The role of Au as a promoter on ammoxidation activity of 2-methylpyrazine

In order to determine the effect of promoter (e.g. 1 wt% Au) on the performance of 10 wt%  $V_2O_5$  catalyst that is used in the ammoxidation of 2-MP (scheme 5.4), we have separately prepared pure gold (1% wt.) and pure  $V_2O_5$  (10% wt.) catalysts supported on  $TiO_2$  and tested for this reaction (Fig. 5.14). The preliminary catalytic tests displayed poor performance of the catalysts containing only monometallic system, i.e. either  $Au/TiO_2$  or  $V_2O_5/TiO_2$ . Single component  $Au/TiO_2$  gave a MP conversion of ca. 40 % and <10 % selectivity of CP. The major products here are mainly  $CO_x$  probably due to high combustion. In a similar way, the  $V_2O_5/TiO_2$  gave > 95 % conversion of MP with very poor selectivity of CP. It is noteworthy that  $Au/TiO_2$  and  $V_2O_5/TiO_2$  catalysts lead to the formation of an undesired dealkylation product, pyrazine, in considerably higher amounts in addition to  $CO_x$ . However, the combination of  $V_2O_5$  with Au as promoter (i.e.  $V_2O_5-Au/TiO_2$ ) substantially improved the catalytic performance (X-MP = 76 % & Y-CP = 50). Such enhancement in the performance is undeniably due to synergistic effects between gold and vanadia (see Fig. 5.14). In other words, Au as an effective promoter exhibit strong influence on the activity, selectivity and the lifetime of the catalyst. However, these are only first results and hence some additional experiments are necessary to identify optimum loading of both  $V_2O_5$  and Au in the whole catalyst. It can be concluded that a significant difference in the activity of both catalysts could be related to the synergistic effect between Au and  $V_2O_5$ .

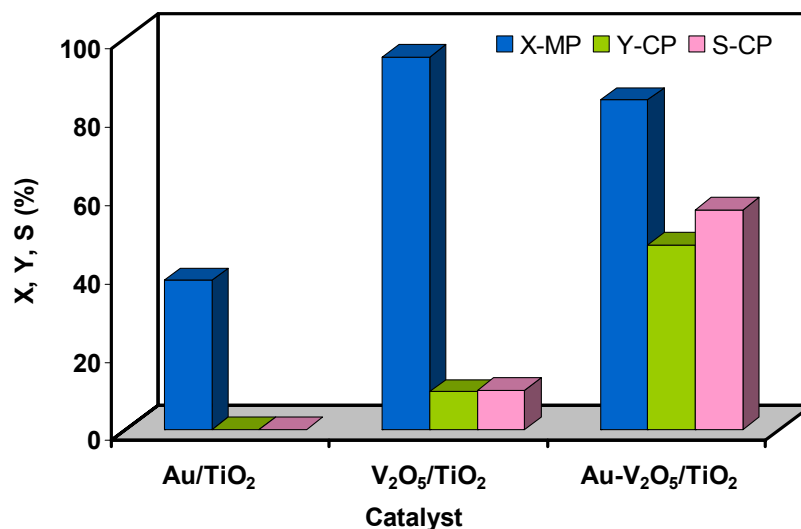


**Fig. 5.14.** Influence of Au as promoter in 10 wt%  $V_2O_5$ -1 wt%  $Au/TiO_2$  on ammoxidation of 2-methylpyrazine to 2-cyanopyrazine. Reaction conditions: (molar ratio of MP :  $H_2O$  :  $NH_3$  : air :  $N_2$  = 1 : 13 : 7 : 26 : 22, T = 360 °C, GHSV = 9506  $h^{-1}$ ). (X=Conversion; Y=Yield; S=Selectivity).



### 5.3.2. Performance of Au promoted $V_2O_5$ catalysts on oxide carriers

The promoting effect of Au on vanadia catalysts supported on different oxides has been tested in the MP ammoxidation reaction. Fig. 5.15 presents the catalytic activity results obtained for the  $V_2O_5$ -Au catalysts supported on MgO, CaO,  $ZrO_2$ ,  $TiO_2$  and  $Al_2O_3$ . It is evident from the figure that the nature of oxide support has a strong influence on the conversion of MP, selectivity and yield of CP, the target product. Additionally, the by-products such as pyrazine, pyrazinamide and  $CO_x$  are also found to depend strongly on the nature of the support. The pyrazine formation is expected from the demethylation of 2-methylpyrazine, which is expected to occur on the stronger acid sites of the catalysts. On the other hand, pyrazinamide might be formed from the partial hydrolysis of 2-cyanopyrazine, the target product. Among all the supports studied,  $TiO_2$  displayed the superior performance while CaO support showed the poor performance. The  $V_2O_5$ -Au/ $TiO_2$  gave 76 % conversion of MP & 47 % yield of CP, whereas  $V_2O_5$ -Au/CaO exhibit very low conversion of MP (ca. 8%) and yield of CP (ca. 2%). On the other hand, the catalysts supported on MgO and  $Al_2O_3$  showed almost complete conversion of MP, but negligible amounts of CP (< 7%). Based on the results obtained, it can be assumed that the differences in the performance of catalysts might be due to the differences in the acidic properties and surface areas of the supports.

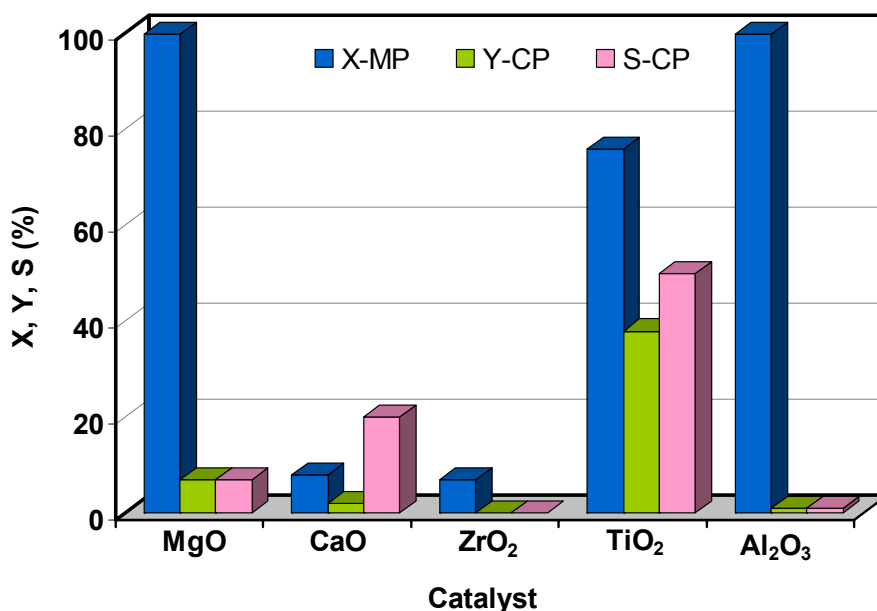


**Fig. 5.15.** Influence of different metal oxides support on ammoxidation of 2-methylpyrazine to 2-cyanopyrazine over Au- $V_2O_5$ /M catalysts, (M= MgO, CaO,  $ZrO_2$ ,  $TiO_2$ ,  $Al_2O_3$ ). Reaction conditions: (molar ratio of MP :  $H_2O$  :  $NH_3$  : air :  $N_2$  = 1 : 13 : 7 : 26 : 22, T = 360 °C, GHSV = 9506  $h^{-1}$ ). (X=Conversion; Y=Yield; S=Selectivity).

### 5.3.3. Performance of Au promoted $V_2O_5$ catalysts on metal oxy-fluorides

We have showed above the influence of various metal oxide carriers on the performance  $V_2O_5$ -Au catalysts. In this part, we present the application their corresponding metal oxy-fluorides as catalyst supports and illustrate their influence on the performance  $V_2O_5$ -Au catalysts with similar composition. These samples are again tested for the same reaction, i.e. ammoxidation of MP to CP. Fig. 5.16 displays the variation in the ammoxidation activity of the Au- $V_2O_5$  catalysts with varying metal oxy-fluorides as novel supports. The metal oxy-fluorides applied in particular are  $MgF_{2-x}(OH)_x$ ,  $CaF_{2-x}(OH)_x$ ,  $ZrF_{2-x}(OH)_x$ ,  $TiF_{4-x}(OH)_x$  and  $AlF_{3-x}(OH)_x$ . As shown above, of all five oxide supports,  $TiO_2$  supported Au- $V_2O_5$  catalyst displayed reasonable performance. However, its corresponding metal oxy-fluoride is surprisingly found to be almost inactive. Furthermore, among all catalysts tested, Au- $V_2O_5$ / $AlF_{3-x}(OH)_x$  displayed the highest activity, with a maximum conversion of MP ca. 20% and selectivity of CP (ca. 65%). Mg, Ca and Zr oxy-fluorides supported Au- $V_2O_5$  catalysts displayed poor activity (X-MP = ca.10% & S-CP =  $\leq$  20%). It can be concluded from these results that oxy-fluorides carriers show relatively much poor performance compared to their corresponding oxide carriers and hence they are not suitable supports for this reaction.

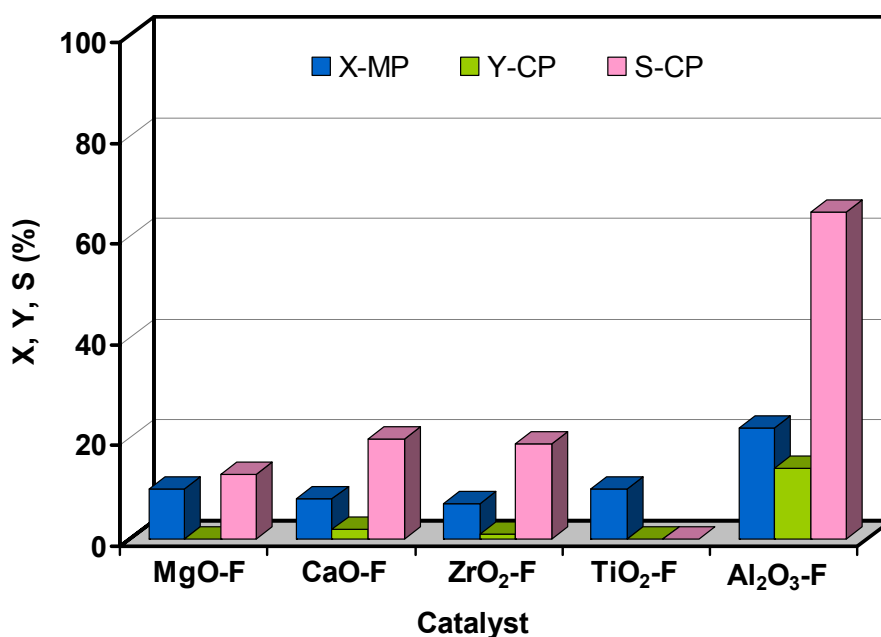


**Fig. 5.16.** Influence of different metal oxy-fluoride supports on the ammoxidation of 2-methylpyridine to 2-cyanopyridine over Au- $V_2O_5$ /M catalysts (M =  $MgF_{2-x}(OH)_x$ ,  $CaF_{2-x}(OH)_x$ ,  $ZrF_{4-x}(OH)_x$ ,  $TiF_{4-x}(OH)_x$ ,  $AlF_{3-x}(OH)_x$ ). Reaction conditions: (molar ratio of MP :  $H_2O$  :  $NH_3$  : air :  $N_2$  = 1 : 13 : 7 : 26 : 22, T = 380 °C, GHSV = 9506 h<sup>-1</sup>). (X=Conversion; Y=Yield; S=Selectivity).

#### 5.3.4. Influence of temperature on the catalytic activity of $V_2O_5$ -Au/TiO<sub>2</sub> solid

Temperature is one of the most important parameters to be considered in increasing the catalytic performance. In terms of activity,  $V_2O_5$ -Au/TiO<sub>2</sub> has been selected as the most active catalyst in ammoxidation of 2-methylpyrazin to 2-cyanopyrazine. Therefore, this catalyst has been examined at different reaction temperatures and their product distributions are plotted in Fig. 5.17. It is evident from this figure that the temperature has a promotional effect on the conversion of MP, which has increased from ca. 67 to 84% with increase in temperature from 360 to 400 °C. The increase in conversion values with increase in reaction temperature is due to kinetic effect. The selectivity of CP is observed to increase continuously from 45 to 62% with increase in temperature 360 to 380 °C and then decrease slightly with further increase in temperature to 400 °C. This result clearly indicates that at higher temperature, the selectivity of CP decreased because at high temperature oxidative dealkylation of MP seems to become prominent, which leads to the formation of undesired pyrazine.

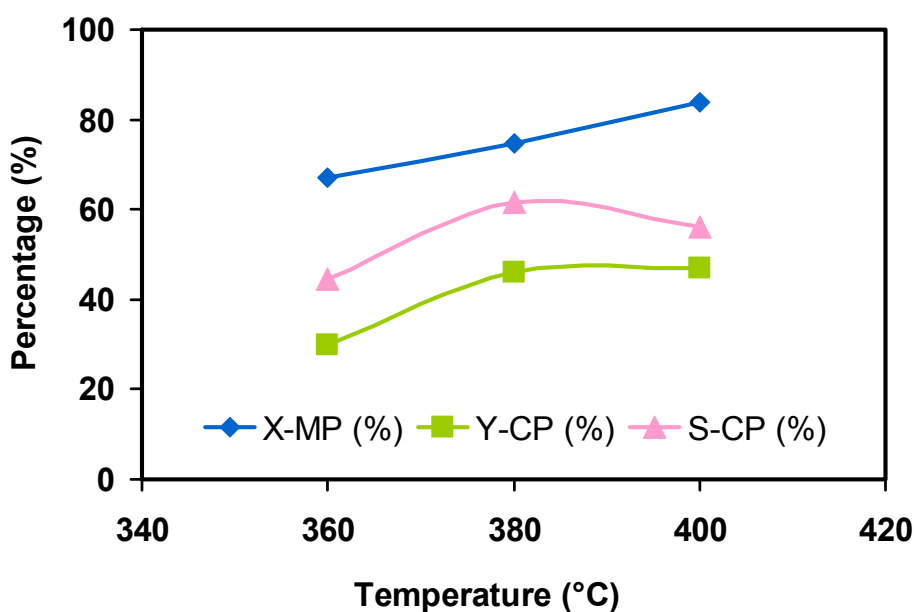


Fig. 5.17. Influence of temperature on the activity and selectivity of  $V_2O_5$ -Au/TiO<sub>2</sub> catalyst (X= Conversion; Y= Yield; S=Selectivity).

---

## **6. Conclusions**

---

## 6.1. Summary and Conclusions

In summary, the conclusions are made mainly based on three aspects such as i) *synthesis* of colloidal AuNPs and other catalysts, ii) *characterization* of colloids and other samples and iii) *catalytic activity* of colloidal, supported and promoted AuNPs. The conclusions drawn from these results are briefly summarized below one after the other.

### *i) Synthesis*

Depending upon the reaction conditions applied, nature of reagents used the size of colloidal AuNPs obtained are varied over a wide range from 1 nm to 50 nm in the initial stages of the investigations. However, better control on the size and stability of AuNPs could be successfully achieved through the experiments performed during the course of this study. Additionally deeper insights on the factors that are responsible for controlling Au size and distribution are identified and optimized. Most of these AuNPs were prepared through a simple one-step chemical reduction of [HAuCl<sub>4</sub>] solution using different reductants and also by varying the reaction conditions. Different reaction parameters (e.g. T, pH, stirring speed, concentration of Au precursor etc.) are found to affect significantly the size and stability of Au particles. In view of this, all such parameters are well optimized with a goal to obtain the smaller and stable AuNPs. The optimized conditions are as follows: T = 60 °C; reductant / [HAuCl<sub>4</sub>] = 4 : 1. pH = 3.0; [HAuCl<sub>4</sub>] = 1.0 mM. Additionally, the nature of reducing agent and also the influence of combination of two such reducing agents on the size of Au are also investigated. For this study, six different reducing agents and two combinations were examined. Gold colloids formed in the presence of citric acid and sodium citrate in aqueous solution without any additional surfactant or stabilizer were found to be stable with particle sizes of 10 and 50 nm, respectively, while unstable colloidal AuNPs were obtained from iso-ascorbic acid, sodium borohydride, tannic acid and sodium thiocyanate with particle size ranging from 3 to 20 nm. Furthermore, application of single reducing agents such as SC and TA gave bigger AuNPs ca. 12 nm and 17 nm, respectively. Nevertheless, combination of reductants (SC & TA) showed strong influence on the rate of reduction, size and reduction steps compared to the reduction using a single reductant. The smallest AuNPs of 3 nm (average size) could be successfully obtained using combination of two reducing agents (SC+TA). Based on the results obtained, it can be said that the size, size distribution, shape, stability, rate of reduction, and formation mechanism are found to depend strongly on the nature of reducing agent and synthesis conditions applied.

In addition, the preparation of supported and promoted gold catalysts using different oxide carriers and their novel corresponding oxy-fluorides have been successfully

carried out using impregnation technique. Besides, the preparation of two different bimetallic catalysts systems (e.g. Au+Ag & Au+Pd) containing AuNPs has also been carried out. These preparations involve the preparation of colloidal AuNPs in the first step and then its further impregnation onto support in the 2<sup>nd</sup> step followed by oven drying and calcination. This preparation gave the small AuNPs in the range from 2 to 10 nm. Interestingly, both mono and bi-metallic catalysts gave comparable size of AuNPs.

### *ii) Characterisation*

UV-Vis, DLS, SEM and TEM are used to examine the morphology, average size, size distribution, and stability of colloidal AuNPs. Microscopic methods (TEM & SEM) proved that a variety of shapes of AuNPs, i.e., spheres, triangles, wires, etc., were obtained using different reducing agents (SC, SB, TA etc.), demonstrating the strong influence of their nature on the shape and stability of AuNPs. UV-Vis and DLS gave good supporting evidence for the observations made from TEM & SEM.

The supported and promoted AuNPs were characterized by various including microscopic and spectroscopic techniques. The metal contents of all samples were estimated by ICP and XRF and found to be in line with theoretical values. BET-SA is found to depend on the nature of support used. The highest surface area (360 m<sup>2</sup>/g) was exhibited by Au/MgF<sub>2-x</sub>(OH)<sub>x</sub>, while the smallest (22 m<sup>2</sup>/g) by CaO supported catalyst. Thermal treatment of the prepared catalysts up to 350 °C did not cause any significant sintering of the Au particles, which however depended on the type of support used. In addition, the nature of support used has a notable influence on the structure, morphology and the size of AuNPs (HRTEM, XRD). Among all supports used, the TiO<sub>2</sub> support displayed the smallest AuNPs (2 nm) with narrow distribution and hence the best catalytic performance. Interestingly, the Au dispersion and active Au area calculated from TEM is observed to be higher for TiO<sub>2</sub> supported solid compared to others. XRD analysis revealed no reflections correspond to crystalline Au in TiO<sub>2</sub> and Al<sub>2</sub>O<sub>3</sub> supported catalysts. This fact suggests that the Au in these samples might be X-ray amorphous and also seem to be well-dispersed on the surface of the support. Activity results gave good support for such assumption. Conversely, MgO, CaO and ZrO<sub>2</sub> showed very weak reflections correspond to crystalline metallic Au phase. Moreover, metal oxy-fluoride supported catalysts mixed phases that correspond to oxide and fluoride in varying proportions. Fluorine and aluminum species in the prepared catalysts are confirmed by solid state NMR, which is attributable to octahedral AlF<sub>6</sub> environments. XPS revealed a clear surface enrichment of Au particularly in TiO<sub>2</sub> supported catalyst compared to other supports. The particle size of Au in supported metal oxide carriers is smaller compared to their corresponding oxy-fluorides. EDX analysis on bi-metallic catalysts, e.g. Au-Pd catalyst reveals that the surface consists of

both metals while Au-Ag seems to form alloy phases. However, XRD analysis did not show any such reflections correspond to metals indicating that the size of the metal crystallites might be less than 5 nm. Such observation is also supported by TEM results. In addition, gold promoted vanadia catalysts are also characterized by various techniques and interesting results were obtained. One such interesting observation is decreased Au size in the promoted samples compared to its corresponding Au alone supported catalysts.

### *iii) Catalytic activity*

The catalytic activity of colloidal (unsupported), supported and promoted AuNPs has been investigated for three different reactions such as a) colloidal AuNPs for homocoupling of phenylboronic acid to biphenyl, b) supported AuNPs for the oxidation of benzyl alcohol to benzaldehyde and also the oxidation of cyclohexane to adipic acid, c) promoted catalysts for ammoxidation of 2-methylpyrazine to 2-cyanopyrazine.

a) It has been found that the colloidal AuNPs are effective catalysts for the homocoupling of phenylboronic acid to biphenyl. The yields of biphenyl are found to depend on the size of AuNPs. The smaller the size of Au, the higher the catalytic performance.

(b) AuNPs supported on metal oxide carriers displayed excellent activity for oxidation of benzyl alcohol to benzaldehyde compared to their corresponding oxy-fluorides. Among all catalysts, TiO<sub>2</sub> supported AuNPs exhibited a higher activity (X-BA = 81%, S-BAI = 95%) in the oxidation of benzyl alcohol. These results are comparable to the existing literature reports. However, in case of oxy-fluoride carriers, again TiF<sub>4-x</sub>(OH)<sub>x</sub> has shown better performance (X-BA = 33%, S-BAI = 67%) compared to all other oxy-fluorides. In addition, using “green chemistry”, supported AuNPs on TiO<sub>2</sub> is found to be active for the production of adipic acid using one-pot oxidation of cyclohexane. Under optimized conditions (400 mg of Au/TiO<sub>2</sub> catalyst, acetonitrile as solvent, TBHP as initiator, 10 bar of O<sub>2</sub>, 150 °C), it is possible to produce adipic acid with ca. 8% yield from the best case. On other hand, metal oxy-fluorides as carriers are found to be not suitable for this reaction. Amazingly, good correlation between Au size, dispersion, Au/M ratio and catalytic activity is obtained.

(c) We have also shown that good synergy between Au and V<sub>2</sub>O<sub>5</sub> could be noticed in Au promoted V<sub>2</sub>O<sub>5</sub> catalysts. Interestingly, the performance of V<sub>2</sub>O<sub>5</sub>-Au/TiO<sub>2</sub> is much superior in the ammoxidation of 2-methylpyrazine to 2-cyanopyrazine (X-MP = 76%) and selectivity (S-CP = 50%), compared to its parent catalysts such as Au alone (Au/TiO<sub>2</sub>) or V<sub>2</sub>O<sub>5</sub> alone (V<sub>2</sub>O<sub>5</sub>/TiO<sub>2</sub>).

Finally, we have proved in the present study that the size of Au plays a key role on the catalytic performance. Such beneficial effect of small AuNPs is commonly observed in all the three reactions investigated in the present study. In particular, it is proved that the production of adipic acid with 8% yield through the one-pot oxidation of cyclohexane is indeed a remarkable achievement of this study.

## 6.2. Outlook

In the last ten years, marked advances have been made in controlling the size, morphology and synthetic methodologies of AuNPs. Researchers have already shown that the final architecture of nanoparticles and the morphology can be controlled by synthetic approaches and by modulating the chemical and redox environments. Synthesis of stable AuNPs on oxide carriers introduces some new possibilities for catalysis because the properties of such AuNPs are different from those of bulk or isolated atoms. Furthermore, such AuNPs are expected to interact effectively with the support and such interaction can stabilize the surface charged species, which act as Lewis sites that are necessary for a catalytic reaction to occur. Nevertheless, the extent of such interaction depends on the type of support used. As a result, the catalytic applications of AuNPs can be expanded to various new reactions. However, highly unsaturated systems are more preferred and ideal to have large number of active Au sites on the surface via an effective interaction between active phase and the support. The mechanistic principles could also serve as a set of design rules for preparing novel nanostructures with desired architecture and unique properties. Furthermore, it is going to be real gift if one could stabilise and control the formation mechanism of various other nanoparticles (e.g. Pd, Pt, Rh, Ir etc.) so that the concepts and reactions developed with the homogeneous catalysis could be directly transferred into heterogeneous catalysis. Coming to commercial application, the main issue in industrial processes is productivity based on activity and selectivity. The productivity is also based on stability and durability of supported AuNPs. The motivation for these investigations made through the present study was provided by the importance of small particles in different catalytic processes and especially the role of gold nanoparticles in the three different reactions studied here in liquid and gas phase. Another research direction is the synthesis of bifunctional and/or multifunctional AuNPs, which might give either new products or existing products in one-pot multistep reactions (e.g. one-pot oxidation of cyclohexane to adipic acid of the present study). The results presented in this work might open new perspectives for future experiments, particularly the results obtained from the direct oxidation of cyclohexane to adipic acid. Nevertheless, further work is still required to gain deeper insights on controlling the size, morphology, growth mechanism etc. and to realize the



potential of such AuNPs for novel applications. The discovery and subsequent research efforts could further improve the fundamental understanding on the dynamics of formation of nanostructured AuNPs and extension of their application into different areas other than catalysis such as bio-medicine, optics, electronics etc.

On the other hand, the ammoxidation is an economic, eco-friendly and valuable tool for one-step syntheses of a large number of industrially important nitriles that can be further used to produce a variety of specialty and fine chemicals. It could be interesting if novel catalytic routes are developed to enable higher selectivity of highly functionalized nitriles. Some new approaches to the rational design and synthesis of improved catalysts would be of great interest for future ammoxidation processes. Therefore, future trends must aim greatly towards the discovery and development of potential catalysts. In parallel to catalyst developments made by chemists, chemical engineers must also develop new concepts, new reactor designs etc. Microstructured reactors may help to master exothermicity, probably membranes can enhance oxygen mobility in a selective direction according to Mars-van Krevelen mechanism and thereby total and non-selective oxidation paths can be avoided. The present ammoxidation is not only important from commercial point of view but also present opportunities for fundamental research and also contribute well to the well-being of modern mankind. Even though great deal has already been achieved in the field of ammoxidation, new approaches and new attempts are certainly necessary to discover novel catalysts capable of activating ammonia relatively at lower temperatures to prevent unavoidable ammonia oxidation, which gives higher amounts of NO<sub>x</sub> and hence reduced nitrile selectivities. Furthermore, rational approaches need to be worked out in the coming years to sequence various functionalities in the direction of developing novel, attractive and eco-friendly ammoxidation processes.

## References

---

- [1] R. F. Service, *Science* 304 (2004) 1732
- [2] A. Henglein, *Chem. Rev.* 89 (1989) 1861
- [3] G. D. Stucky and J. E. MacDougall, *Science* 247 (1990) 669.
- [4] G. Schmid (Ed.): *Clusters and Colloids. From theory to Applications* (VCH, Weinheim, 1994).
- [5] N. Toshima and T. Yonezawa, *New J. Chem.* 22 (1998) 1179.
- [6] N. Toshima and Y. Shiraishi, *Catalysis by metallic colloids*. In: *Encyclopedia of Surface and Colloid Science*, edited by A. T. Hubbard (Marcel Dekker, New York, 2002), pp. 879-886.
- [7] G. C. Bond and D. T. Thompson, *Catal. Rev.* 41 (1999) 319.
- [8] M. Haruta, *Chem. Record* 3 (2003) 75.
- [9] A. G. Sault, R. J. Madix, C. T. Campbell, *Surf. Sci.* 169 (1986) 347.
- [10] B. Hammers and J. K. Nørskov, *Nature* 376 (1995) 238.
- [11] P. A. Sermon, G. C. Bond, P. B. Wells, *J. Chem. Soc.; Faraday Trans.1*, 75 (1979) 385.
- [12] G. J. Hutchings, *J. Catal.* 96 (1985) 292.
- [13] M. Haruta, T. Kobayashi, H. Sano, N. Yamada, *Chem. Lett.* 2 (1987) 405.
- [14] C.-J. Liu, T. Hammer and R. Mallinson, *Catal. Today* (2004) 98.
- [15] J. M.C. Soares, P. Murrall, A. Crossley, P. Harris, M. Bowker, *J. Catal.* 219 (2003) 17.
- [16] A. M. Venezia, L. F. Liotta, G. Pantaleo, V. La Parola, G. Deganello, A. Beck, Zs. Koppány, K. Frey, D. Horváth, L. Gucci, *Appl. Catal., A:General* 251 (2003) 359.
- [17] M. Valden, X. Lai, D.W. Goodman, *Science* 281 (1998) 1647.
- [18] C.T. Campbell, *Science* 306 (2004) 234.
- [19] J.A. van Bokhoven, *Chimia* 63 (2009) 257.
- [20] I.N. Remediakis, N. Lopez, J.K. Nørskov, *Angew. Chem.-Int. Ed.* 44 (2005) 1824.
- [21] N. Lopez, J.K. Nørskov, *J. Am. Chem. Soc.* 124 (2002) 11262.
- [22] G. C. Bond and R. Burch, *Specialist Periodical Reports: Catalysis*, Vol. 6 (Roy. Soc. Chem., London, 1983) p. 27.
- [23] A. H. Guerrero, H. J. Fasoli, J. L. Costa, *J. Chem. Educ.* 76 (1999) 200.
- [24] J. J. Lagowski, *Gold Bull.* 16 (1983) 8.
- [25] G. Bond and D. T. Thompson, *Catalysis Reviews*, 41 (1999) 319.
- [26] U. Kreibitz and M. Vollmer, *Optical Properties of Metal Clusters*, Springer-verlag, 1996.
- [27] M. C. Daniel and D. Astruc, *Chem. Rev.* 104 (2004) 293.
- [28] E. Katz and I. Willner, *Angew. Chem. Int. Ed.* 43 (2004) 6042.
- [29] J. Turkevich and G. Kim, *Science* 169 (1970) 873.
- [30] J. Turkevich, *Gold Bulletin* 18 (1985) 86.
- [31] T. Teranishi and N. Toshima, *Preparation, characterization and properties of bimetallic nanoparticles*. In: *Catalysis and Electrocatalysis at Nanoparticle Surfaces*, edited by E. R. Savinova, et al. (Marcel Dekker, New York, 2002).
- [32] M. A. Debeila, N. J. Coville, M. S. Scurrall and G. C. Hearne, *Appl. Catal. A* 219 (2005) 98.
- [33] J. S. Bradley, *The chemistry of transition metal colloids*. In: *Clusters and Colloids. From Theory to Application*, edited by G. Schmid (VCH, Weinheim, 1994), pp. 459-544.
- [34] G. Schmid, *Clusters and Colloids: From Theory to Applications*, 1994. pp. 469.
- [35] H. Bönemann, R. M. Richards, *Nanoscopic metal particles-synthetic methods and potential applications*. *Eur J. Inorg Chem.* (2001) 2455.
- [36] G. Y. Cha and G. Parravano, *J. Catal.* 18 (1970) 200.
- [37] D. T. Thompson, *Gold Bull.* 32 (1999) 12.
- [38] B. E. Salisbury, W. Wallace, R. L. Whetten, *Chem. Phys.* 262 (2000) 131.

- 
- [39] V. Ponce and G. C. Bond, *Catalysis by Metals and Alloys*, Elsevier, Amsterdam, 1996.
- [40] P. A. Sermon, G.C. Bond and P.B. Wells, *J. Chem. Soc. Faraday Trans.* 75 (1979) 385.
- [41] L. A. Hermans and J. W. Geus, *Stud. Surf. Sci. Catal.* 4 (1979) 113.
- [42] Q. Xu, K. C. C. Kharas and A. K. Datye, *Catal. Lett.* 85 (2003) 229.
- [43] L. Prati, M. Rossi, *Green Chemistry: Challenging Perspectives*, P.Tundo, P. Anastas eds., Oxford 2000, p.183.
- [44] J. D. Grunwaldt, C. Kiener, C. Wogerbauer, A. Baiker, *J. Catal.* 181 (1999) 223.
- [45] F. Boccuzzi, A. Chiorino, M. Manzoli, P. Lu, T. Akita, S. Ichikawa, M. Haruta, *J. Catal.* 202 (2001) 256.
- [46] E. D. Park, J. S. Lee, *J. Catal.* 186 (1999) 1.
- [47] N. A. Hodge, C. J. Kiely, R. Whyman, M. R. H. Siddiqui, G. J. Hutchings, Q. A. Pankhurst, F. E. Wagner, R. R. Rajaram, S. E. Golunski, *Catal. Today* 72 (2002) 133.
- [48] S.-J. Lee, A. Gavriilidis, Q. A. Pankhurst, A. Kyek, F. E. Wagner, P. C. L. Wong, K. L. Yeung, *J. Catal.* 200 (2001) 298.
- [49] R. J. H. Grisel, B. E. Nieuwenhuys, *J. Catal.* 199 (2001) 48.
- [50] S. D. Lin, M. Bollinger and M. A. Vannice, *Catal. Lett.* 17 (1993) 245.
- [51] S. D. Lin, M. Bollinger and M. A. Vannice, *Catal. Lett.* 10 (1991) 47.
- [52] D. A. H. Cunningham, W. Vogel, H. Kageyama, S. Tsubota, M. Haruta, *J. Catal.* 177 (1998) 1.
- [53] G. J. Hutchings, *Gold Bull.* 29 (1996) 123.
- [54] M. Haruta, N. Yamada, T. Kobayashi and S. Iijima, *J. Catal.* 115 (1989) 301.
- [55] S. D. Gardner, G. B. Hoflund, B. T. Upchurch, D. R. Schryer, E. J. Kielin and J. Schryer, *J. Catal.* 129 (1991) 114.
- [56] G. C. Bond and D. T. Thompson, *Catal. Rev. Sci. Eng.* 41 (1999) 319.
- [57] M. Haruta, *Gold Bull.* 37 (2004) 27.
- [58] A. Ueda, T. Oshima and M. Haruta, *Appl. Catal. B* 12 (1997) 81.
- [59] M. A. P. Dekkers, M. J. Lippits and B. E. Nieuwenhuys, *Catal. Today* 54 (1999) 381.
- [60] P. Claus, A. Bruckner, C. Mohr and H. Hofmeister, *J. Am. Chem. Soc.* 122 (2000) 11430
- [61] D. Andreeva, V. Idakiev, T. Tabakova and A. Andreev, *J. Catal.* 158 (1996) 354.
- [62] S. D. Lin, A. C. Gluhoi and B. E. Nieuwenhuys, *Catal. Today* 90 (2004) 3.
- [63] S. Minico, S. Scire, C. Crisafulli, R. Maggiore and S. Galvagno, *Appl. Catal. B* 28 (2000) 245.
- [64] M. Haruta, A. Ueda, S. Tsubota and R. M. Torres Sanchez, *Catal. Today* 29 (1996) 443.
- [65] W. D. Provine, P. L. Mills and J. J. Lerou, *Stud. Surf. Sci. Catal.* 101 (1996) 191.
- [66] British Patent 1 372 245; *Gold Bull.* 8 (1975) 63.
- [67] German Offen. 2 315 570; *Chem. Abstr.* 83 (1975) 63384.
- [68] T. Mallat and A. Baiker, *Chem. Rev.* 104 (2004) 3037.
- [69] L. Prati, L. and M. Rossi, *J. Catal.* 176 (1998) 552.
- [70] F. Porta, L. Prati, M. Rossi, S. Colluccia and G. Martra, *Top. Catal.* 13 (2000) 231.
- [71] L. Prati, *Gold Bull.* 32 (1999) 96.
- [72] S. Carretin, P. McMorn, P. Johnston, K. Griffin and G. J. Hutchings, *Chem. Commun.* 4 (2002) 696.
- [73] S. Carretin, P. McMorn, P. Johnston, K. Griffin, C. J. Kiely and G. J. Hutchings, *Phys. Chem. Chem. Phys.* 5 (2003) 1329.
- [74] A. Abad, P. Concepción, A. Corma and H. Garcíá, *H. Angew. Chem., Int. Ed.* 44 (2005) 4066.
- [75] D. I. Enache, J.K. Edwards, P. Landon, B. Solsona-Espriu, A. F. Carley, A. A. Herzing, M. Watanabe, C. J. Kiely, D. W. Knight and G. J. Hutchings, *Science*, 311 (2006) 362.
- [76] P. J. Miedziaka, Q. Heb, J. K. Edwardsa, S. H. Taylora, D. W. Knighta, B. Tarbitc, C. J. Kielyb, G. J. Hutchingsa, *Catal. Today* (2010) in press.

- 
- [77] U. Schuchardt, D. Cardoso, R. Sercheli, R. Pereira, R. S. da Cruz, M. C. Guerreiro, D. Mandelli, E. V. Spinace and E. L. Pires, *Appl. Catal. A* 211 (2001) 1.
- [78] K. Weissmehl and H.-J. Harpe, *Industrial Organic Chemistry*, Wiley-VCH, Weinheim, 4<sup>th</sup> edn, 2003.
- [79] P. V. Saji, C. Ratnasamy. S. Gopinathan, S. U.S. Patent 6,392,093, B1, 2002.
- [80] W. Morris, GB Patent 1304 855 (1973).
- [81] J. G. Schulz and A. C. Whitaker, US Patent 3390174 (1968).
- [82] F. T. Starzyk, *Studies in Surf. Sci. and Catal.*, 84 (1994) 1419.
- [83] Y. J. Xu, P. Landon, D. Enache, A. F. Carley, M. W. Roberts, G. J. Hutchings, *Catal. Lett.* 101 (2005) 175.
- [84] G. Lu, R. Zhao, G. Qian, Y. Qi, X. Wang, J. Suo, *Catal. Lett.* 97 (2004) 115.
- [85] G. Lu, D. Ji, G. Qian, Y. Qi, X. Wang, J. Suo, *Appl. Catal. A*. 280 (2005) 175.
- [86] A. Corma, J. Lopez Nieto, (2007) US Patent, 7, 166, 751.
- [87] L.X. Xu, C.H. He, M.Q. Zhu, K.J. Wu, Y.L. Xu, *Catal. Lett.* 118 (2007) 248.
- [88] B. P. C. Hereijgers, B. M. Weckhuysen, *J. Catal.* 270 (2010) 16.
- [89] V. N. Kalevaru, B. D. Raju, V. V. Rao and A. Martin, *Catal. Commun.* 9 (2008) 715.
- [90] F. K Hannour, A. Martin, B. Kubias, B. Lücke, E. Bordes and P Courtine, *Catal. Today*. 40 (1998) 263.
- [91] A. Martin and V. N. Kalevaru, *ChemCatChem.* 2 (2010) 1.
- [92] M. Ai, K. Ohdhan and J. Mol., *Catal. A*. 159 (2000) 19.
- [93] P. Scherrer and *Nachr. K. Ges. Wiss., Göttingen* 98 (1918).
- [94] G. H. Jiang, L. Wang, T. Chen, H. J. Yu and A. K. Chen, *Mater. Chem. Phys.* 98 (2006) 76.
- [95] J. M. Petroski, Z. L. Wang, T. C. Green and M. A. El-Sayed, *J. Phys. Chem. B* 102 (1998) 3316.
- [96] J. Turkevich, *Gold Bull.* 18 (1985) 86.
- [97] K. S. Mayya, V. Patil and M. Sastry, *Langmuir* 13 (1997) 3944.
- [98] M. M. Alvarez, J. T. Khoury, T. G. Schaaf, M. N. Shafiqullin, I. Vezmar and R. L. Whetten, *J. Phys. Chem. B* 101 (1997) 3706.
- [99] J. A. Creighton and D. G. Eadon, *J. Chem. Soc., Faraday Trans.* 87 (1991) 3881.
- [100] M. M. Alvarez, J. T. Khoury, T. G. Schaaff, M. N. Shafiqullin, I. Vezmar and R. L. Whetten, *J. Phys. Chem. B* 101 (1997) 3706.
- [101] J. C. Valmalette, L. Lemaire, G. L. Hornyak, J. Dutta and H. Hofmann, *Anal. Mag.* 24 (1996) 23.
- [102] S. Link and M. A. El-Sayed, *J. Phys. Chem.* 103 (1999) 3073.
- [103] M. Yamada and H. Nishihara, *ChemPhysChem.* 5 (2004) 555.
- [104] G. Frens, *Phys. Sci.* 241 (1973) 20.
- [105] A. I. Kirkland, P. P. Edward, D. A. Jefferson and D. G. Duff, *Annu. Rep. Prog. Chem.* 87 (1990) 247.
- [106] S. Link, C. Burda, Z. L. Wang and M.A. El-Sayed, *J. Chem. Phys.* 111(1999) 1255.
- [107] J. L. Yao, G. P. Pan, K. H. Xue, D. Y. Wu, B. Ren, D. M. Sun, J. Tang, X. Xu and Z. Q. Tian, *Pure Appl. Chem.* 72 (2000) 221.
- [108] S. Link, M. A. El-Sayed, *Annu. Rev. Phys. Chem.* 54 (2003) 331.
- [109] G. Mie, *Ann. Phys.* 25 (1908) 377.
- [110] C. L. Haynes and R. P. Van Duyne, *J. Phys. Chem. B* 105 (2001) 5599.
- [111] R. Jin, Y. Cao, C. A. Mirkin, K. L. Kelly, G. C. Schatz, J. G. Zheng, *Science* 294 (2001) 1901.
- [112] M. D. Malinsky, K. L. Kelly, G. Schatz, R. P. Van Duyne, *J. Am. Chem. Soc.* 123 (2001) 1471.
- [113] P. Mulvaney, *Langmuir* 12 (1996) 788.

- 
- [114] I. O. Sosa, C. Noguez and R. G. Barrera, *J. Phys. Chem. B* 107 (2003) 6269.
- [115] U. Kreibig and L. Genzel, *Surf. Sci.* 156 (1985) 678.
- [116] B. K. Jena and C. R. Raj, *Langmuir* 23 (2007) 4064.
- [117] C. D. Chen, Y. T. Yeh and C. R. Wang, *J. Phys. Chem Solids* 62 (2001) 1587.
- [118] S. Link, M. B. Mohamed and M. A. El-Sayed, *J. Phys. Chem. B* 103 (1999) 8410.
- [119] B. K. Pong, H. I. Elim, J. X. Chong, B. L. Trout and J. Y. Lee, *J. Phys. Chem. C*, 111 (2007) 6281.
- [120] M. H. Lee and D. G. Park, *bull. Korean Chem. Soc.* 24 (2003) 1437.
- [121] M. J. Hologado, V. Rives and S. San Román, *J. of Mate. Sci. Lett.*, 11 (1992) 1708.
- [122] P. J. Chupas, M. F. Ciruolo, J. C. Hanson and C. P. Grey, *J. Am. Chem. Soc.*, 123 (2001) 1694.
- [123] R. König, G. Scholz, T. H. Thong and E. Kemnitz, *Chem. Mater.*, 19 (2007) 2229.
- [124] J. Hutchings, M.S. Hall, A.F. Carley, P. Landon, B.E. Solsona, C.J. Kiely, A. Herzing, M. Makkee, J.A. Moulijn, A. Overweg, J.C. Fierro-Gonzalez and B.C. Gates, *J. Catal.* 242 (2006), 71.
- [125] S. Schimpf, M. Lucas, C. Mohr, U. Rodemerck, A. Brückner, J. Radnic, H. Hofmeister and P. Claus, *Catal. Today* 72 (2002), 63.
- [126] G. C. Bond in *Handbook of Heterogeneous Catalysis*, G. Ertl, H. Knoezinger and J. Weitkamp, (eds.) VCH, Weinheim, 1997, Vol. 2, p. 752.
- [127] R. Narayanan and M. A. El-Sayed, *Top. Catal.* 47 (2008)15.
- [128] G. A. Somorjai and F. Tao, J. Y. Park, *Top. Catal.* 47 (2008) 1.
- [129] C. González-Arellano, A. Corma, M. Iglesias and F. Sánchez, *J. of Catal.* 238 (2006) 497.
- [130] Yang Li, Xiaobin Fan, Junjie Qi, Junyi Ji, Shulan Wang, Guoliang Zhang and Fengbao Zhang, *Mat. Res. Bulletin*, 45 (2010) 1413.
- [131] P. Beltrame, M. Comotti, C. D. Pina and M. Rossi, *J. Applied Catal. A*, 297 (2006) 1.
- [132] B. Imelik (Eds.), *Metal-support and Metal-Additive Effects in Catalysis* (Elsevier Scientific Pub. Co., Amestrdam, 1982).
- [133] K. Foger, in: J. R. Anderson and M. Boudart (Eds.), *Catalysis, Science and Tchnology*, Vol. 6 (Springer, Berlin, 1984) p.227.
- [134] G. C. Bond and R. Burch, *Specialist Periodical Reports: Catalysis*, Vol. 6 (Roy. Soc. Chem., London, 1983) p. 27.
- [135] R. Burch, *Specialist Periodical Reports: Catalysis*, Vol. 7 (Roy. Soc. Chem., London, 1995) p. 149.
- [136] T. Ishihara, K. Harada, K. Eguchi and H. Arai, *J. Catal.* 136 (1992) 161.
- [137] A. Y. Stakheev and L. M. Kustov, *Appl. Catal. A* 188 (1999) 3.
- [138] S. J. Taustr, S. C. Fung and R. L. Garten, *J. Am. Chem. Soc.* 100 (1978) 170.
- [139] S. J. Taustr, S. C. Fung and R. T. K. BarKer and J. A. Horsley, *Science*. 221 (1981) 1121.
- [140] P. J. Chupas and C. P. Grey, *J. Catal.* 224 (2004) 69.
- [141] B. Bureau, G. Silly, J.Y. Buzare, J. Emery, *Chem. Phys.* 249 (1999) 89.
- [142] A. Alshammari, A. Köckritz, V. N. Kalevaru, A. Martin, EU Patent P08285EP, (2010).
- [143] C. A. Tolman, J. D. Druliner, M. J. Nappa and N. Herron, *Alkane oxidation studies in Functionalization of Alkanes*, first ed., Wiley-Interscience, New York, 1989, p. 316.
- [144] U. Schuchardt, D. Cardoso, R. Sercheli, R. Pereira, R. S. da Cruz, M. C. Guerreiro, D. Mandelli, E. V. Spinacé and E. L. Pires, *J. Appl. Catal. A* 211 (2001) 1.

---

# Appendix

---

## List of Abbreviations, Acronyms and Symbols

Å	Angstrom
BE	Binding Energy
BET	Brunauer-Emmett-Teller and their adsorption model
°C	degree Celsius
DTA	Differential Thermal Analysis
DTG	Differential Thermogravimetry
DLS	Dynamic Light Scattering
EDX	Energy-Dispersive X-ray emission spectroscopy
FTIR	Fourier transformation Infrared spectroscopy
GC	Gas Chromatography
ICP	Inductively Coupled Plasma
K	Kelvin
NMR	Nuclear Magnetic Resonance
RT	Room Temperature
SEM	Scanning Electron Microscopy
TEM	Transmission Electron Microscopy
TG	Thermogravimetric analysis
UV-Vis	Ultraviolet-Visible Spectroscopy
XRD	X-Ray Diffraction
XRF	X-ray Fluorescence Spectrometry
XPS	X-ray Photoelectron Spectroscopy

## List of Chemicals

### Solids

Adipic acid (Alfa, 99%)  
Aluminum (Strem, 99.9%)  
Aluminum *tert*-butoxide (Aldrich, 99.9%)  
Aluminium triisopropoxide (Aldrich, 99.8%)  
Ammonium metavanadate (Aldrich, 98%)  
 $\alpha$ -aluminum oxide (Degussa)  
 $\gamma$ -aluminum oxide (Alfa Aesar)

---

Calcium nitrate (Aldrich, ≥98.0%)  
Cerium oxide (Aldrich)  
Citric acid (Aldrich, 99.5%)  
D-(-)-iso-ascorbic acid (Fluka, 99.0%)  
Palladium chloride (Aldrich, 99%)  
Phenylboronic acid (Aldrich, 98.5%)  
Potassium carbonate (Fluka, 99%)  
Potassium hydroxide (Merck, 90%)  
Sodium borohydride (Aldrich, 98%)  
*tri*-Sodium citrate dehydrate (Fluka, 99.5%)  
Sodium thiocyanate (Fluka, 99%)  
Tannic acid (Aldrich, 98%)  
Tetrachloroauric acid (Fluka, 99%)  
Magnesium (Aldrich, 99.98%)  
Magnesium hydroxide (Fluka, 99%)  
Magnesium nitrate (Aldrich, ≥98.0%)  
Oxalic acid (Aldrich, 99%)  
Titanium oxide (Degussa)  
Zinc oxide (Degussa)  
Zirconium isopropoxide (Fluka)  
Zirconium oxide (Fluka, 99.0%)

## **Liquids**

Benzyl alcohol (Aldrich, 99.8%)  
1-butanol (Aldrich, 99.9%)  
tert-Butyl hydroperoxide (Aldrich, 98%)  
Cyclohexane (Acros, 99%)  
Methanol (Cross, 99.8%)  
Hydrofluoric acid (Merck, 95%)  
2-propanol (Aldrich, 99.5%)  
Pentane (Aldrich, 99%)



---

## Chapter 2

### Preparation of $\text{HAuCl}_4 \cdot 3\text{H}_2\text{O}$

- 1- 10.32 g of metallic gold was cut in very small pieces and placed into a 100 mL beaker at room temperature.
- 2- 60 mL of aqua regia (13 mL of 35% v/v  $\text{HNO}_3$  and 39 mL of 65% v/v  $\text{HCl}$ ) were slowly added into the beaker.
- 3- This mixture was stirred and the temperature gradually increased to 50 °C; if the dissolution of Au metal was not completed, temperature should be increased to 80 °C.
- 4- Once metallic gold was completely dissolved (after ca. 1 h.), the mixture was continuously heated until it was concentrated to 30 mL.
- 5- 3 mL of  $\text{HCl}$  was used to wash the gold chloride solution from  $\text{HNO}_3$ .
- 6- The presence of acid vapors was controlled by a pH paper, which was put into the vapors; this operation (addition of  $\text{H}_2\text{O}$ , concentration of the solution under heating) was repeated until pH 7 was obtained.
- 7- The mixture was concentrated to 10 mL by heating at 80 °C.
- 8- The mixture was placed in an oven for 1 day at 60 °C, until crystals of an intense yellow color were obtained.

### Preparation of metal oxide powders

#### *Synthesis of $\text{CaO}$*

105.2 g of  $(\text{Ca}(\text{NO}_3)_2 \cdot 6\text{H}_2\text{O})$  (mixture A) was dissolved in 800 mL of distilled water. 74.0 g of  $(\text{NH}_4\text{HCO}_3)$  (mixture B) was dissolved on 600 mL of distilled water and the pH was fixed at 10.2 using  $(\text{NH}_4\text{OH}, 25\%)$ . Mixture A was added dropwise to B under stirring, a solid precipitated and the stirring was continued overnight. The solid was then filtered off, washed 4 times with water and a small amount of ethanol. The obtained solid was oven dried at 120 °C for 16 h and then calcined at 900 °C for 5 h in air.

#### *Synthesis of $\text{MgO}$*

160 g of  $(\text{Mg}(\text{NO}_3)_2 \cdot 6\text{H}_2\text{O})$  (mixture A) was dissolved in 1.0 L of distilled water. 74.0 g of  $(\text{NH}_4\text{HCO}_3)$  (mixture B) was dissolved on 600 mL of distilled water and the pH was

---

fixed at 10.2 using (NH<sub>4</sub>OH, 25%). Then the same procedure was carried out as described above for CaO.

### **Synthesis of metal-oxy fluorides powders**

#### *Synthesis of CaF<sub>2-x</sub>(OH)<sub>x</sub>*

1.56 g (64.2 mmol) of Ca metal was dissolved in methanol (200 mL) in a Schlenk flask attached to a reflux condenser. The reaction started with the evolution of hydrogen gas to give a whitish colored magnesium methoxide solution which was used for the fluorination. Calcium methoxide was fluorinated using 1 mole of HF. The mixture concentrated to dryness under vacuum at 50 °C and gentle stirring to obtain the Ca(OH)<sub>x</sub> F<sub>2</sub> precursor. The obtained solid was oven dried at 120 °C for 16 h and then calcined at 350 °C for 5 h in air.

#### *Synthesis of MgF<sub>2-x</sub>(OH)<sub>x</sub>*

64.8 g (0.80 mol) of Al(O<sup>i</sup>Pr)<sub>3</sub> was dissolved in 200 ml of isopropanol and 1.2 moles of HF/H<sub>2</sub>O was added under stirring. The mixture was concentrated to dryness under vacuum at 50 °C and gentle stirring to obtain Mg(OH)<sub>x</sub> F<sub>2</sub> precursor. The obtained solid was oven dried at 120 °C for 16 h and then calcined at 350 °C for 5 h in air.

#### *Synthesis of ZrF<sub>2-x</sub>(OH)<sub>x</sub>*

57.32 g (0.17 mol) of Zr(O<sup>i</sup>Pr) was placed in a Schlenk flask under stirring for 5 min in an ice bath. 10.2 g of 48% HF was added slowly. The stirring of the reaction mixture was continued for 2 h. The mixture was concentrated to dryness under vacuum at 50 °C and gentle stirring to obtain Zr(OH)<sub>x</sub> F<sub>2</sub> precursor. The obtained solid was oven dried at 120 °C for 16 h and then calcined at 350 °C for 5 h in air.

#### *Synthesis of Ti<sub>4-x</sub>(OH)<sub>x</sub> and AlF<sub>3-x</sub>(OH)<sub>x</sub>*

These compounds were prepared following the above procedure for ZrF<sub>2-x</sub>(OH)<sub>x</sub> with varying the metal precursors (Ti(O<sup>i</sup>Pr), Al(O<sup>i</sup>Pr)).

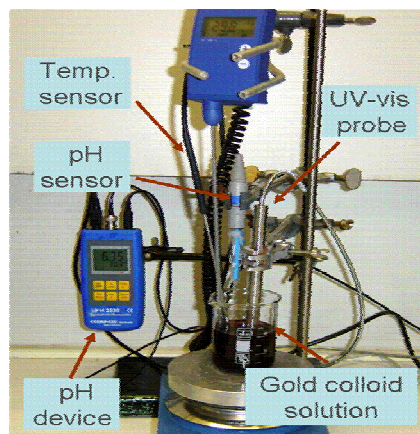


**Fig. App. 1(a).** Apparatus used for colloidal AuNPs preparation.



**Fig. App. 1(b).** Photographs of autoclaves used for oxidation reactions.

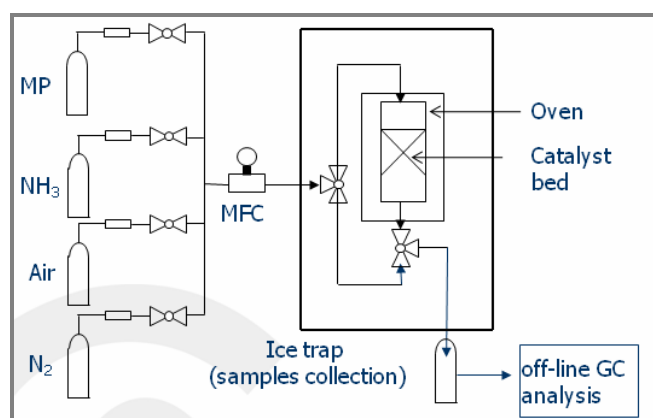


**Fig. App. 1(c).** Schematic picture of the flow system used for ammoxidation reaction. MP: 2 methylpyrazine, MFC: mass flow controller, GC: gas chromatograph.

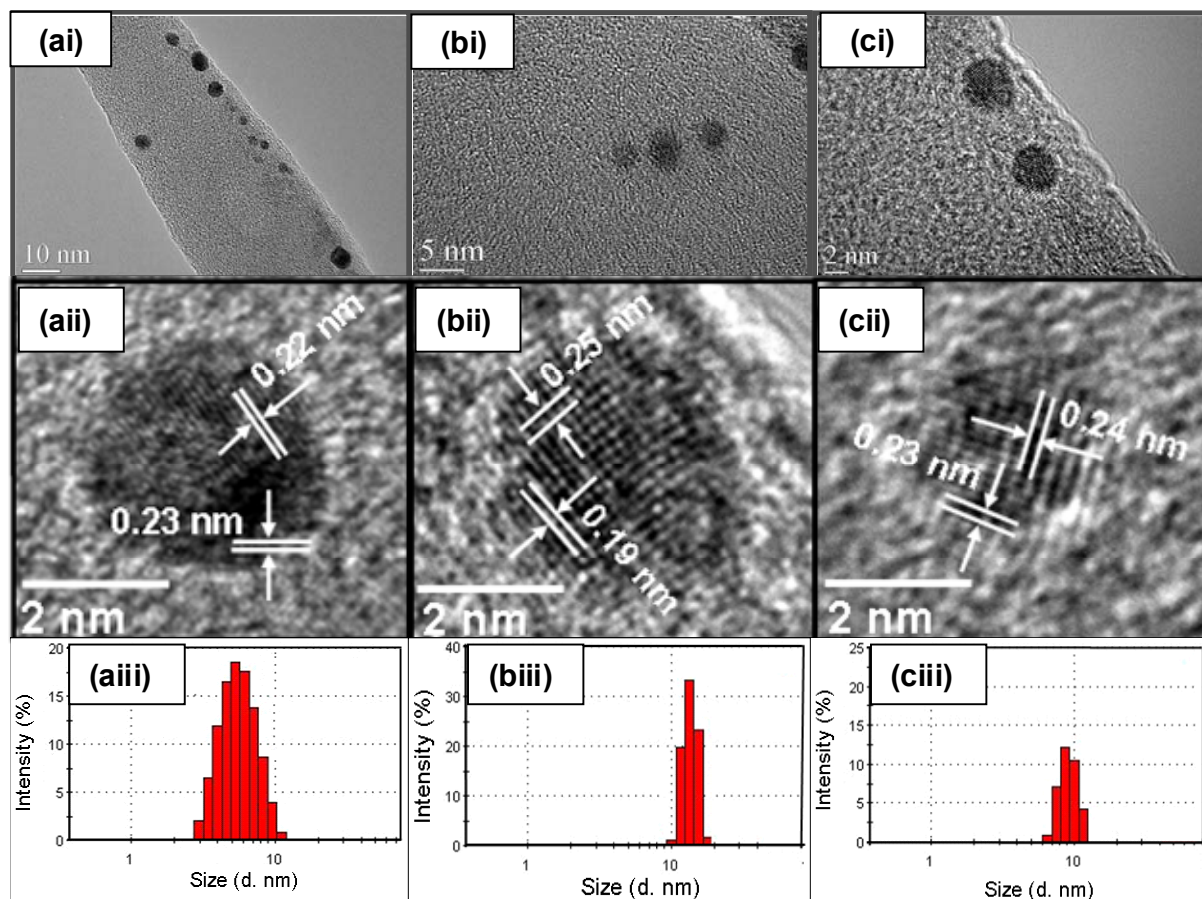


**Fig. App. 2.** TEM-(i), HRTEM-(ii) and DLS-(iii) of colloidal Au prepared using precursors a, b and c.

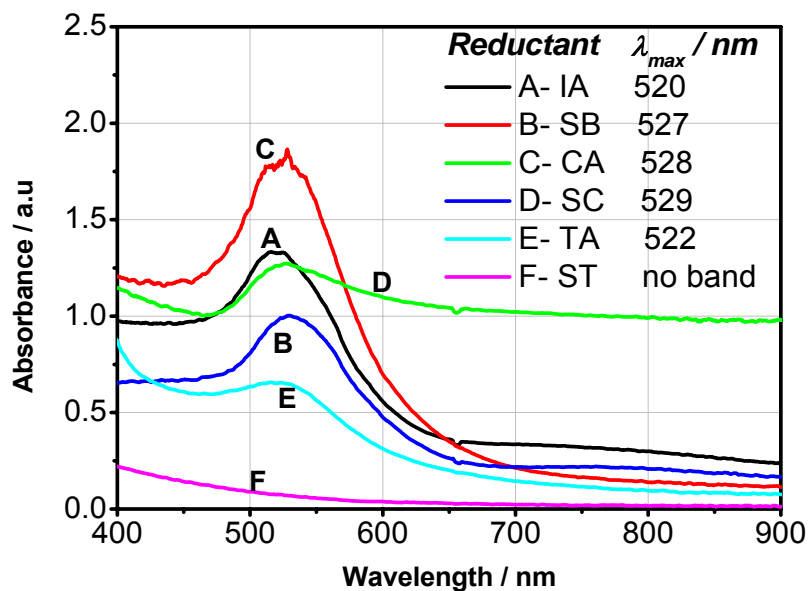


**Fig. App. 3.** UV-Vis spectra of colloidal nano-gold particles prepared by reduction of 1.0 mM HAuCl<sub>4</sub> solution using different reducing agents (IA, SB, CA, SC, TA and ST).

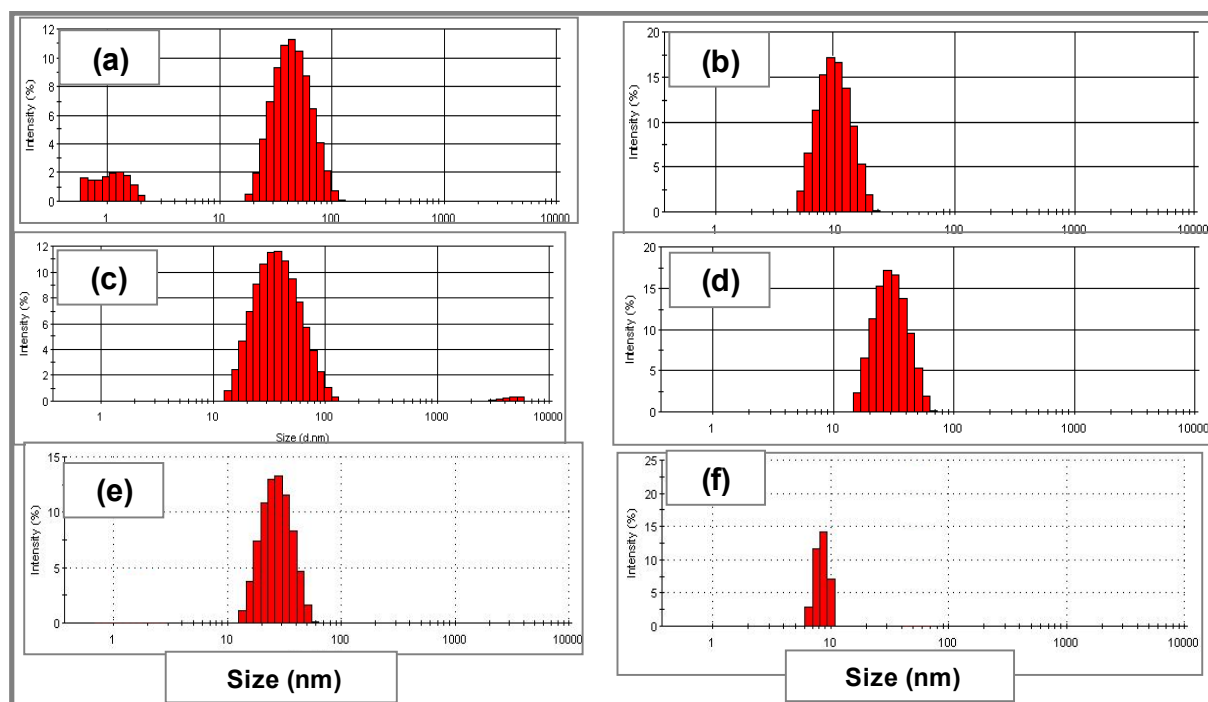


**Fig. App. 4.** DLS size distribution of colloidal AuNPs prepared by reduction of 1.0 mM HAuCl<sub>4</sub> using different reducing agents (a- CA, b- SC, c- IA, d- SB, e- TA, f-ST).

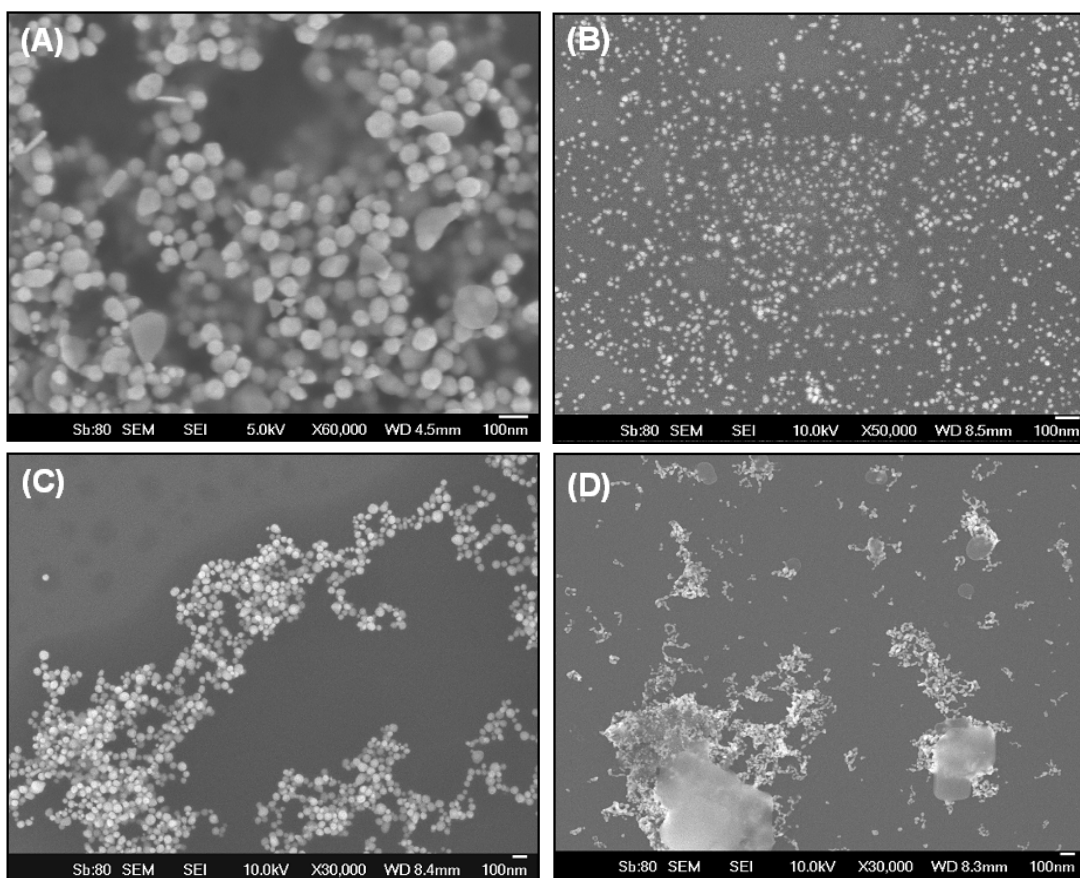


**Fig. App. 5.** Representative SEM images of colloidal AuNPs prepared by reduction of 1.0 mM HAuCl<sub>4</sub> using different reducing agents (15 mM): (A) CA, (B) SC, (C) IA, (D) SB at 60 °C.

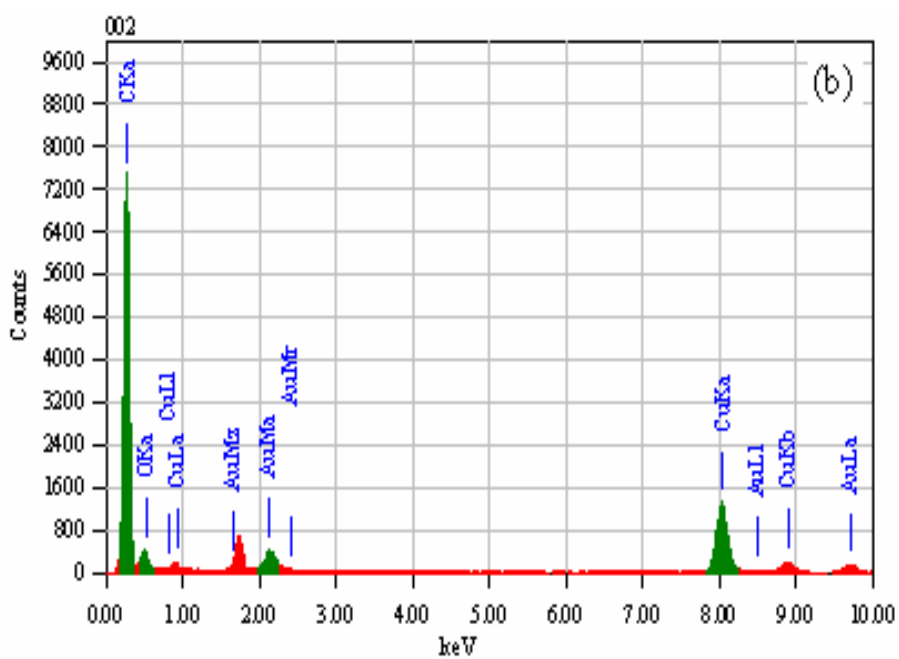
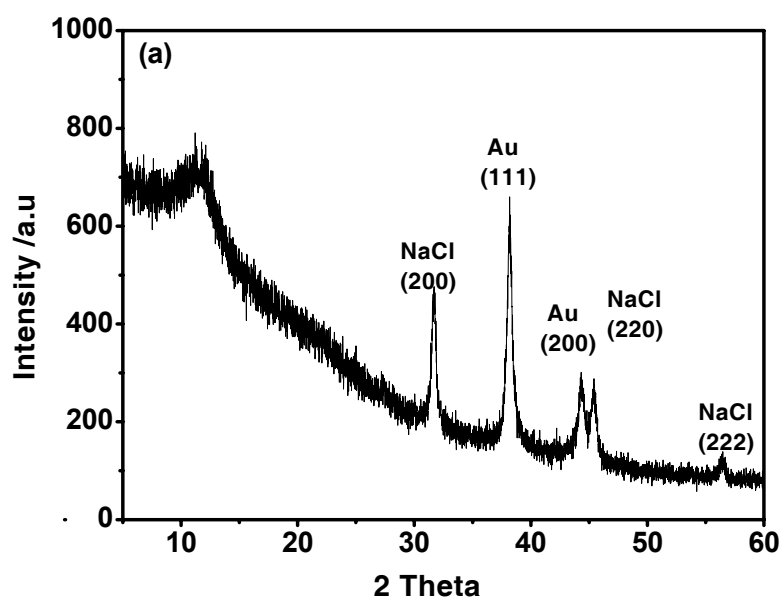
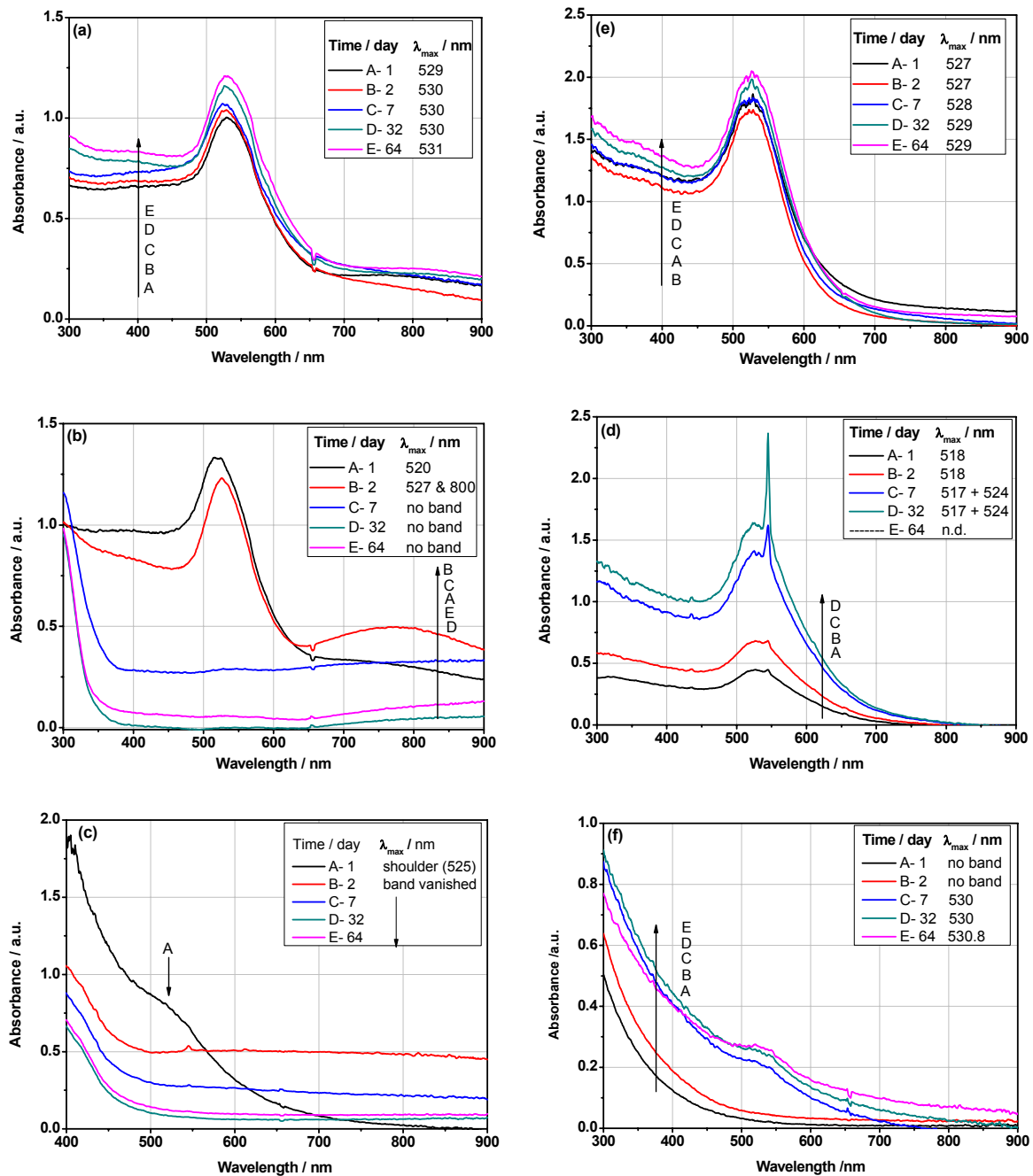
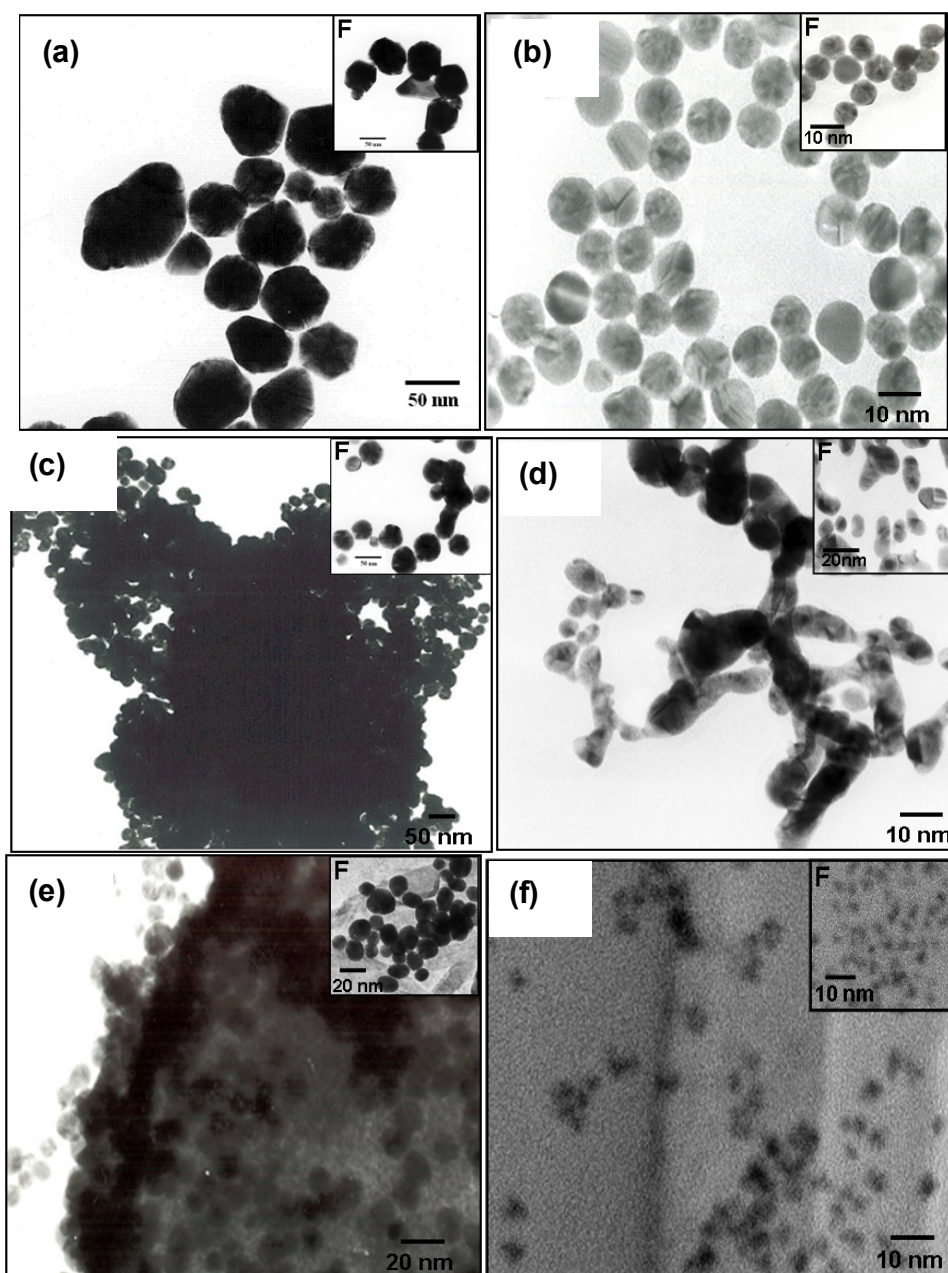


Fig. App. 6. XRD (a) and EDX (b) results of colloidal AuNPs prepared using SC as reductant.



**Fig. App. 7.** UV-Vis absorption spectra of colloidal AuNPs prepared using (a) CA, (b) SC, (c) IA, (d) SB, (e) TA, and (f) ST. The samples were taken at different storage time.





**Fig. App. 8.** TEM images of stored prepared colloidal AuNPs using different reductants: (a) CA, (b) SC, (c) IA, (d) SB, (e) TA, (f) ST. Images F corresponding to fresh samples.

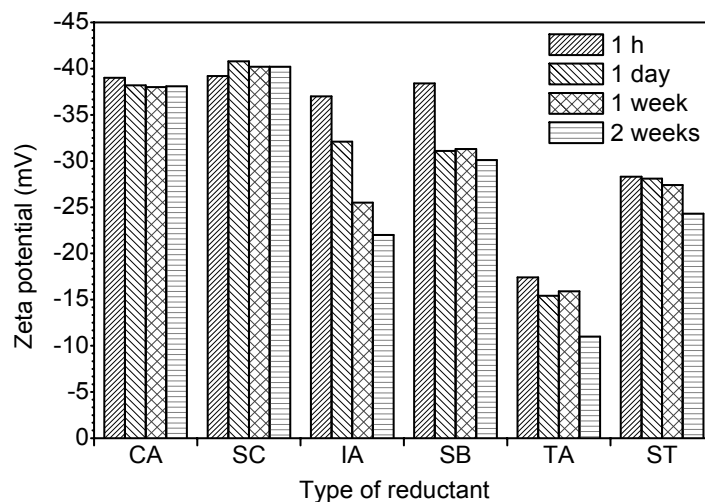


**Fig. App. 9.** Zeta potential of colloidal nano-gold particles prepared using CA, IA, TA, SB, SC and ST. The  $\zeta$  was recorded at different storage times of the samples.

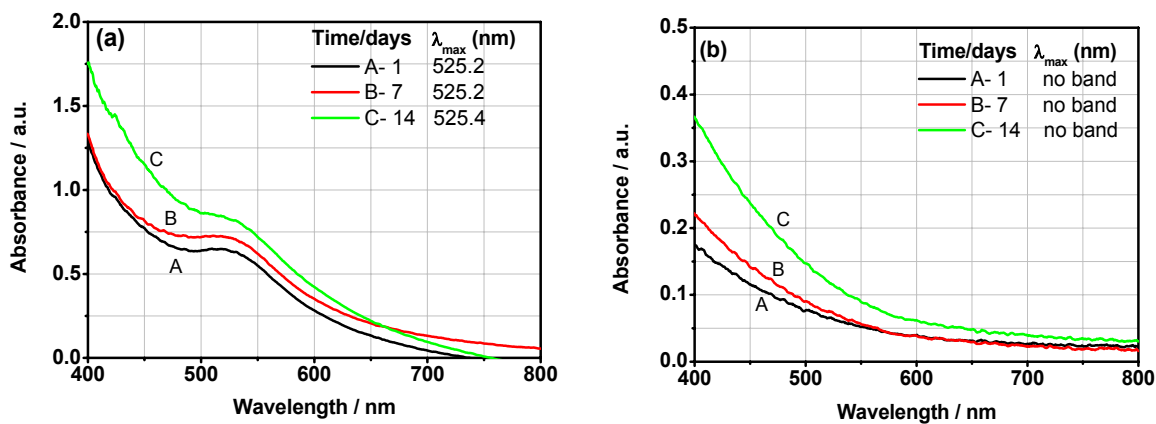


**Fig. App. 10.** UV-Vis absorption spectra of colloidal AuNPs prepared using (a) TA and (b) ST in the presence of ST. The samples were taken at different storage time.

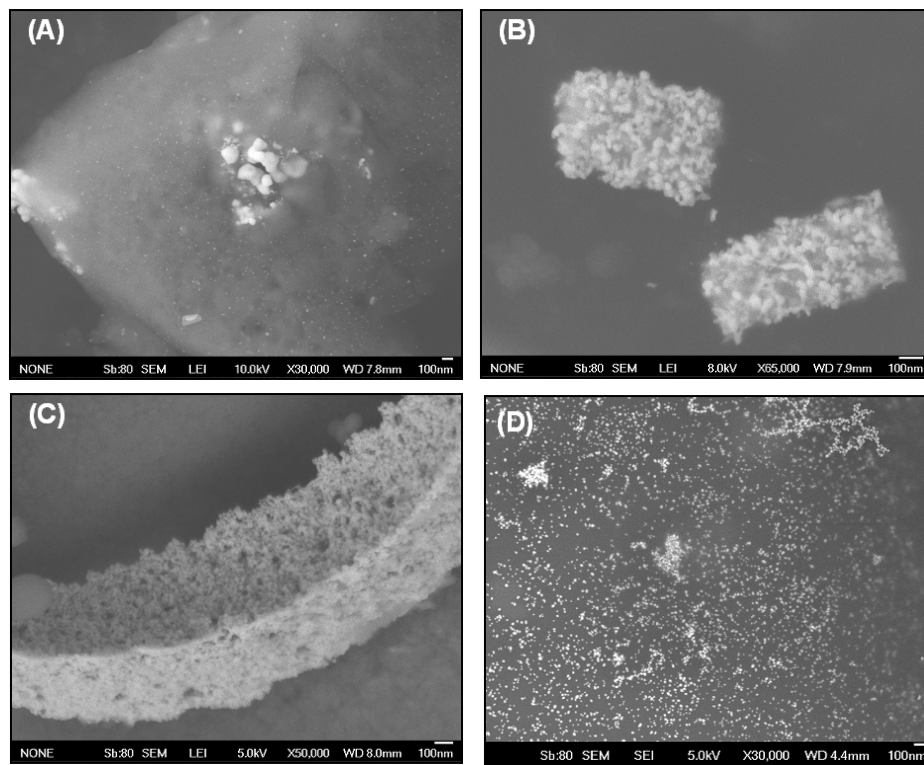


**Fig. App. 11.** SEM images taken from various time steps during the formation of colloidal AuNPs obtained by reduction of 1.0 mM  $\text{HAuCl}_4$  with 15 mM SC at 60 °C and an  $[\text{Au}^{3+}]/[\text{SC}]$  ratio of 1:4 at reaction time of (A) 1 min, (B) 10 min, (C) 30 min, and (D) 60 min.

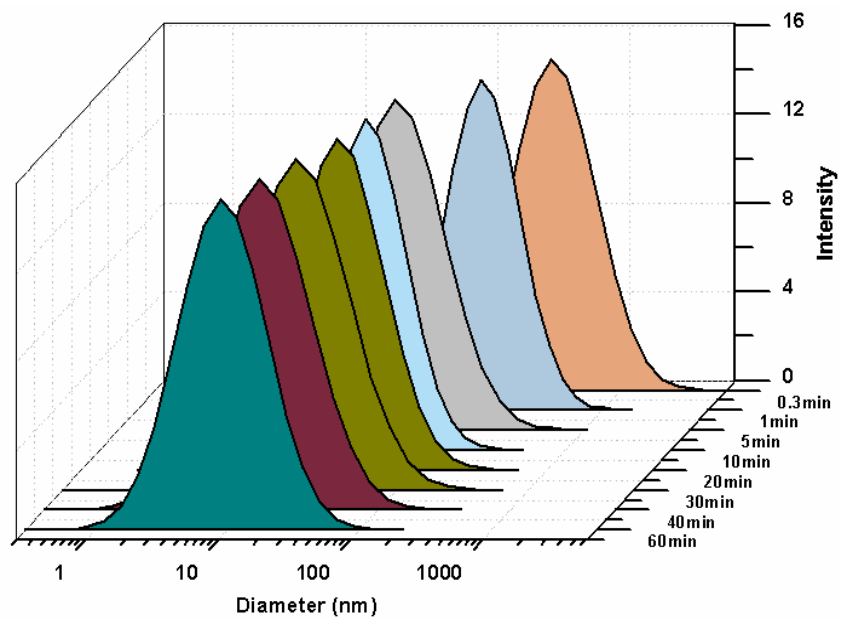


**Fig. App. 12.** Time-resolved plot of the size distribution of colloidal AuNPs achieved by DLS (reaction conditions: 186 mL of 1.0 mM HAuCl<sub>4</sub> solution, 50 mL 15 mM SC, 60 °C, [Au<sup>3+</sup>]/[SC] ratio 1:4).

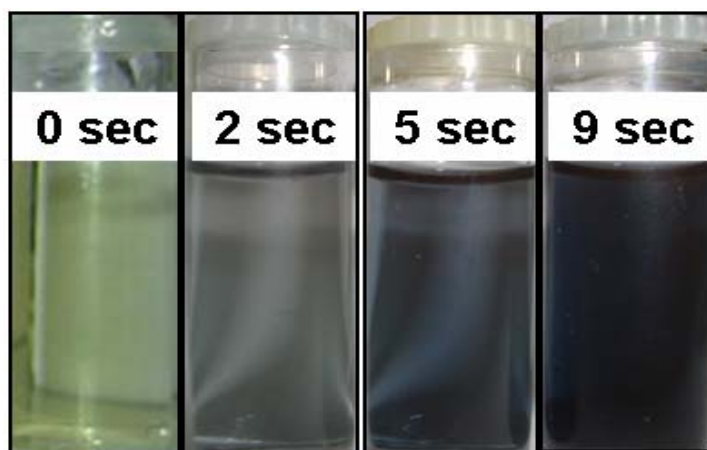


**Fig. App. 13.** Color changes of the reaction solution during the course of colloidal AuNPs formation with TA as reducing agent.

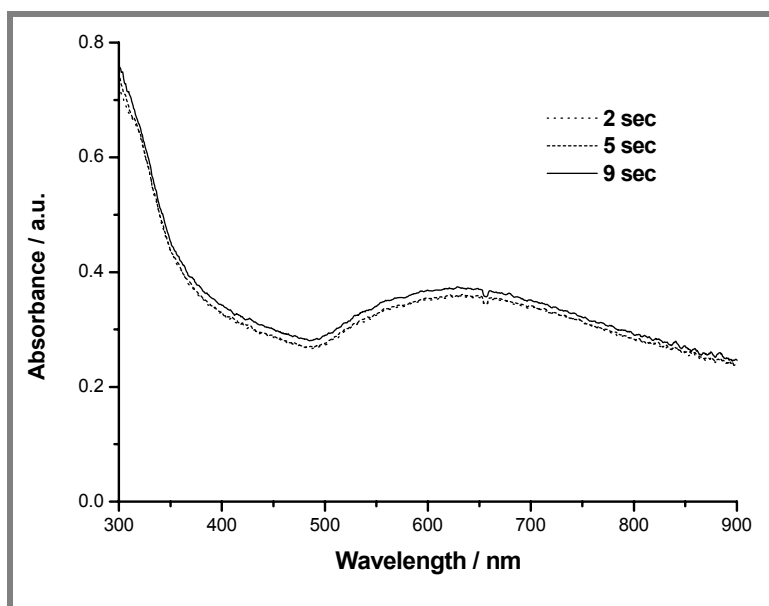


**Fig. App. 14.** Time-resolved UV-vis spectra during the reduction of 1.0 mM HAuCl<sub>4</sub> solution with 15 mM TA at 60 °C and an [Au<sup>3+</sup>]/[TA] ratio of 1:4.

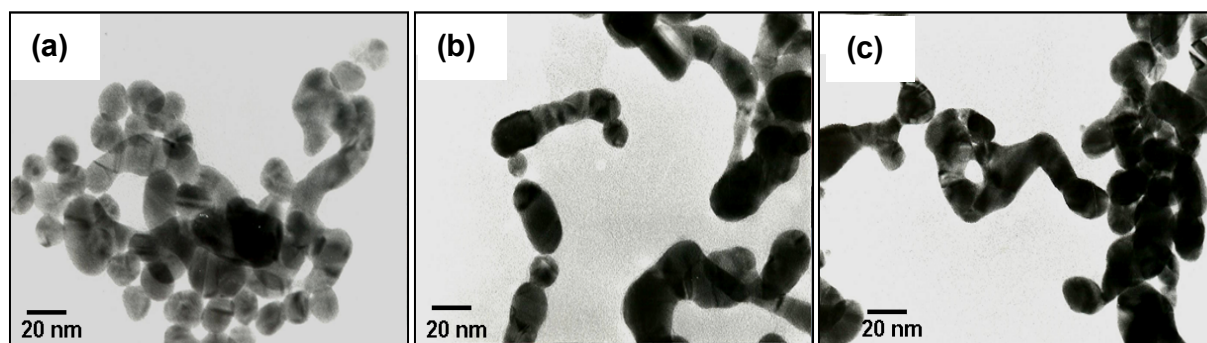


**Fig. 3.15.** TEM images taken during the formation of colloidal AuNPs obtained by reduction of 1.0 mM HAuCl<sub>4</sub> solution with 15 mM TA solution at 60 °C and an [Au<sup>3+</sup>]/[TA] ratio of 1:4 at reaction time of (A) 2 sec, (B) 5 sec, and (C) 9 sec.

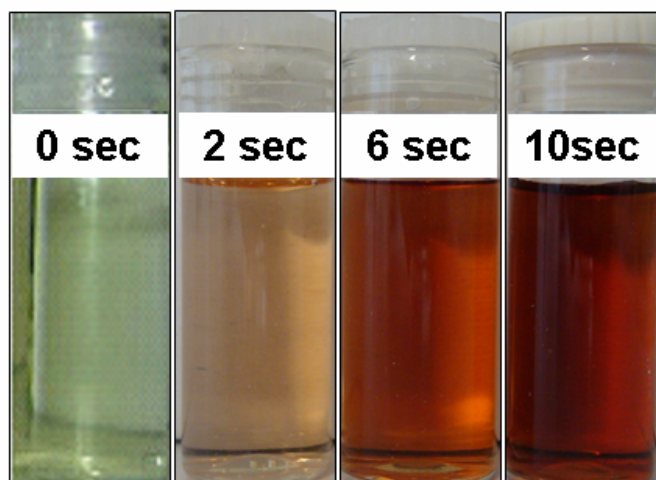


**Fig. App. 16.** Color changes of the reaction solution during the course of colloidal AuNPs formation with a combination of SC and TA as reducing agent.

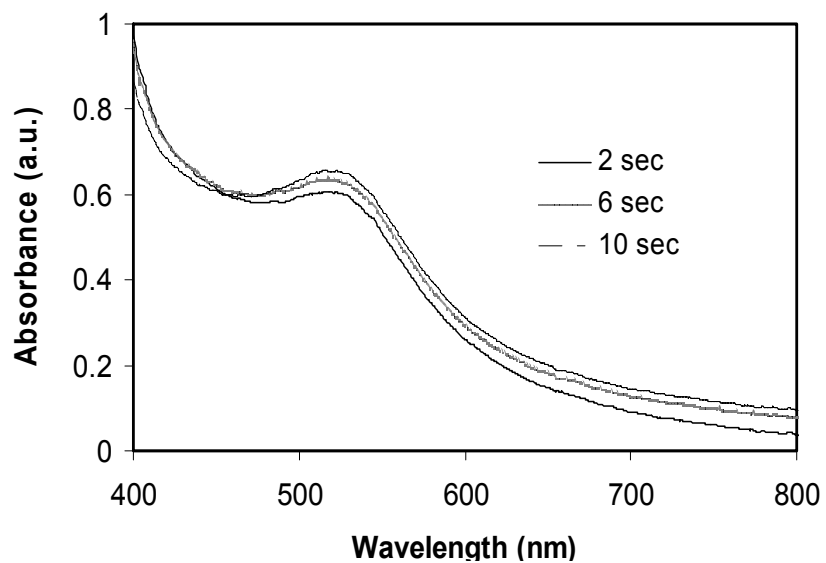


**Fig. App. 17.** Time-resolved UV-vis spectra during the reduction of 1.0 mM  $\text{HAuCl}_4$  solution with 15 mM SC solution in the presence of TA at 60 °C and an  $[\text{Au}^{3+}]/[\text{SC}]$  ratio of 1:4.

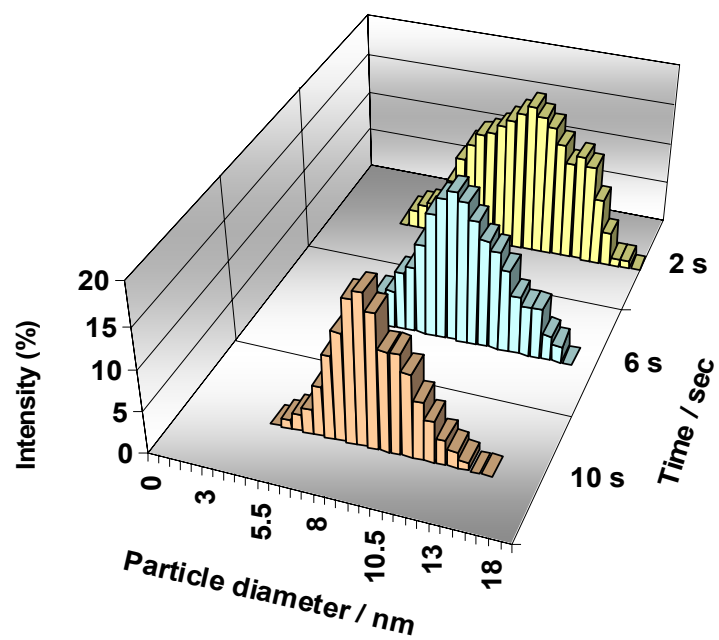


**Fig. App. 18.** Time-resolved plot of the size distribution of colloidal AuNPs achieved by DLS (reaction conditions: 186 mL of 1.0 mM HAuCl<sub>4</sub>, solution, 50 mL of 15 mM SC, 0.5 ml of 6 mM TA, at 60 °C, [Au<sup>3+</sup>]/[SC] ratio 1:4).



## Chapter 4

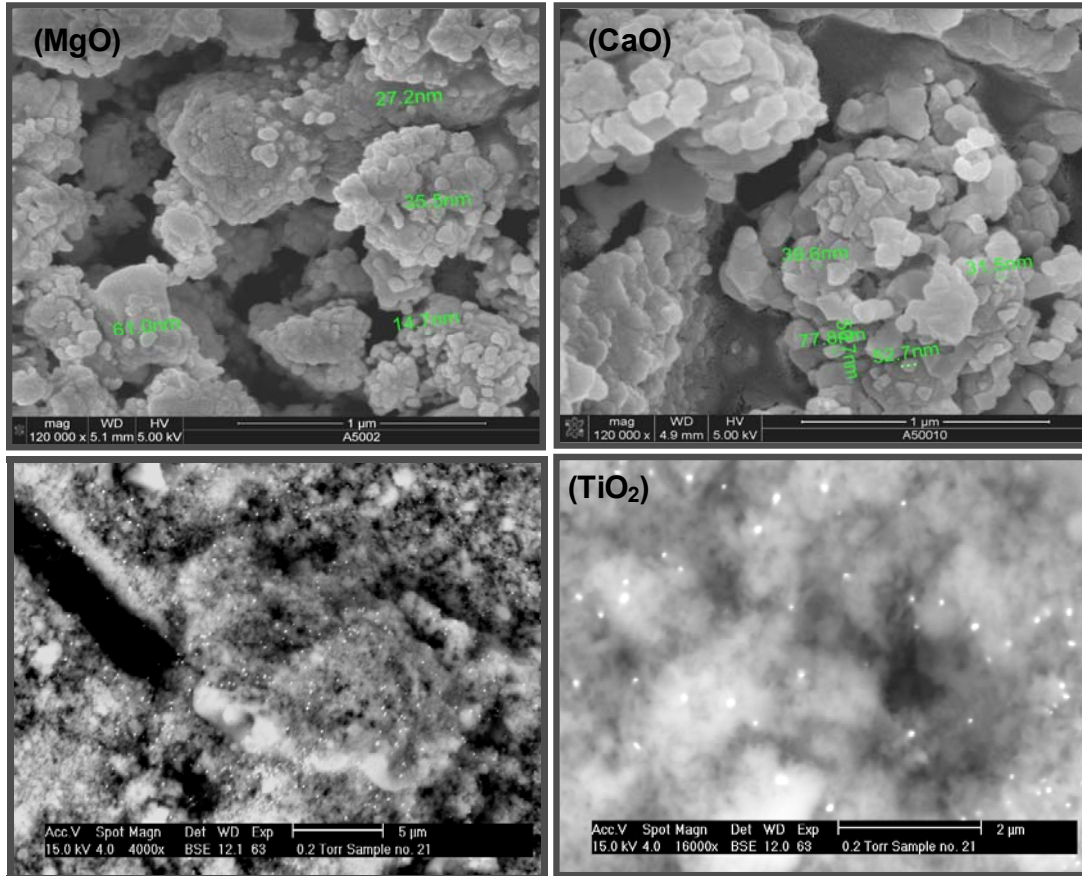


Fig. App. 4.19. SEM images of fresh AuNPs supported on different metal oxide carries.



---

C.V.

---

## **Versicherung**

Hiermit versichere ich, dass ich die Arbeit selbständig und nur unter Verwendung der angegebenen Hilfsmittel angefertigt und verfasst habe.

Rostock, den 25.11.2010

Ahmad Alshammari

---

## List of contributions

1. A. Alshammari, A. Köckritz, V.N. Kalevaru, A. Martin  
Method for preparation of dicarboxylic acids from saturated hydrocarbons or cycloaliphatic hydrocarbons by catalytic oxidation  
EP P08285 (2010). (Patent)
2. A. Alshammari, A. Köckritz, V.N. Kalevaru, A. Martin  
Influence of precursor on the particle size and stability of colloidal gold nanoparticles  
Studies in Surf. Sci. and Catal., 175 (2010) 409. (Paper)
3. A. Alshammari, A. Köckritz, V.N. Kalevaru, A. Martin  
Influence of single use and combination of reductants on the size, morphology and growth steps of gold nanoparticles in colloidal mixture  
Nanoscale research Letter (submitted 2010) (Paper)
4. A. Alshammari, A. Köckritz, V.N. Kalevaru, A. Martin  
One-pot oxidation of cyclohexane to adipic acid over gold catalysis  
ChemCatChem. (in preparation 2010). (Paper)
5. A. Alshammari, A. Köckritz, V.N. Kalevaru, A. Martin  
Study on the preparation and formation of colloidal gold nanoparticles by various spectroscopic and microscopic techniques  
J. Nanosci. and nanotech (in preparation 2010). (Paper)
6. A. Alshammari, A. Köckritz, V.N. Kalevaru, A. Martin  
One-pot oxidation of cyclohexane to adipic acid over gold catalysis  
The 8<sup>th</sup> International Conference and Exhibition on Chemistry in Industry, Bahrain, 2010. (Oral presentation)
7. A. Alshammari, A. Köckritz, V.N. Kalevaru, A. Martin  
Comparison of the catalytic activity of supported gold nanoparticles on Ti-oxide and Ti-(oxy)-fluoride  
14<sup>th</sup> Nordic Symposium on Catalysis August ,2010 Marienlyst, Denmark. (Poster)
8. A. Alshammari, A. Köckritz, V.N. Kalevaru, A. Martin  
Morphology and stability of colloidal gold nanoparticles synthesized using various reductants  
6<sup>th</sup> World Congress of Oxidation catalysis in Lille, 2009. (Poster)
9. A. Alshammari, A. Köckritz, V.N. Kalevaru, A. Martin  
Influence of the combination of reductants on the formation mechanism of colloidal gold nanoparticles  
Jahrestreffen Deutscher Katalytiker, March 2009, Weimar, Germany (Poster)
10. A. Alshammari, A. Köckritz, V.N. Kalevaru, A. Martin  
Applications of metal hydroxyfluorides as novel supports for gold nanoparticles  
Jahrestreffen Deutscher Katalytiker, March 2009, Weimar, Germany (Poster)
11. A. Alshammari, A. Köckritz, V.N. Kalevaru, A. Martin  
Investigations on the formation mechanism of gold nano-particles  
Jahrestreffen Deutscher Katalytiker, March 2008, Weimar, Germany (Poster).

---

## **Lebenslauf**

### **Persönliche Daten**

Name: Ahmad Alshammari

Geburtsdatum : 16.05.1980

Geburtsort : Hail, Saudi Arabian

Nationalität : Saudi

Geschlecht : männlich

Familienstand : verheiratet

### **Bildung**

1986 – 1998 Grund – und sekundäre Bildung Hail – Saudi.

1998 – 2002 B.Sc. in Chemie; Naturwissenschaftliche Fakultät – König-Saud-Universität, Riad, Saudi Arabien.

2003 – 2005 M.S.c. Designing chemical solutions, Newcastle Universität, England.

2007 – 2010 Doktorand im institut für chemie an der Rostock – Universität in kooperation mit dem Leibniz-Institut für Katalyse, Rostock.

### **Berufstätigkeit**

2002 – 2003 Forscher-Assistent in der Erdöl-und Petrochemie-Forschungs-institut, Riad, Saudi Arabien.

2005 – 2007 Forscher-Assistent in der Petrochemie-Forschungs-institut, Riad, Saudi Arabien.